On-Line Consolidation of Thermoplastic Composites

by
Po-Jen Shih

Dissertation submitted to the Faculty of the
Virginia Polytechnic Institute and State University
in partial fulfillment of the requirements for the degree
of
DOCTOR OF PHILOSOPHY
in
ENGINEERING MECHANICS

Approved:

_____
Alfred C. Loos, Chairman

_____	_____
Mark S. Cramer	Zafer Gürdal
_____	_____
Robert A. Heller	Eric R. Johnson

February 19, 1997

Blacksburg, Virginia

On-Line Consolidation of Thermoplastic Composites

by
Po-Jen Shih

Committee Chairman: Alfred C. Loos
Engineering Science and Mechanics

(ABSTRACT)

An on-line consolidation system, which includes a computer-controlled filament winding machine and a consolidation head assembly, has been designed and constructed to fabricate composite parts from thermoplastic towpregs. A statistical approach was used to determine the significant processing parameters and their effect on the mechanical and physical properties of composite cylinders fabricated by on-line consolidation. A central composite experimental design was used to select the processing conditions for manufacturing the composite cylinders. The thickness, density, void content, degree of crystallinity and interlaminar shear strength (ILSS) were measured for each composite cylinder. Micrographs showed that complete intimate contact and uniform fiber-matrix distribution were achieved. The degree of crystallinity of the cylinders was found to be in the range of 25-30%. Under optimum processing conditions, an ILSS of 58 MPa and a void content of <1% were achieved for APC-2 (PEEK/Carbon fiber) composite cylinders.

An in-situ measurement system which uses a slip ring assembly and a computer data acquisition system was developed to obtain temperature data during winding. Composite cylinders were manufactured with eight K-type thermocouples installed in various locations inside the cylinder. The temperature distribution inside the composite cylinder during winding was measured for different processing conditions.

ABAQUS finite element models of the different processes that occur during on-line consolidation were constructed. The first model was used to determine the convective heat transfer coefficient for the hot-air heat source. A convective heat transfer coefficient of 260 $w/m^{2}°K$ was obtained by matching the calculated temperature history to the in-situ measurement data. To predict temperature distribution during winding an ABAQUS winding simulation model was developed. The winding speed was modeled by incrementally moving the convective boundary conditions around the outer surface of the composite cylinder. A towpreg heating model was constructed to predict the temperature distribution on the cross section of the incoming towpreg. For the process-induced thermal stresses analysis, a thermoelastic finite element model was constructed. Using the temperature history obtained from thermal analysis as the initial conditions, the thermal stresses during winding and cooling were investigated.

Acknowledgments

I wish to express gratitude to my advisor, Dr. Alfred Loos for his continuous support and guidance through this work. Thanks are also extended to Dr. Mark S. Cramer, Dr. Zafer Gürdal, Dr. Robert A. Heller and Dr. Eric R. Johnson for serving on my advisory committee.

This work was supported by the NSF Science and Technology Center; High-Performance Polymeric Adhesives and Composites (NSF grant number DMR-912004). The author would like to acknowledge Mr. Steven Garrette of Fiberite, Inc. for supplying the APC-2 towpreg.

Special gratitude must be expressed to my parents, Lung-Chin Shih and Wen-Chia Shihhsu, and parents in law, Hui-An Chiang and Chieh-Chu Lin, for their continuous support, understanding, and their unshakable faith in me. Finally, the deepest appreciation is expressed to my wife, Tzu-Hui Chiang, for her silence sacrifice and endless love throughout this long journey as a graduate student.

To my family,
Jonathan, Jerry, Jimmy, and Tzu-Hui.

Table of Contents

List of Figures

List of Tables

1 Introduction

1.1 Motivation and Objective

When considering replacing conventional materials with composite ones, costs are the major concerns. While the cost of raw materials will usually decline as the demand goes up, the production costs can be reduced only through the use of low-cost, automated manufacturing technology. Yet automated processes sometimes raise concerns about product quality. For the thermoplastic composites, the newly developed on-line consolidation technique may have the potential to achieve both desired quality and lower production costs.

On-line consolidation is a composite manufacturing process where the resin impregnated fiber bundles ("towpreg" or "prepreg") are continuously oriented, laid down, consolidated, and cured onto the tool surface in a single step. Once the surface of the designed structure has been covered and the thickness has been achieved, the part is finished. Secondary processing steps such as autoclave or hot-press consolidation are eliminated. When integrated with a computer controlled system, the process can be fully

automated which leads to further cost savings in fabrication by increasing productivity and reducing labor cost.

In addition to the reduced cost, on-line consolidation also offers benefits for design flexibility and performance. With localized heating, this process is inherently suitable for manufacturing parts with large surfaces and moderate curvatures, such as fuselage structures and deep submersibles [1]. Because the towpreg is fully consolidated and locked in the vicinity of the melting point as it is placed onto the structure, conceptually there is no limitation on producing parts with thick cross-sections and large surface areas [2]. Furthermore, complex, non-geodesic, and even concave winding paths are also achievable, thus allowing design flexibility [3].

Thick-section thermoplastic composites experience a build-up of residual stresses caused by the large volumetric changes during melting and solidification in post consolidation [4]. The effects of residual stresses on the mechanical properties of composite structures have received considerable attention [5-14]. It has been demonstrated that the high level of residual stresses may lead to dimensional instability and premature failure. However, due to localized heating and solidification, the on-line consolidation process has the potential to prevent the build-up of residual stresses and, in turn, to produce better quality composite structures.

The objectives of this study were to design and develop low cost on-line consolidation techniques that can be used for reliable and consistent fabrication of composite structures using thermoplastic towpreg. This investigation will experimentally determine the processing window and

thereby evaluate the feasibility of the on-line consolidation technology. Process simulation models will be developed and used to calculate the temperature field and the associated thermal stresses and to relate the processing parameters to the quality of the consolidated parts.

1.2 On-Line Consolidation

On-line consolidation techniques are commonly used in manufacturing processes such as filament winding and tape laying. Despite differences in the machines used to implement these two manufacturing processes, similar procedures are required to ensure complete bonding between the composite layers. The basic components of on-line consolidation process are illustrated in Figure 1.1.

A focused heat source is aimed at the interface between incoming towpreg and substrate to create a molten zone. The intensity of the heat source must be properly adjusted to ensure melting on both mating surfaces. Once the proper molten zone has been created by the heating system, adequate pressure must be applied via fiber tension and/or roller compaction to compress the uneven melting surfaces and to squeeze the matrix flow to fill the gaps. Subsequently, intimate contact and diffusion bonding in the interface can be established. The roller pressure should be held constant until the temperature at the exit of the molten zone drops below the melting point of the resin to prevent void formation by either volumetric shrinkage or the release of spring energy from the fiber network.

Continuous operation of the on-line consolidation process is achieved by either rotating the mandrel and moving the carriage during filament winding or, in the case of tape laying, by moving the lay-up head. However, the speed of on-line consolidation is limited by the time required for intimate contact and diffusion bonding. In general, the speed of consolidation, the heat intensity, and the roller pressure are used to describe the processing window of on-line consolidation.

For the purpose of analysis, the on-line consolidation process can be divided into the three stages shown in Figure 1.2, and discussed in detail in the following section. These include localized melting, non-isothermal consolidation, and controlled cooling.

1.2.1 Localized Melting

For the on-line consolidation process, it is preferred that melting occurs only in the neighborhood of the nippoint where the incoming towpreg and consolidated substrate meet. If the required speed of consolidation is so high that a single nippoint heater is unable to achieve the designed temperature, a pre-heating system could be adapted to elevate the temperature of incoming towpreg.

Since the towpreg must be heated to well above melting temperature in seconds, highly focused heaters must be used to guarantee melting of the mating surfaces. However, excessive heating may lead to matrix degradation by polymer chain scission and oxidation, and consequently may affect the crystallization, adhesion of the fiber/matrix interface, and matrix properties

[15]. Therefore, appropriate selection and arrangement of the heating sources are the most important factors for a successful on-line consolidation system.

Many heat sources, including hot-gas, focused infra-red, laser, ultrasonic, microwave, induction, and conductive energy can be used for diffusion bonding of thermoplastic composites. Among these, the highly focused heat sources, such as hot-gas and laser energy, are commonly used for nippoint heating and the infra-red heaters are mostly found in the pre-heating stage [16-23].

1.2.2 Non-Isothermal Consolidation

On-line consolidation is a non-isothermal manufacturing process that involves continuous heating, compacting, and solidification which results in a large temperature variation in the deformation zone. However, it is very difficult, if not impossible, to physically measure the rapid change in temperature in the deformation zone. Therefore, a model which takes into account all mechanisms involved in the non-isothermal consolidation must be established to obtain the vital information.

Three major mechanisms, including resin flow, intimate contact, and diffusion bonding (healing), must be carefully investigated in the model. It is believed that to form good contact and bonding, the above mentioned mechanisms of consolidation must occur sequentially or simultaneously [24-26]. A schematic description of the physical phenomena in non-isothermal on-line consolidation is shown in Figure 1.3. The variation of thicknesses of the towpreg is used as an indicator to show the occurrence of each

mechanism. The time scale in on-line consolidation is generally less than a few seconds.

It is well known that the surfaces of commercially available prepregs are uneven. When two surfaces are brought into contact without applying pressure, gaps exist at interface. It is clear that polymer chains cannot diffuse without intimate contact. Hence, providing a proper pressure field to compress the viscous matrix, fill the gaps, and form perfect contact are essential for a successful fusion bonding.

The time needed for polymer chains of semi-crystalline thermoplastics to diffuse across the interface and randomization is relatively short compared with the time needed for resin flow. Therefore, it is believed that diffusion bonding is completed immediately after the two molten surfaces merge; and the micro- structure of the contact zone is also assumed to be identical to that of any other bulk sections [27,28].

However, some portion of the applied pressure is taken by the fiber network, and the energy stored in the deformed fiber network may be released at the exit of the roller and form voids. Therefore, the fiber network must be locked in the matrix before the exit. In other words, the roller should act as a heat sink to decrease the temperature of the deformation zone and to initiate crystallization before exiting. This is critical due to the fast consolidation speed.

1.2.3 Cooling

The last step of on-line consolidation is to cool and to solidify the consolidated parts. It is well known that, in addition to the reinforcement, the physical and mechanical properties of composites are determined by the microstructure of the matrix, while the morphology of the thermoplastics is determined by its thermal history [29-32].

For semi-crystalline thermoplastics, crystallization will occur during cooling. The equilibrium between crystalline and non-crystalline phases is delicate. Moreover, the presence of the reinforcing fibers, which provide a large surface for nucleation, further complicates the crystallization kinetics for a thermoplastic composite [29-32]. In order to thoroughly understand changes in the mechanical properties of thermoplastic composites processed under different conditions, we must study more than just the degree of crystallinity. Nucleation density, spherulite sizes, and the degree of crystalline perfection should also be taken into account [32]. However, correlating the changes in the mechanical properties with the changes in the morphology of matrix material is not within the scope of the present study. Instead, the effect of the degree of crystallinity on the mechanical properties of thermoplastic composites will be investigated.

While the physical and mechanical properties of bulk thermoplastic composites are influenced by the entire processing cycle, the cooling rate has been identified as the most important influence on the morphology of the matrix and the degree of crystallinity. In general, slower cooling rates yield higher degrees of crystallinity which correspond to an increase in tensile strength, compressive strength, and solvent resistance of the matrix [33]. Due

to the rapid temperature change in on-line consolidation, the cooling rate may be too high to achieve a designated crystallinity. Therefore, a controlled cooling rate or a secondary annealing process may be incorporated into the overall process.

For on-line consolidation, cooling starts immediately after the nippoint heating. This makes it more difficult to monitor and control the thermal history. However, the physics involved through the process must be well understood and carefully analyzed in order to control each step in the processing-structure-property loop and thus predict the mechanical properties of a consolidated laminate.

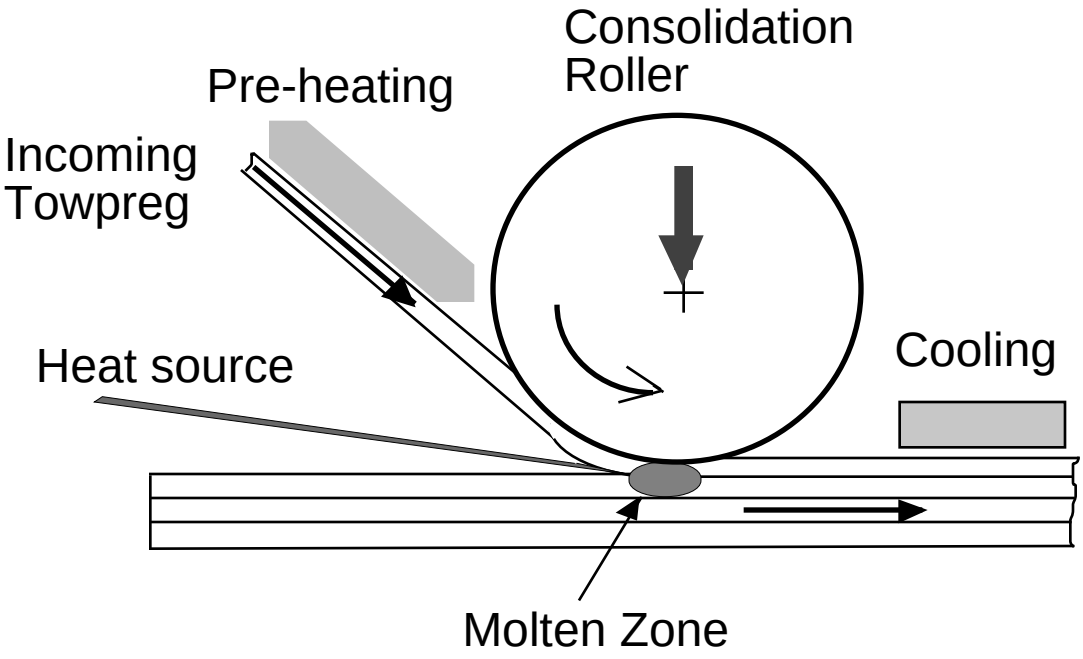

Figure 1.1 Schematic diagram of the on-line consolidation process.

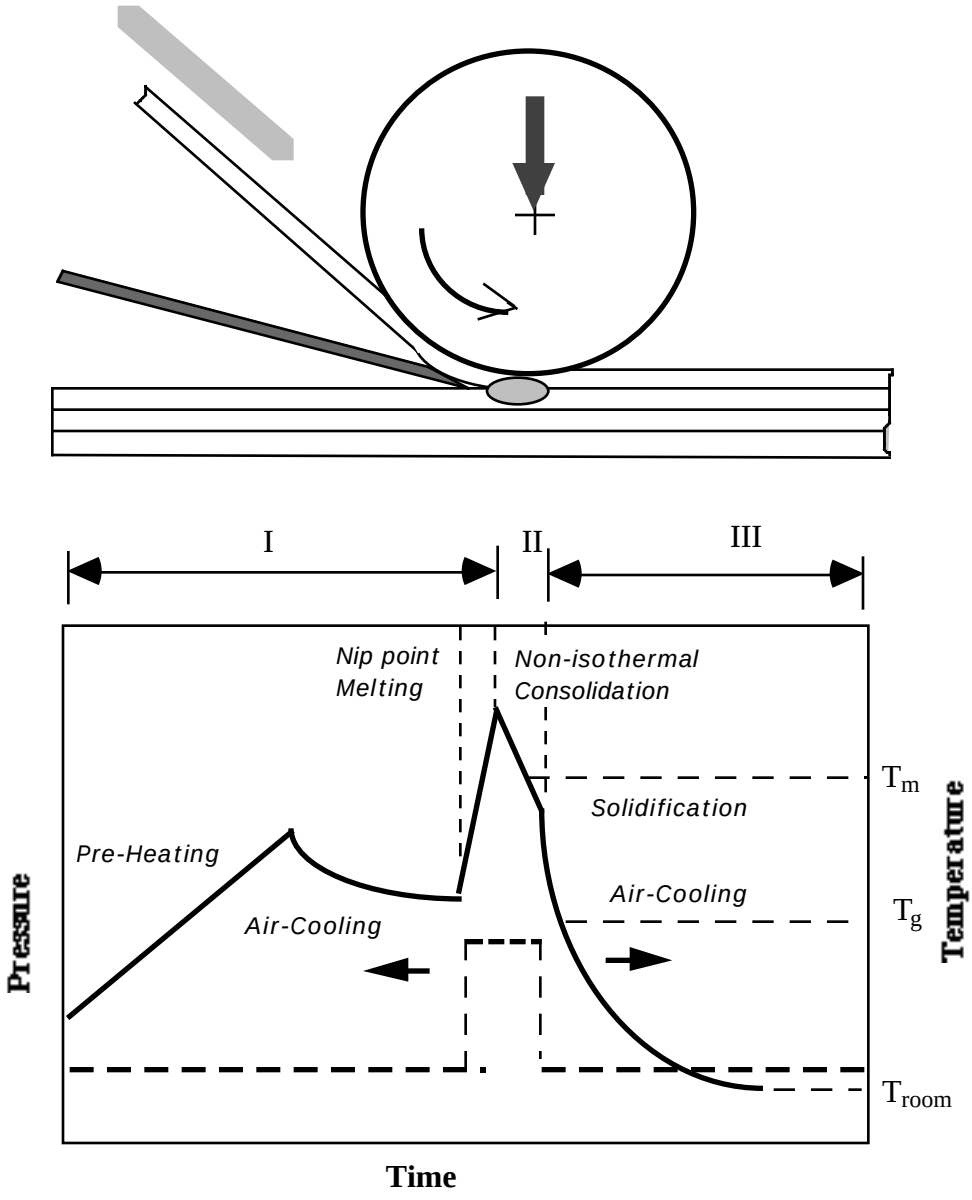

Figure 1.2 Suggested temperature and pressure profiles during on-line consolidation.

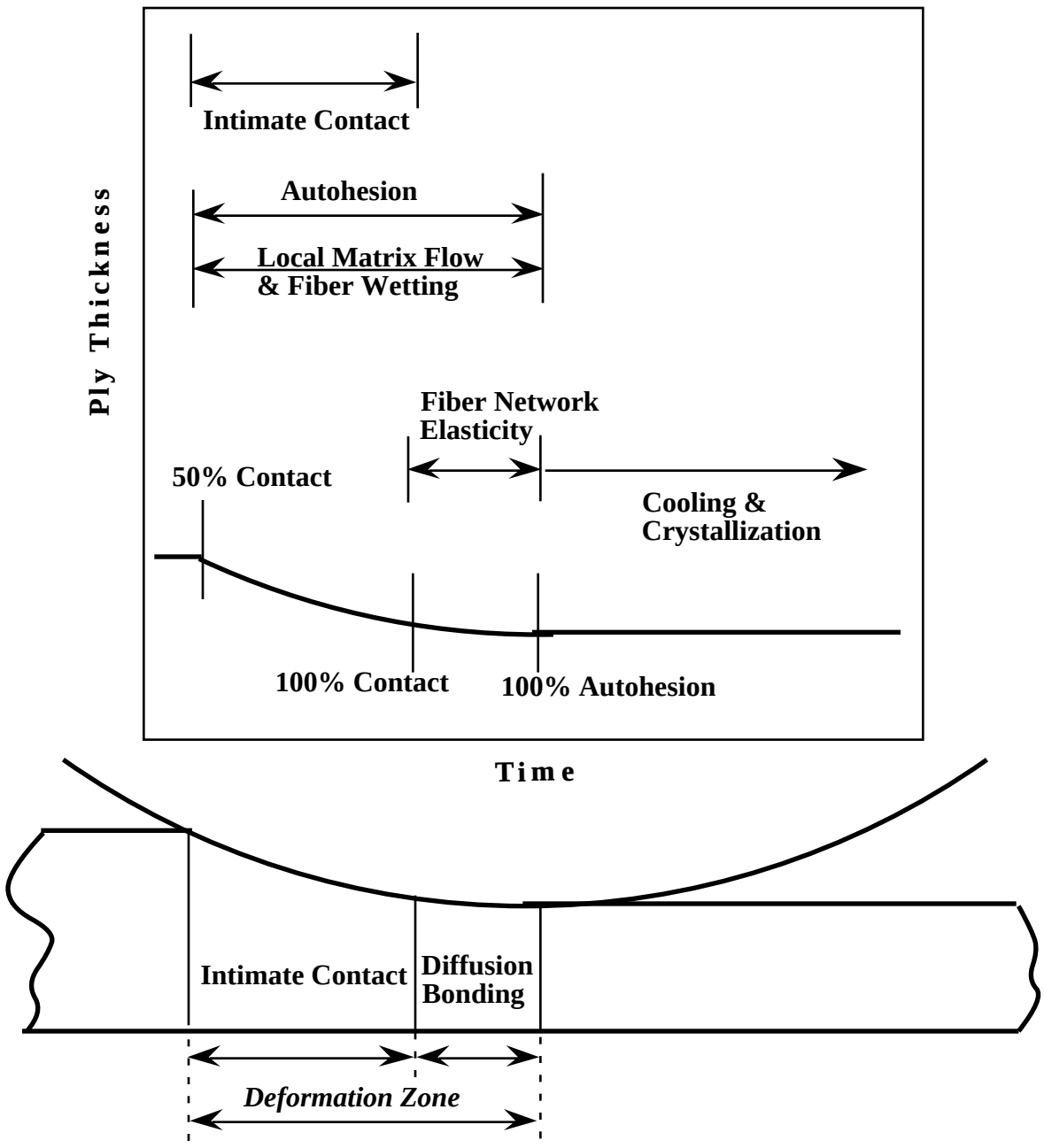

Figure 1.3 The variation of thickness during on-line consolidation.

2 Literature Review

2.1 On-Line Consolidation System

Over the past decade, the on-line consolidation of thermoplastic composites has attracted attention. Many studies have been devoted to develop this promising composite manufacturing technique [1-2, 4, 17, 20-22, 34-49]. The present review will briefly describe the previous research.

Almost all existing on-line consolidation systems have similar processing steps that start with unwinding preimpregnated towpreg from the spool. The continuous towpreg passes through a tensioner and guide rollers, and then arrives at the nippoint, where the towpreg and composite substrate meet. Energy from a highly focused heater melts the surfaces of the towpreg and composite substrate while, at the same time, the compacting roller compresses the material and squeezes out excess resin. Finally, the towpreg is solidified and consolidated onto the tool surface. However, the choice of apparatus for each system is unique and depends largely on its applications. For production, the capability of producing large structures with high throughput is the major concern. For laboratory research purposes, the

custom-made, single-purpose setups are the most common and have been proved sufficient for evaluating project feasibility and for studying the involved physics. The following reviews some of the existing on-line consolidation systems organized by different heating methods.

2.1.1 Laser Heating

Utilizing a laser as the heat source was first introduced by Beyeler and Güçeri [36]. An 80 watt CO_2 laser was used to partially melt the incoming tape and substrate. A horizontal rotating table combined with air cylinder and linear bearing provided the necessary rotation for hoop winding RYTON® AC40-60 towpregs onto a vertical mandrel. Micrographs of rings with various thickness indicated high quality composites. Furthermore, with the help of a motion controller, helical springs using APC-2 prepreg tows were successfully produced [22].

The laser-assisted processing technique was adapted by Mazumdar and Hoa [41]. A 65 watt CO_2 laser with a wavelength of 10.6 mm was used as the heat source. The steel consolidation roller driven by a speed controlled motor compacted the APC-2 towpregs onto the steel mandrel. In addition to the microstructure study, process-induced deformation and interlaminar fracture have been assessed. The impact of processing parameters on consolidated rings were investigated and the results from double cantilever beam tests assured that the laser could be a promising heat source for producing quality composites using the on-line consolidation technique.

For mass production purposes, McDonnell Douglas Aerospace (MDA) had developed a laser-assisted fiber placement machine that is capable of producing parts up to 52 inches in diameter and up to ten feet in length. The fiber placement facility included a winding machine and a gantry which housed optics to control the size of the heating zone, a compliant compaction shoe for pressure application, and a band-cut-and-add head for handling the towpregs. Their scale-up venture will fabricate submarine structures 35 feet long and 20 feet in diameter [50].

2.1.2 Hot Gas Heating

Due to the lack of flexibility and narrow processing window for satisfactory consolidation using laser energy, alternative heating methods need to be investigated. Because hot-gas welding of thermoplastic resins has been a common practice, the idea of applying the same heating technique in thermoplastic composites comes naturally for many researchers.

Although Gruber [51] reported on the use of hot gas as the heat source for on-line consolidation, the author chose to reveal few details. The first experimental demonstration of utilizing hot gas heating in on-line consolidation systems was done by Werdermann et al. [52]. They developed a hybrid system that consisted of two types of heating elements. In addition to a hot gas heater that aims at the nippoint, an infrared radiation oven was used to preheat the incoming towpreg. The basic set-up of the hybrid system had been extended by Buijs and Nederveen [40]. The preheating stage consisted of two sections, each of which housed a pair of 1000 watt opposite placed line heaters. Two hot gas torches, one aimed at incoming tow and the other at

substrate, were also installed to promote melting. Recently, the hybrid system has evolved one step further. A prewarmed chamber was used to house the material delivery system which included towpreg feeder and tensioner. In addition to the preheating section and two hot air heaters, an infrared line heater placed right on top of the heated mandrel was used to provide a constant nippoint temperature. This arrangement helped to realize consolidation speeds as high as twelve meters per minute for Glass fiber/PET thermoplastic composite [53].

Another approach is to integrate a compact consolidation mechanism into existing commercial automatic machines, such as robotic arms and filament winding machines. Automated Dynamic Corporation (ADC) developed a robotic winding system (ROWS) to place and consolidate towpregs onto a stationary mandrel [54]. Steiner [55] integrated a compact thermoplastic consolidation head with a six-axis AEG-Westinghouse PUMA 762 robot to place the towpreg onto a rotating mandrel. This robotic winding system was modified by Hümmler et al. [56] to accomplish double-concave winding. Felderhoff and Steiner [57] reported the latest development on the compact robotic head design which contained a cut-restart mechanism, tension control, infrared preheaters, and an additional hot-gas torch.

Combined with a computer-controlled filament winding machine, a thermoplastic processing head which included a tow cut-restart mechanism, a constant-load compaction roller, and a hot gas torch was developed through a cooperative team effort [39]. The hot-gas torch is capable of heating the nitrogen up to 1200°C. This allowed the successful fabrication of many

complex composite structures such as integrally stiffened cylinders and cylindrical sandwich structures with a phenolic honeycomb core. Mazumdar and Hoa [42, 58] have chosen the same hot gas torch to replace the laser energy. Optimum processing conditions for on-line consolidation of APC-2 composites using hot Nitrogen gas have been studied.

Due to its flexibility and minimum equipment cost, the hot-gas heating system has received much attention from researchers [34, 39, 40, 43, 45, 59-61] and has been chosen as the major heat source for the thermoplastic towpregs. Despite the specific design and different components required in various systems, most of the on-line consolidation systems using hot gas energy are conceptually similar to the one developed by ICI and ADC.

2.1.3 Continuous Ultrasonic Heating

Ultrasonic welding utilizes high-frequency vibration energy to join two thermoplastic towpregs. The heat is generated through deformation and friction in the interface which melts and becomes solid again to form molecular bonds. Benatar and Gutowski [16] reported that a relative bonding strength of 80 percent was achieved in welding PEEK composites. The limitations of their approach were the requirement of the triangular energy director made of the same material as the matrix. As a result, these energy directors will then form resin rich areas in the interface and may introduce voids in the interface as well.

Recognizing these limitations, Bullock and Boyce [62] modified the traditional method of energy input in ultrasonic welding and developed an

Ultrasonic Tape Lamination (UTL) apparatus. The developed a proprietary wave guide and transducer system to efficiently couple the ultrasonic energy into the tapes without the help of a energy director. The hoop wound rings produced by the UTL winding apparatus at a feeding rate up to 3.5 cm/sec ware tested and shown to achieve 96 percent consolidation. Details of the rings' mechanical properties, however, were not revealed.

One of the most important features distinguishing Ultrasonic on-line consolidation from other heating methods is that the strength of bonding can be monitored in-situ by gauging power consumption. The power absorbed in the interface increases dramatically when the glass transition temperature is reached. In a very short period of time, the polymer becomes viscous then the ultrasonic vibration energy compacts both surfaces and forms intimate contact. In the mean time, the polymer chains migrate across the interface, develop entanglements and bond the interface. The energy absorbed by towpregs drops when bonding is complete. The ultrasonic energy has been successfully shown to be a cost-effective alternative for on-line consolidation systems. However, the greatest challenges lie in scaling up and process control.

2.1.4 Summary

From the various available combinations, we chose one that consists of a commercial filament winding machine and a hot-air heating system. The rationale is twofold. First, we need a computer-controlled winding machine to expand our ability to manufacture parts such as tubes and cylinders in the lab. Second, the cost of the hot-air heating system is lower and most of the

required components are commercially available. The challenge lies in integrating all ingredients into a consolidation head that can be attached to the horizontal carriage of the filament winding machine. The head assembly must be easy to remove from the winding machine since the machine may be used regularly for other purposes; and the control devices for both electrical and pneumatical systems should be well placed inside a metal enclosure to avoid interference with the winder.

These guidelines for our design are concise but sufficient. Mass production is not within the scope of our study. We are most interested in investigating the fundamental physics involved in the process and how we can utilize the obtained knowledge to push the on-line consolidation technology a step further.

2.2 Heat Transfer Analysis

Virtually all manufacturing processes for thermoplastic composites involve heating and cooling cycles. In the on-line consolidation process, melting and solidification occur in seconds and the associated thermal history in the laminate is quite complicated. It is well-known that mechanical properties of consolidated parts depend on their thermal history during manufacture. Therefore, a transient heat transfer analysis is needed to investigate this thermal history.

Colton and Leach [34] solved the transient heat transfer problem by using the one-dimensional finite difference method. The energy required for

localized melting and heating methods, including radiant heating, conductive heating and convective heating, were discussed. The thermal analysis for the on-line consolidation process included four stages: infrared oven pre-heating, nippoint hot gas heating, roller conductive cooling, and atmosphere free convective cooling. However, both heat generation due to crystallization and the effect of roller speed have been neglected in this study.

Grove [35] has developed a two-dimensional finite element model to investigate the temperature profile of the tape laying process with a single laser heat source. A fixed finite element mesh, representing the neighboring area of the tape/substrate interface, was used. The movement of the laying head has been taken into account by using a coordinate system moving with the tape laying head. Furthermore, by assuming that the moving tape-laying head travels much faster than the rate of longitudinal heat conduction in a unidirectional carbon fiber prepreg, movement of the laying head was modeled by incrementally shifting the calculated temperature distribution from the previous step through the mesh at an appropriate time interval. For the boundary conditions, the effect of air cooling was also evaluated, and the consolidation roller as well as the lay-up table were considered as heat sinks.

Beyeler and Güçeri [36] investigated the anisotropic heat conduction phenomena of the laser-assisted tape laying process using a two-dimensional finite difference technique. In order to simplify the geometric complexity of the present problem they employed a boundary-fitted coordinate system technique which transforms a complex physical domain into a uniform

rectangular computational domain. Heat release from crystallization and local material velocity were also included in their thermal analysis.

In addition to heat release and tape motion during tape laying process, Ghasemi Nejhad et al. accounted for the size effect of the heating area [2]. Their two-dimensional, steady-state approach and numerical grid generation method were similar to those proposed by Beyeler and Güçeri [36]. Ghasemi Nejhad et al. found that, as the size of the heating area decreased, the processing window narrowed. The identical finite difference approach for the parametric study were later extended to include a three-dimensional thermal analysis of thermoplastic filament winding [37]. The effect of the winding angle was modeled by an orthotropic conductivity tensor obtained by transforming the tow conductivity tensor into the mandrel coordinate system. A large temperature gradient in the vicinity of the consolidation point was predicted in both tape laying and filament winding.

The transient heat transfer models described above were carefully formulated for their particular use. They were not programmed to be applied in all cases. Therefore, to simulate the on-line consolidation process, we had to develop our own models that incorporated both the geometry of the mandrel and the thermal properties of the composite materials. Since the domain of interest is fairly complicated, it required a special transformation technique as stated in Ref. 36 when using the finite difference analysis. Therefore, on its own merits of versatility and ease of implementation, a commercial finite element package, ABAQUS, was adapted to analyze the rapid temperature change during the manufacturing process.

2.3 Non-Isothermal Consolidation

The consolidation of thermoplastic composites can be considered as an autohesion process in which the molecular chains diffuse across the interface and entangle with their new neighbors. The interface is formed by bringing two identical polymers into contact through an applied pressure.

Thus, it is believed that the strength of the interply bonds depends strongly upon two basic mechanisms, namely intimate contact and diffusion bonding. Many theories, models, and experimental results have been published to describe these controlling mechanisms both qualitatively and quantitatively. The following sections discuss the previous research on intimate contact and diffusion bonding.

2.3.1 Models for Intimate Contact

It has been recognized that the thickness and surface topology of commercially available prepregs are not uniform. Dara and Loos [28] used the two-parameter Weibull function to model the tow height of AS4/P1700 prepregs (AS4 graphite fiber and Udel P1700 polysulfone resin). A reinforcement/viscosity factor "c" has been introduced to account for the presence of carbon fibers in prepregs. A power law viscosity model was adapted and the non-Newtonian viscosity coefficient and the power law exponent were obtained by matching the model results to degree of intimate contact versus time data.

Simplifying the model developed by Dara and Loos [28], Lee and Springer [63] used a series of uniform rectangles with two geometric parameters, namely generalized width and height, to describe the variations in prepreg thicknesses. They treated the deformation of the rectangular elements as a one-dimensional laminar squeezing flow in the transverse direction. For the verification of the proposed model, a single ply APC-2 prepreg was consolidated in a hot-press under various conditions of temperature, pressure, and compression time. The percentage of the uncompressed area was correlated to the degree of intimate contact. The temperature dependent matrix-fiber viscosity and the geometric parameters were obtained by matching the model to degree of intimate contact versus time data.

Mantell and Springer [49] extended the Lee-Springer model [63] to incorporate the tape laying and filament winding processes. By assuming that the temperature and pressure were constant during the manufacturing process, a simplified expression for the degree of intimate contact was derived and related to contact time. For the tape laying process, the contact time is equal to the arc length of contact between the roller and composite, divided by the roller speed. For the filament winding process, the same expression for degree of intimate contact was used except that the roller speed was replaced by the product of the speed of mandrel rotation and the radius of the cylinder at the contact interface. For model verification, Mantell et al. [64] fabricated sixteen-ply short beam shear specimens and two-ply lap shear specimens made of unidirectional APC-2 prepreg by compression molding and tape laying. By assuming that autohesion proceeded much faster than intimate

contact, the degree of intimate contact approximated the degree of bonding. Ultrasonic C-Scan was used to visually determine the ratio of contact area at the interface, while shear fracture tests were used to physically measure the strength and modulus of the specimens. The geometric parameters in the intimate contact model formulation were obtained by matching the model to degree of intimate contact versus time data obtained from the C-Scan results.

For processing the thermoplastic composites in a hot-press, the predicted degree of bonding which was modeled as a function of degree of intimate contact and degree of autohesion, agreed well with data. However, in the case of tape laying, large discrepancies between the prediction and the measured degree of bonding were found in short beam shear tests. This suggested that the nitrogen gas heating at the selected processing speed may not have provided enough energy to completely melt the interface. Thus, even though sufficient pressure was applied to compress the prepreg and achieve high degree of intimate contact, the autohesion process was not complete due to lower temperature achieved at the interface during the tape laying process.

Li and Loos [65] measured the surface of the prepreg plies by using a surface topology characterization machine. The prepreg geometric parameters were measured directly and consequently eliminate the necessity of determining the geometric parameters by matching the intimate contact data with models [49. 64]. The surface roughness of prepregs can be best described as a sinusoidal curve and can be simplified as a rectangular step for modeling purposes. After Lee and Springer [63], a series of uniform rectangles

was used to represent the waviness of the prepreg. The consolidation process of the thermoplastic composites in a hot press was also modeled as a squeezing flow between two rigid parallel plates of infinite width. Zero-shear-rate viscosity was used in the model; interfaces of both unidirectional and cross-ply laminate have been studied. The experimental data agreed well with the simulation results.

A power law squeezing flow model was proposed by Wang and Gutowski [66] to study the transverse spreading of unidirectional thermoplastic composites. Liu and Tsai [48] combined the Wang-Gutowski model with the intimate contact model of Lee and Springer [63] to simulate numerous microscopic viscous flows during the on-line consolidation of thermoplastic composites. To investigate transverse spreading of thermoplastic tow during on-line (in-situ) consolidation, a tow placement machine was used to place an AS4/PEEK towpreg on top of the heated tool plate. Tow widths at various locations after in-situ consolidation were measured and the experimental results agreed with the model prediction. The intimate contact portion of the model was not directly verified by the experiments. Instead, an interply bonding model similar to the one proposed by Mantell and Springer [49] was used to investigate the combined effect of intimate contact and autohesion. Lap shear test coupons were fabricated under three torch temperatures and four external forces. After taking into account the thermal degradation at the interface, corrected prediction agreed with the data.

2.3.2 Diffusion Bonding

There have been many attempts to model diffusion bonding of thermoplastic polymers [67-68]. Micro-mechanical models, including the widely accepted reptation theory are commonly based on the motion of molecular chains. However, in the current research, we focus mostly on the effects of variables on the property of diffusion bonding. It is our purpose to model and to correlate the experimental parameters to the interlaminar shear strength of composite laminate.

The strength of the autohesion bonding is generally described by the interface fracture property. Many investigators have shown that variables such as molecular weight, time, pressure, and temperature play decisive roles in governing the autohesion bonding developed in thermoplastic polymers [67-70]. It has been experimentally determined that the development of the interface fracture energy (G_{IC}) is inversely proportional to the molecular weight of the polymer and proportional to the square root of time [67]. Wool et al. [67] also concluded that the effect of pressure can be neglected once intimate contact has achieved 100 percent. As for the effect of temperature, higher temperature promoted diffusion bonding, thus shortening the required time to achieve complete bonding. However, it should be noted that too high a temperature may cause polymer degradation.

For on-line consolidation of semi-crystalline thermoplastic composites, the heating energy must be sufficient to raise the temperature in the interface well above the melting point. Therefore, it is reasonable to assume that diffusion bonding is complete as soon as the two molten surfaces are brought

into contact. Nevertheless, the validity of this assumption must be further investigated by related experiments.

2.3.3 Summary

Using squeezing flow between two parallel platens to describe the consolidation mechanism of thermoplastic composites under hot press has proven successful. Yet, the consolidation mechanism under compaction roller and mandrel has not been investigated thoroughly. Just by looking at the complexity of the geometry involved in on-line consolidation, one would expect the consolidation mechanism under a roller to be far different from the one under a hot press. For the tape laying and the filament winding processes which involved a roller and a flat platen, Mantell and Springer [49] proposed models to estimate the degree of intimate contact. However, their models requires isothermal conditions at towpreg and composite substrate which might not be valid under on-line consolidation conditions. Further investigations on non-isothermal consolidation mechanism are required. For the present study, micrographs taken at the cross-section of the composite cylinder are used to study the intimate contact under different filament winding conditions.

2.4 Formation Of Residual Stresses

The heterogeneous and anisotropic natures of composite materials offer the flexibility of tailoring the mechanical properties for a given application. However, this flexibility does come with a price. Different

properties of the constituent materials during processing may cause undesirable residual stresses. These process-induced residual stresses have been widely observed to reduce the performance of the composite. The interfacial micro-debonding and matrix crazing inside a lamina and the delamination in the laminate are attributed to the pre-existence of processed induced residual stresses. Therefore, it is important to study how to reduce or optimally to eliminate the residual stresses and consequently learn how to make better composite parts.

Minimization is not possible without knowing how the residual stresses have formed during processing. For convenience, the process-induced residual stresses are divided into micro, macro and global levels [71]. Though they occur simultaneously during processing, the mechanisms that cause these stresses are totally different. It is clear that differences in the thermal expansion coefficients and the discontinuity of elastic properties of the constituent materials cause the micro-residual stresses in laminae. For laminates, the macro-residual stresses are formed by the different elastic and thermal properties due to orientation of the plies. In addition, the various thermal gradients in the individual processes will introduce the global level of stresses.

In on-line consolidation of thermoplastic composites where rapid heating and cooling are required to instantaneously achieve intimate contact and bonding of the layer, transient thermal effects become the important factor of the formation of residual stresses. Therefore, in the present study,

we will focus mainly on the formation of global thermal stresses and investigate their effects on the quality of the consolidated parts.

3 On-Line Consolidation System Development

3.1 Introduction

To develop an on-line consolidation system is the most important task in the present study. In other words, we want to build the most concise system using minimal parts, yet still be able to demonstrate the feasibility of the concept, that is to produce quality thermoplastic composite cylinders without a post-consolidation process.

Through reviews on the existing design, we concluded that a successful on-line consolidation system should at least include a computer-controlled filament winding machine and a well designed consolidation head which houses a compaction roller and a hot-air heater. The basic apparatus as schematically illustrated in Figure 3.1, includes a towpreg delivery system, a computer-controlled filament winding machine and a thermoplastic consolidation head assembly. Figure 3.2 shows a photograph of the on-line consolidation system. The detail of each piece of equipment is discussed in the following sections.

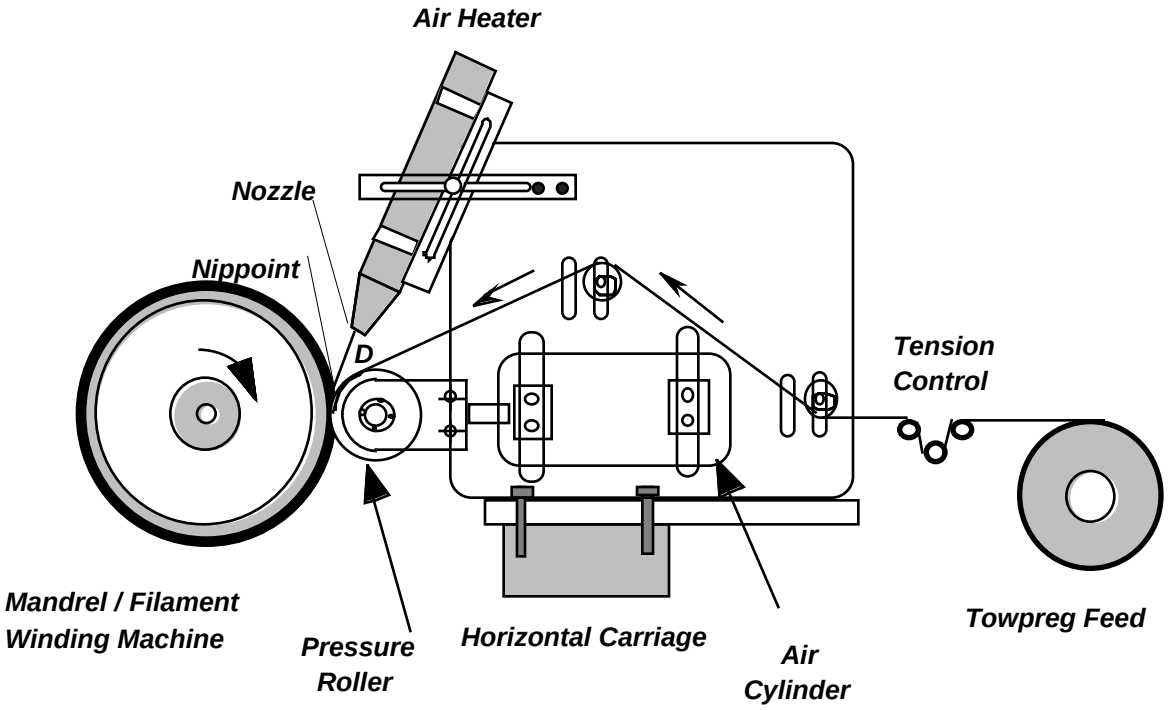

Figure 3.1 Illustration of the on-line consolidation system.

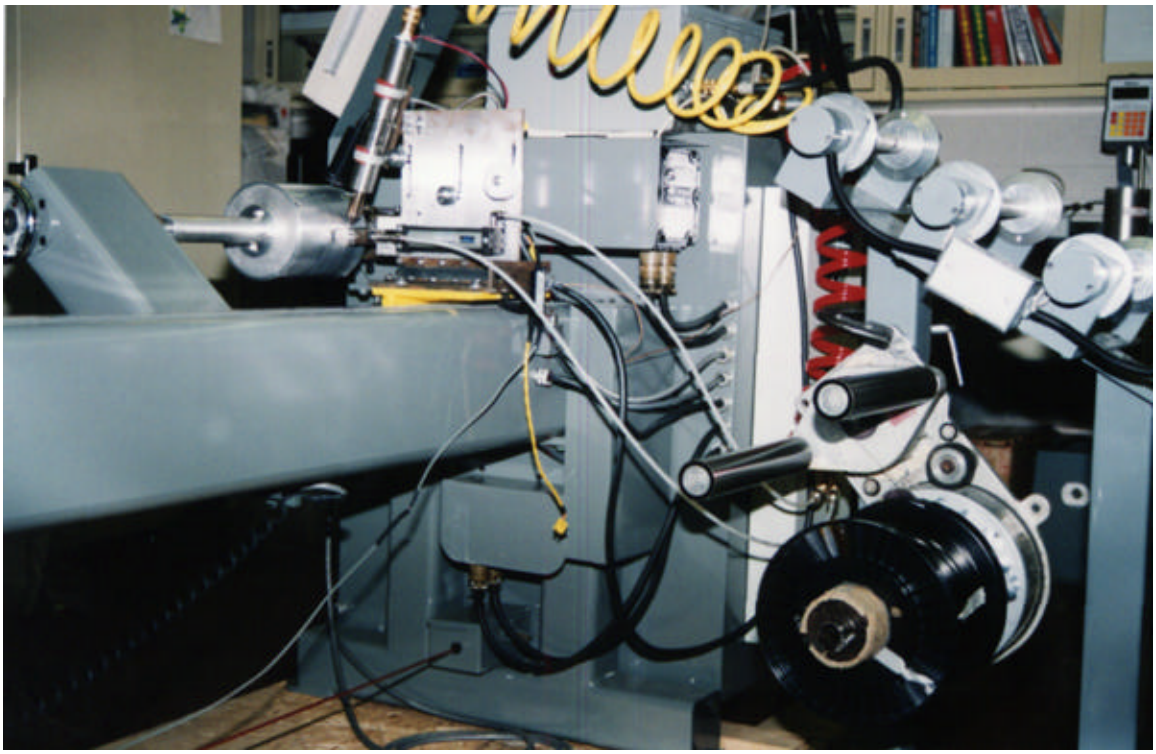

Figure 3.2 Photograph of the on-line consolidation system.

3.2 System Description

3.2.1 Towpreg Delivery System

The first step in the on-line consolidation process is to unwind the thermoplastic towpreg from the spool. The towpreg then passes through a tensioner which applies pre-selected back tension on the towpreg to ascertain a smooth, consistent delivery to the consolidation head assembly. It should be noted that the use of towpreg tension here is only for the purpose of material handling. We believe that there would be essentially no impact on the quality of resulting composite cylinders by changing the tension level. Therefore, a constant fiber tension of two and half pound will be used throughout the present study. A photograph of the towpreg delivery system is shown in Figure 3.3.

3.2.2 Consolidation Head Assembly

Compaction pressure and highly focused heat sources are the most significant ingredients required for making quality parts using the on-line consolidation technique. Pressure can be provided by a roller, contact shoe and/or fiber tension, while commonly used heat sources include hot-air torches, focused infrared spots, laser, direct electrical heating and ultrasonic energy [51, 62, 72]. Of the many possible combinations the most common one is that of a steel roller and a hot-air gun due to its low construction cost. Thus, it is adapted for the present study.

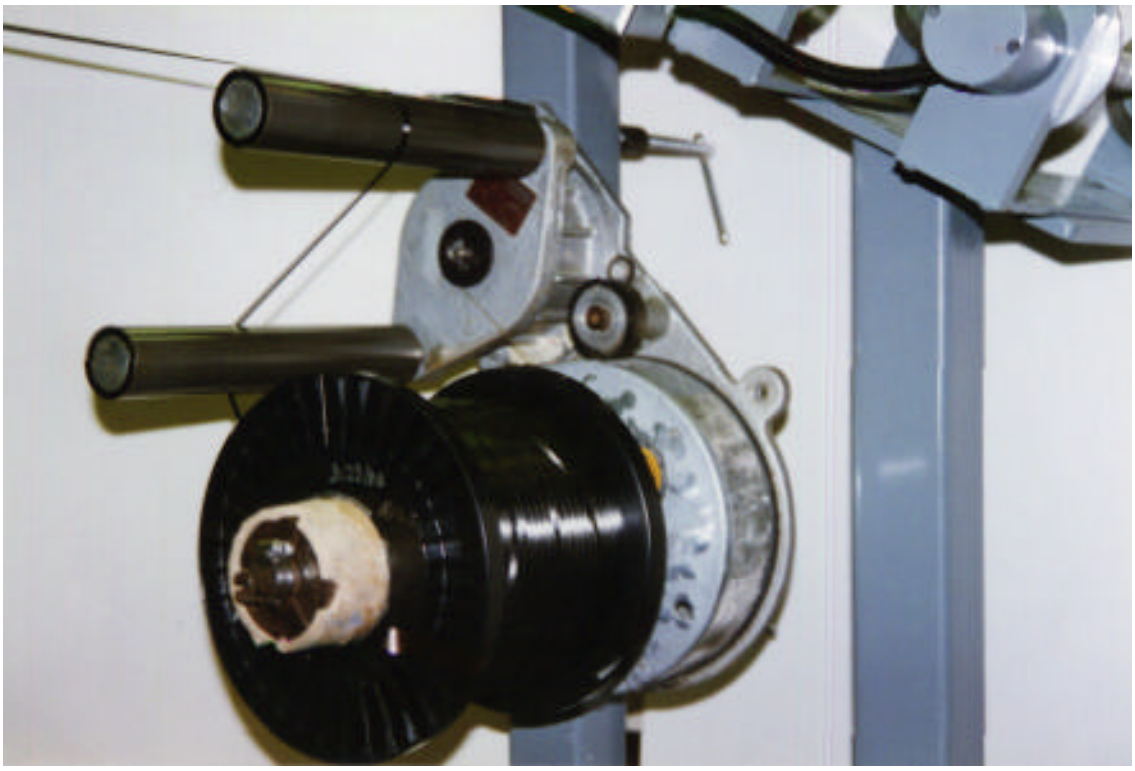

Figure 3.3 Photograph of the towpreg delivery system.

The consolidation head assembly is designed so that it can be easily mounted on the horizontal carriage of the filament winding machine. As shown in Figure 3.4, all components including air heater, pressure cylinder, compaction roller, and guiding rollers are installed on a simple T-shaped structure consisting of two perpendicular tool steel platens bolted together with reinforcing steel angles.

The Serpentine Heat Exchanger Type II by Osram Sylvania Inc. was chosen as the single heat source. It has a maximum operational temperature of 870°C (1600°F) which will ensure melt of the thermoplastic resin towpreg. The control of temperature is via a temperature controller also by Osram Sylvania Inc. The temperature controller, pressure gauges, and adjusting knobs are integrated into a metallic chassis sitting on top of the winding machine console for ease of access during operation.

The 25.4 mm (1 in) O.D. steel compaction roller and its holder were manufactured in the ESM machine shop. The assembly was then mounted on a small bore pneumatic cylinder. The cylinder can operate on compressed air pressure up to 1034.3 kPa (150 psi). With a force factor of 442.2 Newtons (99.4 lbs) per 689.5 kPa (100 psi) air pressure, the cylinder will provide sufficient compaction on the incoming towpreg

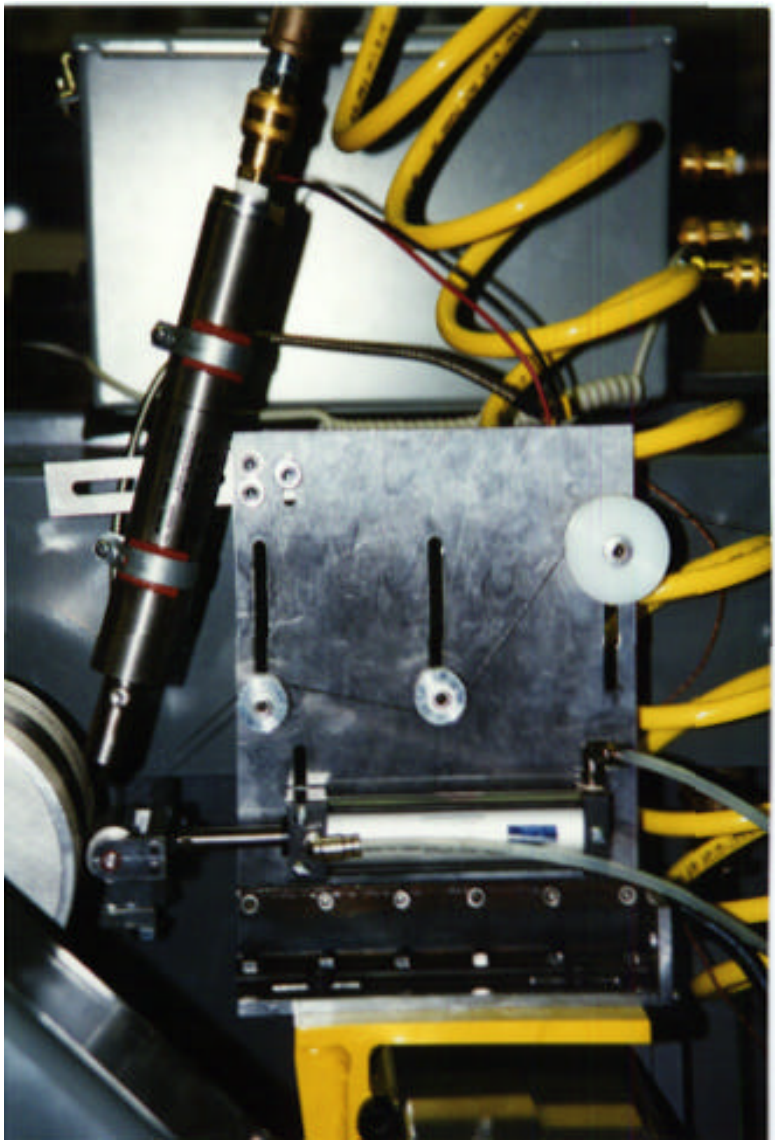

Figure 3.4 Photograph of the on-line consolidation head assembly.

3.2.3 Computer-Controlled Filament Winding Machine

The model ULD computer-controlled filament winding machine from Composite Machines Company (CMC) was purchased for the present study. This "laboratory-sized" filament winder is capable of controlling dual-axis motion, namely spindle rotation and linear carriage motion, via the CMC machine control system. The control system uses a programmable multi-axis controller (PMAC) card made by Delta Tau Data Systems. The PMAC card accepts output from the feedback encoders and produces an analog signal for driving the motor controller. A 486 based personal computer (PC) is used to provide supervisory control, to display information, and to store and load the machine's motion and control program. This particular winder can wind objects 12 inches in diameter and 72 inches in length using both wet winding and tape winding techniques. A photograph of the filament winding machine is given in Figure 3.5. Winding patterns for symmetric shapes and for some non-symmetric shapes such as elbows are generated off-line by CADWIND™ pattern generation software.

3.3 Manufacturing Composite Cylinders

The present on-line consolidation system, described above, is used to manufacture composite cylinders from commercial thermoplastic towpreg. In this section we discuss the selection of material systems, mandrel construction, winding pattern generation, and finally the procedure of the actual winding process.

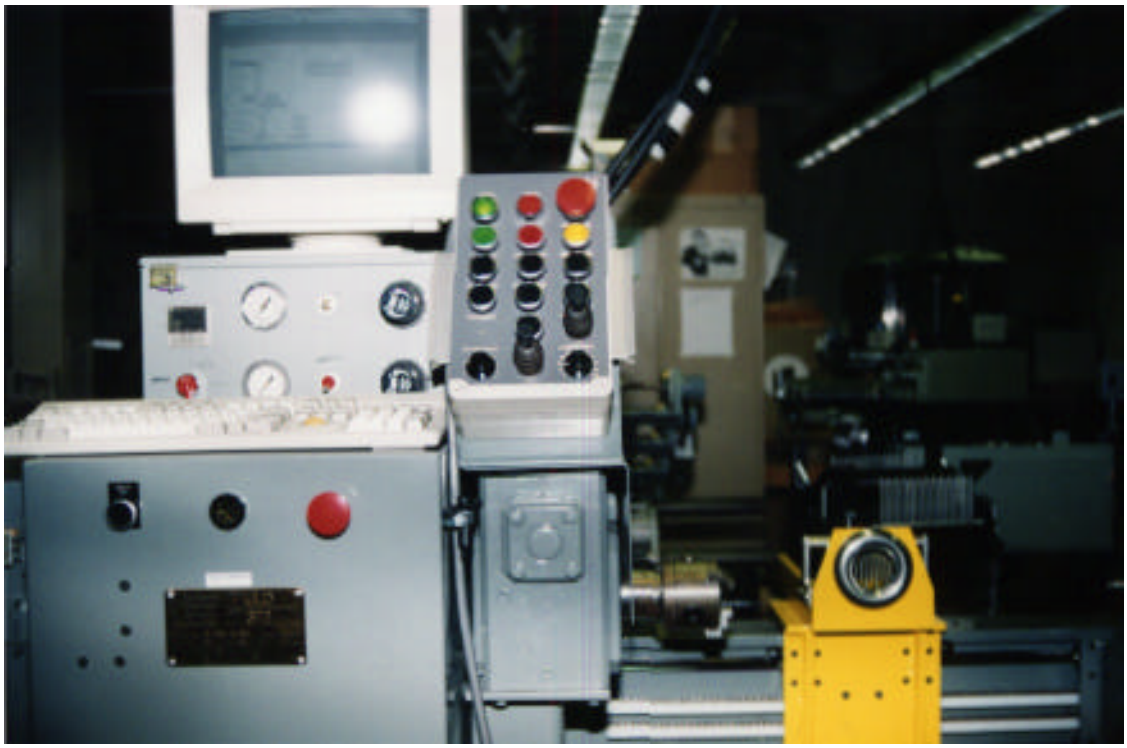

Figure 3.5 Photograph of the filament winding machine.

3.3.1 Selection of Material Systems

Fiber reinforced semi-crystalline thermoplastic composites have been utilized in many applications due to their superior mechanical properties and fracture toughness. The most commonly used thermoplastic systems include Polyphenylene Sulfide (PPS) developed by Phillips Petroleum, Polyether-etherketon (PEEK) developed by ICI and Polyether-keton-keton (PEKK) developed by DuPont. At present, we use 6.35 mm wide APC-2 towpreg (carbon fiber and PEEK) from Fiberite, Inc.

As we examine the surfaces of the towpreg visually, different roughness are observed on the two sides. The difference may result from the prepregging process where only one surface was in contact with the impregnation roller. This observation was later verified by the Environment Scanning Electron Micrographs (ESEM). On the smooth side, individual carbon fiber is clearly observed and only very little resin is found, as shown in Figure 3.6. On the rough side, the resin distribution is uneven. Figure 3.7(a) shows a resin rich area while we find only a thin layer of resin stretching across a few fibers in Figure 3.7(b).

Based on the observations, the topology of the towpreg might have an impact on the quality of consolidated parts. For the present study, the hot-air heater is directed at the rough surface of the towpreg since it is easier to melt the resin rich surface of the towpreg.

(a)

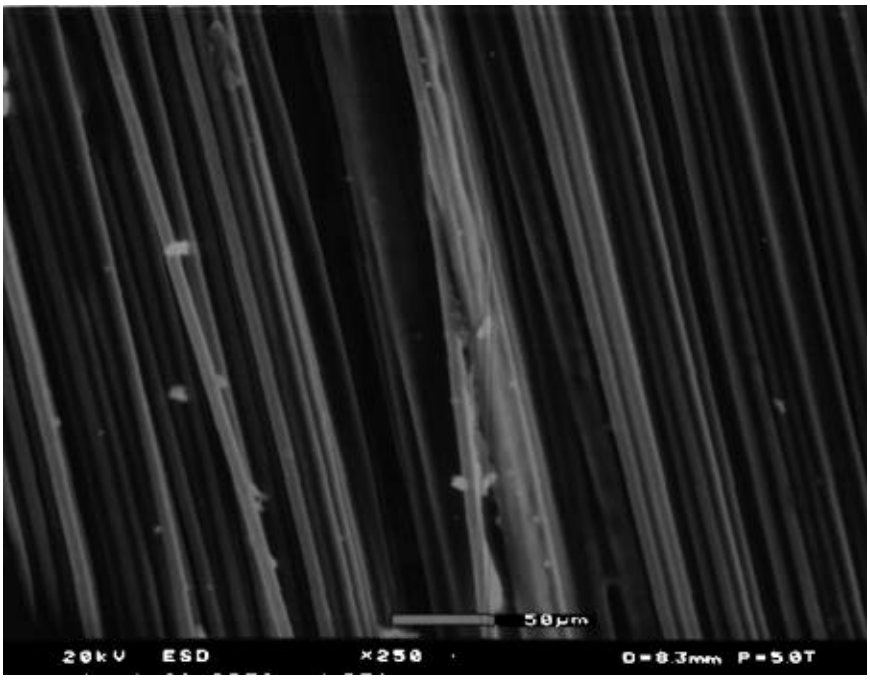

(b)

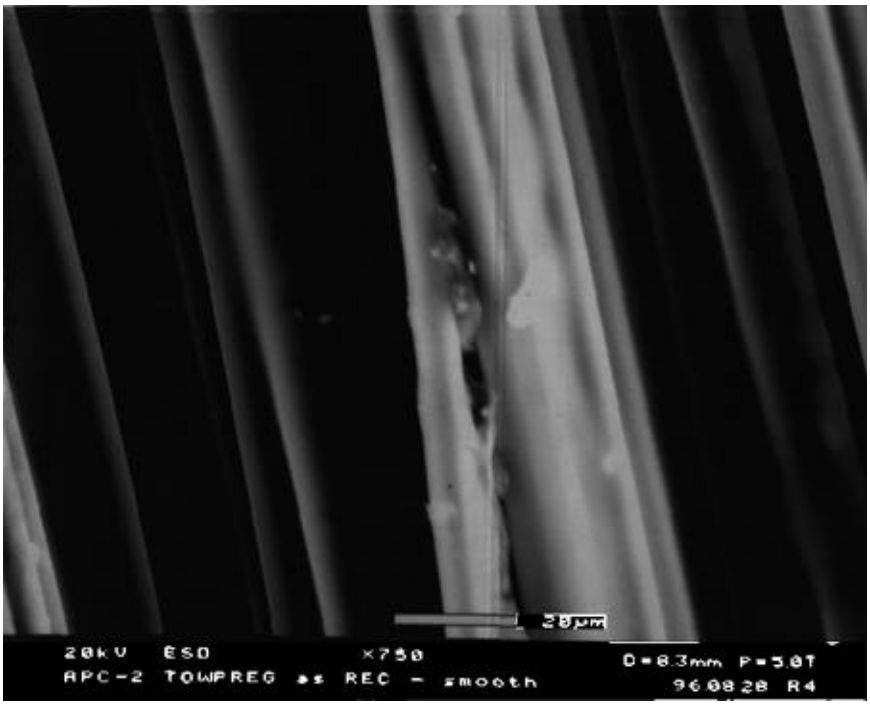

Figure 3.6 Environment Scanning Electron Micrographs on the "smooth" surface of the APC-2 towpreg.

(a)

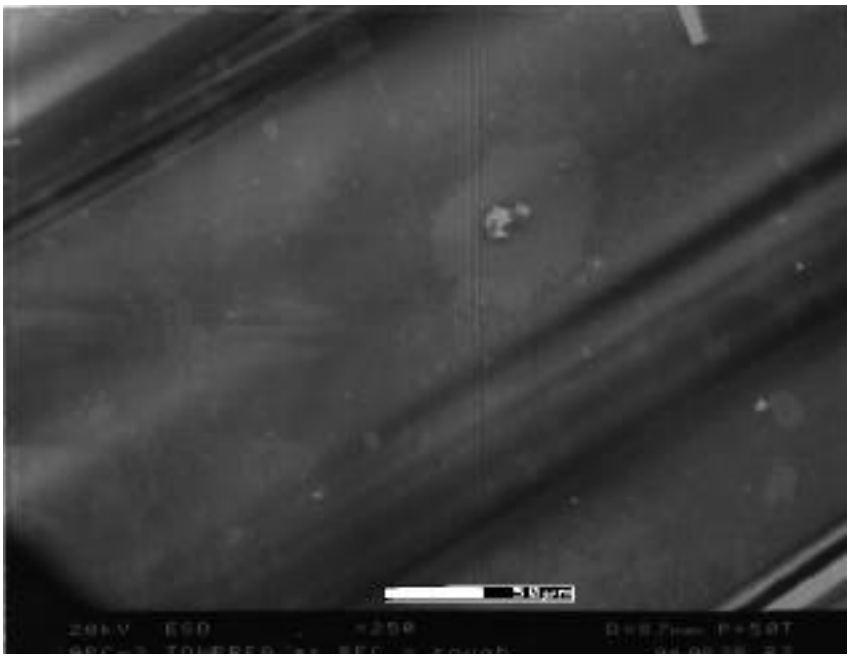

(b)

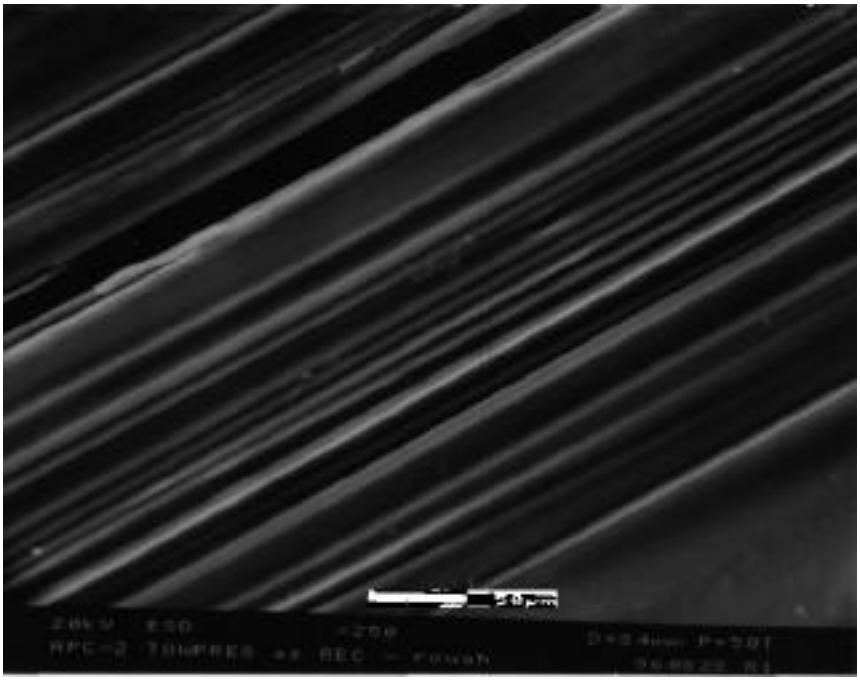

Figure 3.7 Environment Scanning Electron Micrographs on the "rough" surface of the APC-2 towpreg. (a) resin rich, (b) thin layer of resin.

3.3.2 Mandrel Assembly

The aluminum mandrel assembly consists of a 6.35 mm thick hollow circular tube, two circular platens and a pair of shafts for attaching the mandrel onto the winding machine. The mandrel is 152.4 mm (6 in) long and 146 mm (5.75 in) in diameter. The circular platens are bolted onto both ends of the cylinder and the shafts are screwed into the circular platens.

3.3.3 Winding Pattern Generation

Although the computer controlled winder is capable of winding complicated shapes and close-end bottles, only circular cylinders will be produced and tested throughout this work. After the desired winding pattern is generated, displayed, and checked in real-time on the computer screen, it is then converted to the control code listed in Figure 3.8 for the winding machine. The control code shows the machine position for an entire winding process. The X-variable indicates the horizontal movement of the carriage and the A-variable indicates mandrel rotation. It is also noted that the Q variables, Q97 and Q98, are used as the limit and counter, respectively. That is, for a 26 layer composite cylinder, the program must loop 13 times. For every loop the towpreg will cover the surface twice. Figure 3.9 shows a typical computer generated pattern for hoop-wound cylinder.

3.3.4 Winding Procedure

The towpreg was unwound from the spool mounted on the tensioner, then passed through the guide rollers, and secured by heat-resistant tape onto

the mandrel surface. Since we want the towpreg to absorb as much energy from the hot-air heater as possible, a large angle between towpreg and heater is preferred. Therefore, the passage of the towpreg through the guide rollers given previously in Figure 3.4 was changed to that shown in Figure 3.10. It should be noted again that the hot-air heater is aimed at the rough surface of the towpreg for all cylinders.

To set the air temperature and roller pressure, we simply adjust the knobs on the control box. The winding speed is adjusted from the control panel. After the set temperature is stabilized, the winding program that was loaded onto the computer earlier is started by hitting the start button in the control panel. After this, all the winding is automatic. The last thing is to cut the towpreg when the cylinder is completed. Figure 3.11 shows a consolidated cylinder and a composite ring.

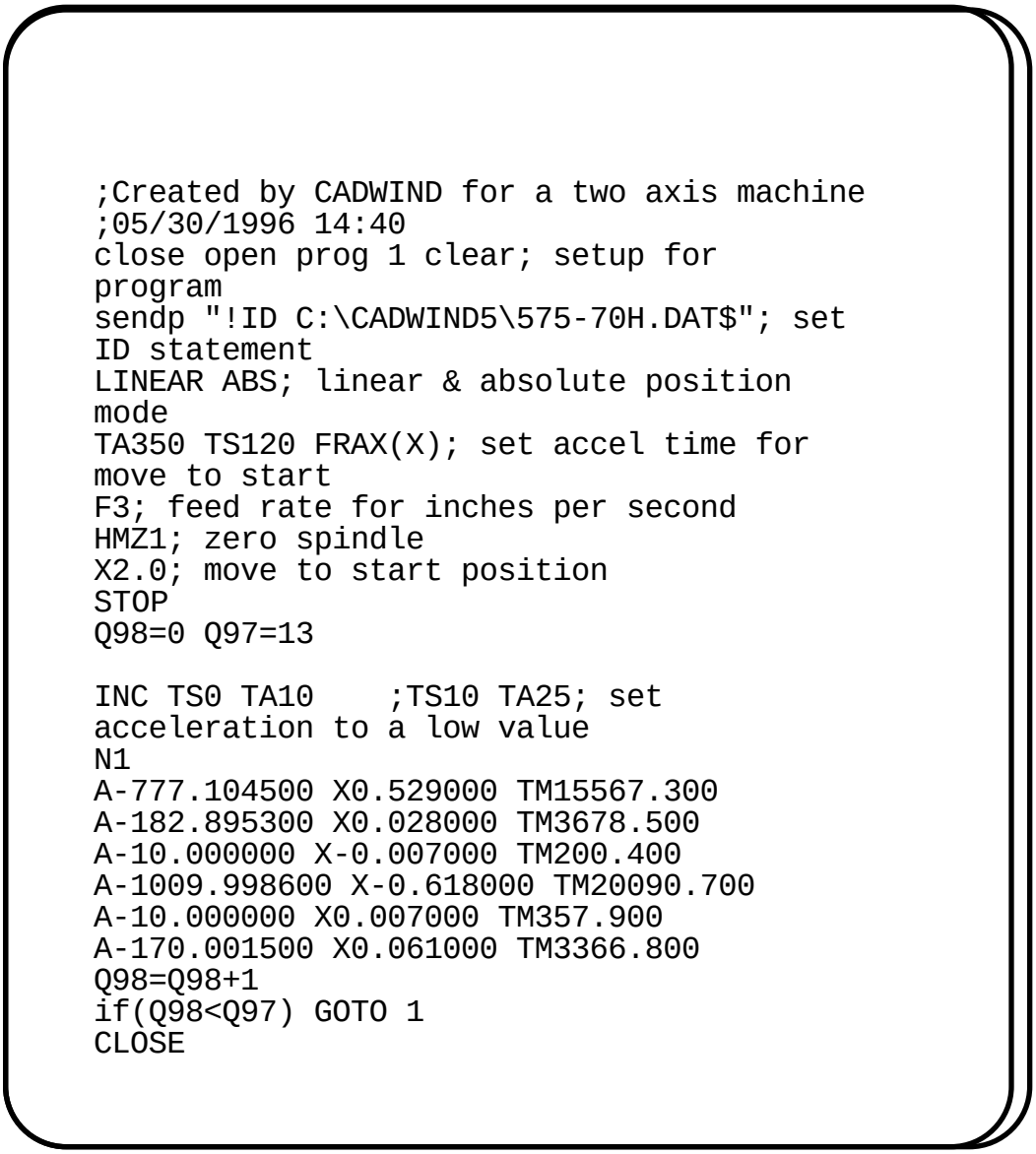

```
;Created by CADWIND for a two axis machine
;05/30/1996 14:40
close open prog 1 clear; setup for
program
sendp "!ID C:\CADWIND5\575-70H.DAT$"; set
ID statement
LINEAR ABS; linear & absolute position
mode
TA350 TS120 FRAX(X); set accel time for
move to start
F3; feed rate for inches per second
HMZ1; zero spindle
X2.0; move to start position
STOP
Q98=0 Q97=13

INC TS0 TA10    ;TS10 TA25; set
acceleration to a low value
N1
A-777.104500 X0.529000 TM15567.300
A-182.895300 X0.028000 TM3678.500
A-10.000000 X-0.007000 TM200.400
A-1009.998600 X-0.618000 TM20090.700
A-10.000000 X0.007000 TM357.900
A-170.001500 X0.061000 TM3366.800
Q98=Q98+1
if(Q98<Q97) GOTO 1
CLOSE
```

Figure 3.8 List of control code for filament winding machine.

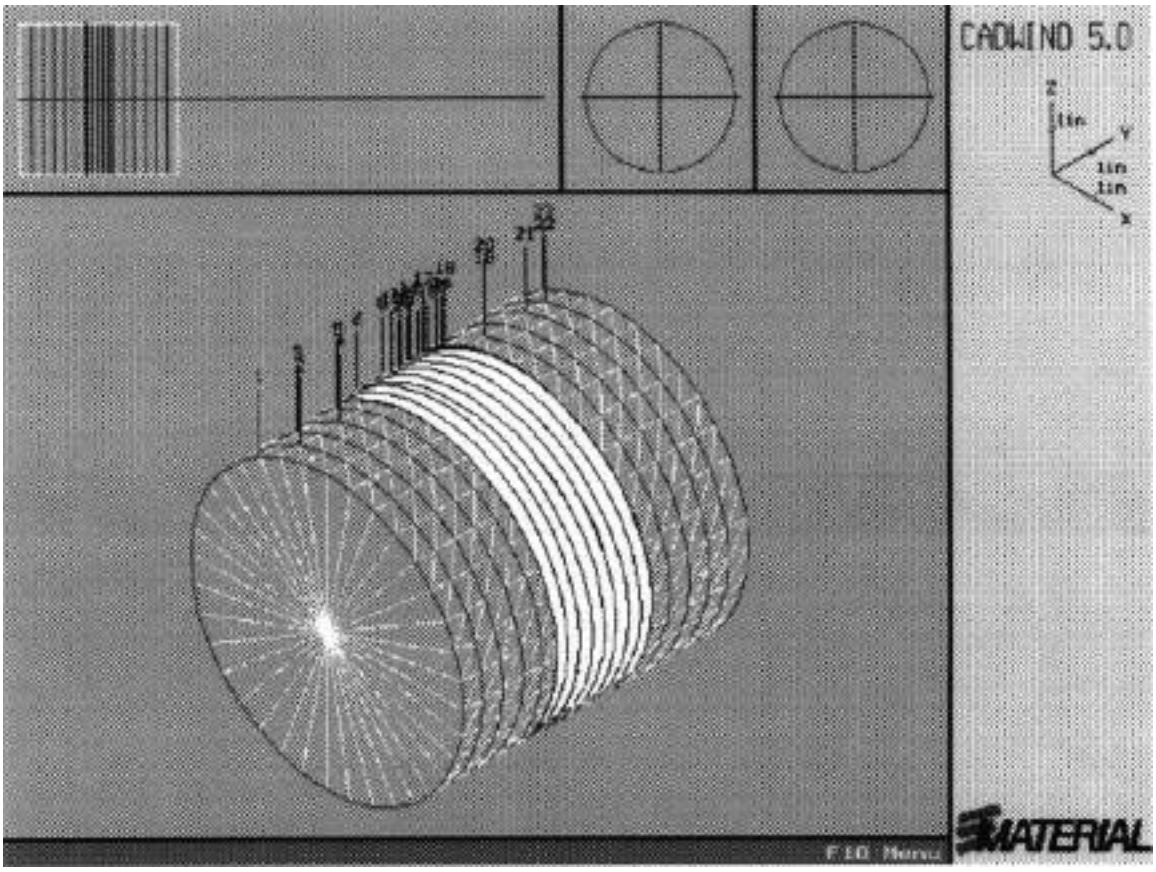

Figure 3.9 Computer generated pattern for hoop-wound cylinder.

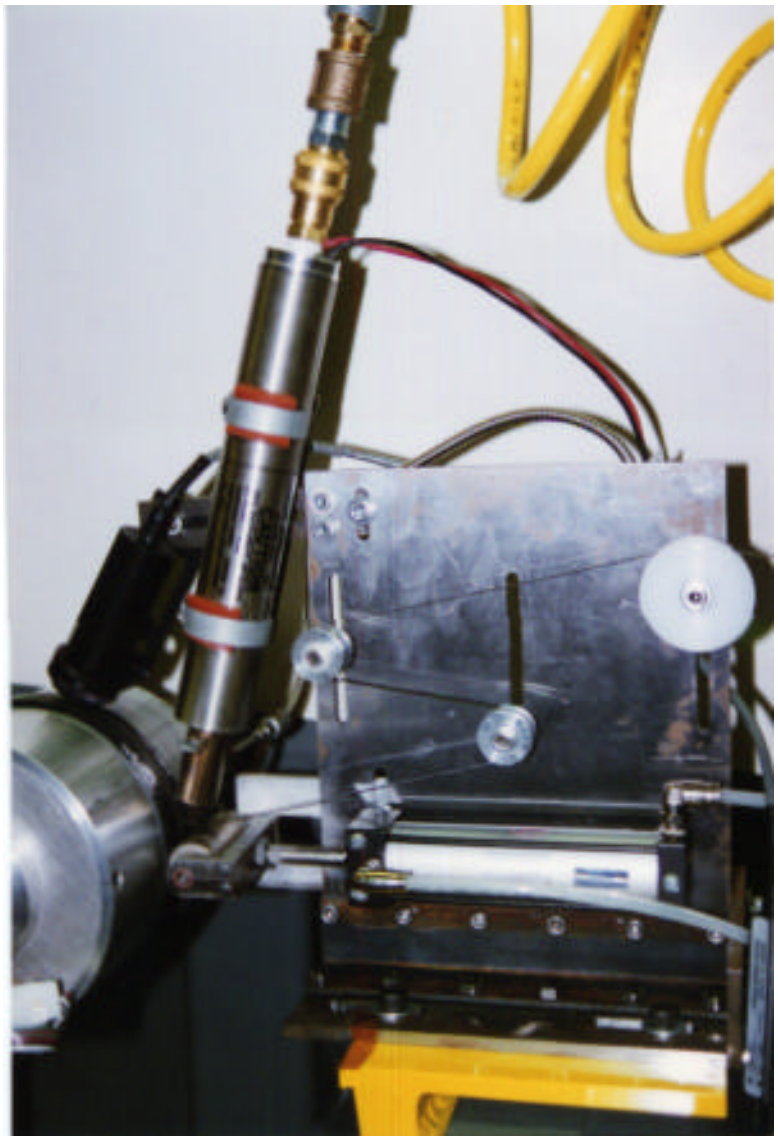

Figure 3.10 Modified passage of the towpreg through guiding roller.

Figure 3.11 Photograph of a consolidated cylinder and a composite ring.

3.4 Mechanical and Physical Tests

As stated previously, one objective of this study is to test whether or not the quality of the composite cylinders made by the on-line consolidation system can compete with the quality of those made by conventional hot press consolidation. Therefore, emphasis should be placed on mechanical properties resulting directly from the manufacturing process such as interlaminar shear strength (ILSS), and not on the material properties themselves. In addition to mechanical testing, it is equally important to determine the overall quality. Next, we'll discuss the specimen preparation and general procedures for quality evaluation and mechanical testing.

Once the composite cylinders have been produced their thickness was measured, recorded at twenty different locations around the circumference, and then the composite cylinders were sent to the machine shop to trim off rough edges. After the composite cylinders were cleaned and marked, they were again sent back into the machine shop for fabricating test coupons. First, a 6.35 mm (quarter-inch) wide ring was cut out from the center portion of the cylinder. Second, a thin diamond cutter was used to cut open the ring and the opening dimension was then recorded. Different displacements indicate that the process-induced residual stresses might have varied due to different processing conditions. Third, fifteen coupons were machined and ground to conform to the dimensional requirements as described in ASTM standard D2344-84 and as shown in Figure 3.12.

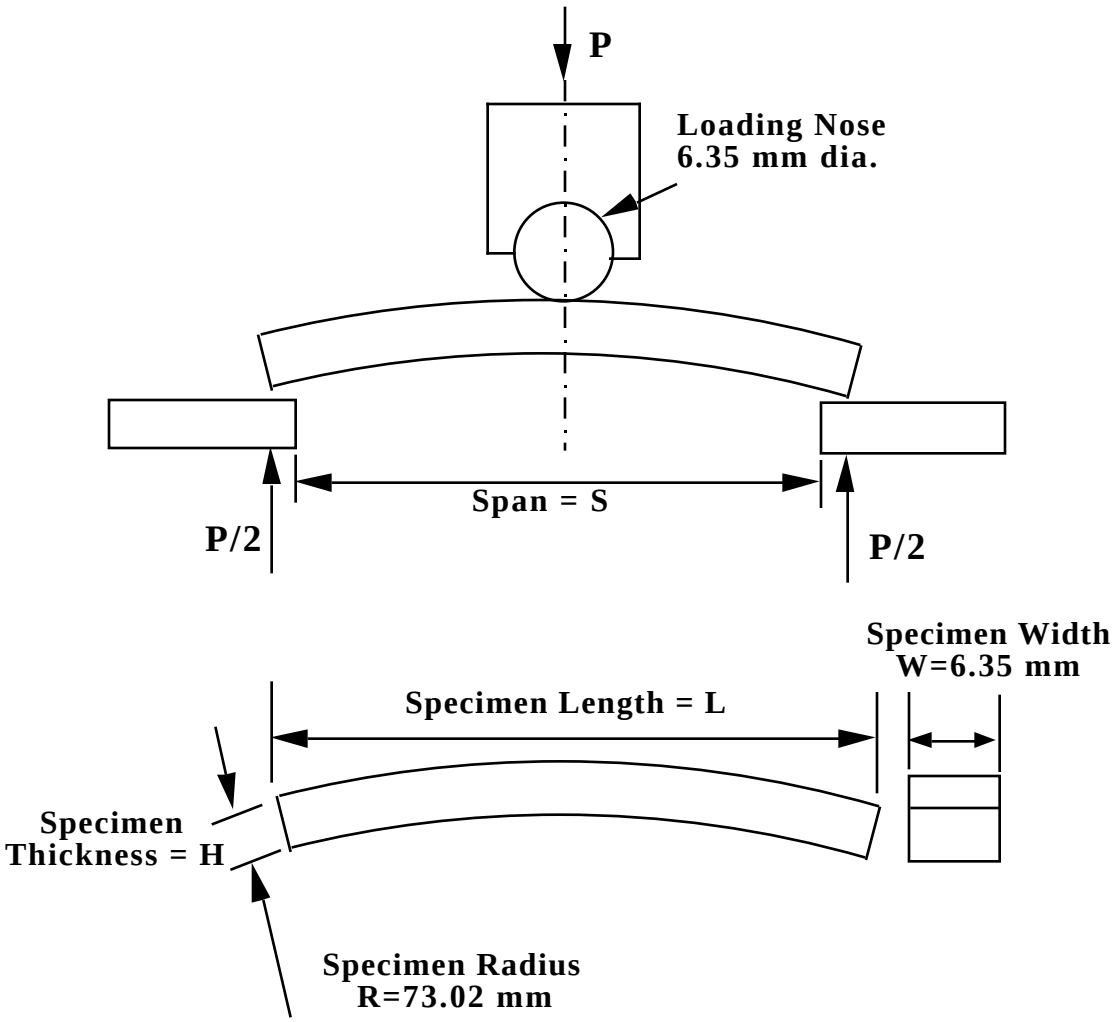

Figure 3.12 Apparent interlaminar shear strength test standard

It should be noted that the length-to-thickness ratio of five was taken for each cylinder to ensure the occurrence of shear failure, since, when incorrect length-to-thickness ratio is chosen, the specimens do not always fail in shear mode.

During the mechanical testing, the crosshead speed was 1.27 mm per minute. The load applied on the specimen was recorded twice every second and displayed on the computer screen. Figure 3.13 shows the INSTRON testing machine and the fixture for interlaminar shear test. As observed by sharp audible reports during tests as well as by the first drop in load in the load-displacement curve, it is noted that noncatastrophic cracking initiated before the final failure was reached. For a designer, the point at which crack initiates is much more important than the shear strength itself. However, for the calculation of apparent interlaminar shear strength, maximum load alone is used. The equation for calculating the apparent shear strength is given as follows:

$$S_H = 0.75\ P_B / b\ d \tag{3.1}$$

where:

S_H = shear strength, (MPa),

P_B = maximum load, (N),

b = width of specimen, (mm), and

d = thickness of specimen, (mm).

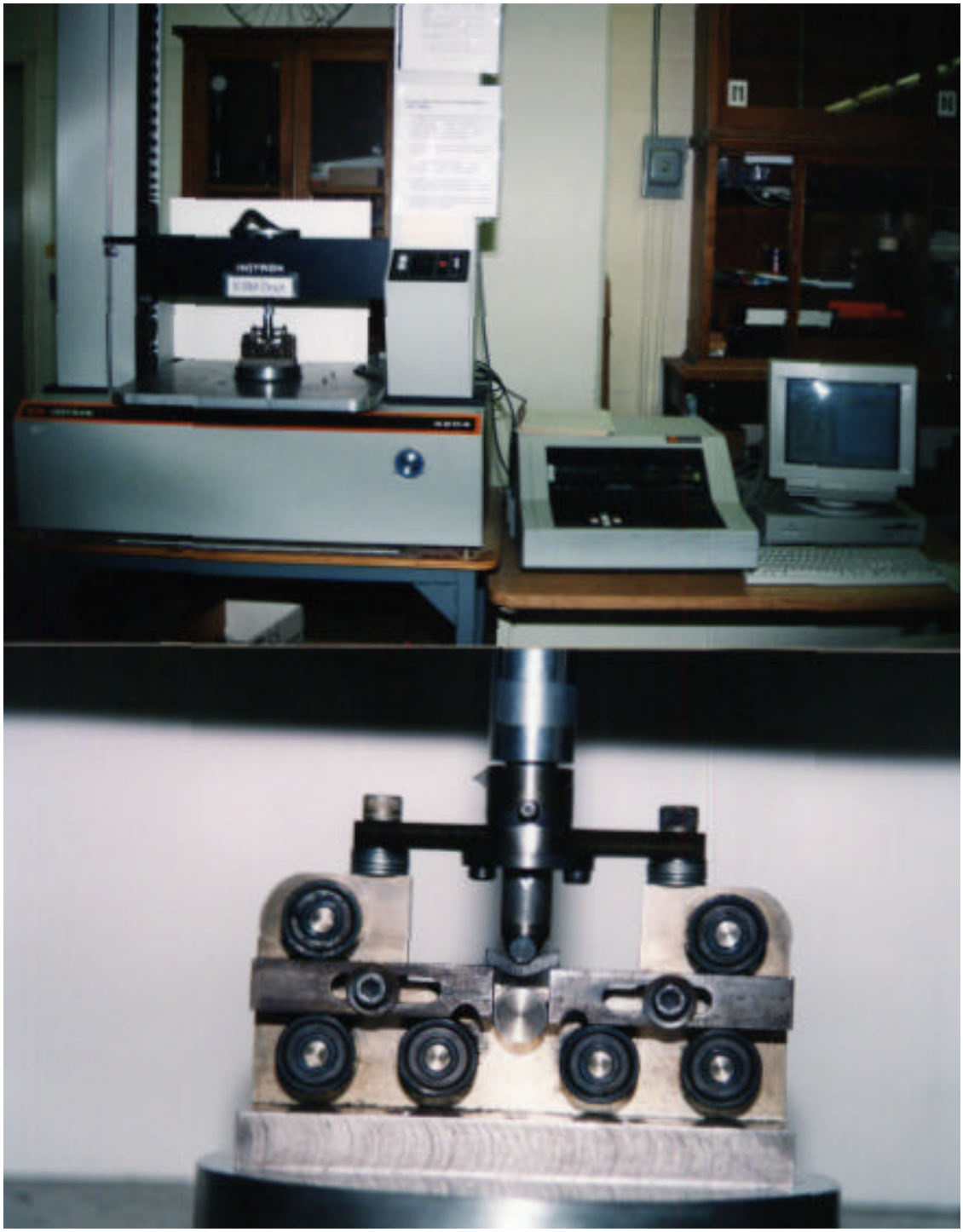

Figure 3.13 INSTRON testing machine and fixture for interlaminar shear strength test.

To gauge the overall quality, density and void content tests were performed on all composite cylinders. The density measurements followed ASTM standard D792-91. Each specimen was hand sanded to remove rough edges caused by cutting. The specimens were then weighed in air (dry) and in isopropyl alcohol (IPA). The density of the composite can be obtained by

$$\textit{CompositeDensity}\ (C_D) = W_1 \times \textit{IPA Density} \Big/ (W_1 - W_2) \tag{3.2}$$

where W_1 is the initial dry weight of specimen and W_2 is the weight of the sample immersed in IPA.

It is well known that the void content of a composite may significantly affect its mechanical properties and therefore it is an important indicator for composite quality. However, to determine the void content of a semi-crystalline thermoplastic composite such as APC-2 is no easy task, because the level of crystallinity that results from different processing conditions causes variation in the resin density and thus variation in composite density. Although differential scanning calorimetry (DSC) can measure the actual degree of crystallinity, DSC does require the fiber and resin weight fraction which is affected as well by void content. Ideally, the resin and fiber content should be determined by ASTM standard D3171-76 using matrix digestion. Unfortunately, we cannot safely conduct this test in our laboratory due to a lack of training in handling concentrated nitric acid and of the equipment required to perform the standard test. Nevertheless, in order to obtain theoretical density of a thermoplastic composite, we assumed the degree of crystallinity to be 30% based on the DSC data from all consolidated cylinders

fabricated during the present study. The resin density can be obtained approximately by

$$\rho_r = \nu_{Am}\rho_{Am} + \nu_{Cr}\rho_{Cr} \tag{3.3}$$

where:

ρ_r = density of resin, g/cm^3,

ν_{Am} = volume fraction of amorphous resin, volume percent,

ρ_{Am} = density of amorphous resin, g/cm^3,

ν_{Cr} = volume fraction of crystalline, resin volume percent, and

ρ_{Cr} = density of crystalline resin, g/cm^3.

The calculation of theoretical density of the composite is as follows:

$$\boldsymbol{T_d} = \nu_f\rho_f + \nu_r\rho_r \tag{3.4}$$

where:

$\boldsymbol{T_d}$ = theoretical density of a void-free composite, g/cm^3,

ν_f = fiber volume fraction, volume percent,

ρ_f = density of reinforcement, g/cm^3, and

ν_r = resin volume fraction, volume percent.

Finally, the void content of a composite, based on ASTM standard D2734-91, was calculated as follows:

$$\boldsymbol{V = 100(T_d - M_d)/T_d} \tag{3.5}$$

where:

$\boldsymbol{V}$ = void content, volume percent, and

$\boldsymbol{M_d}$ = measured composite density.

3.5 Summary

The on-line consolidation system, consisting of a filament winding machine and consolidation head assembly, has been designed, constructed, and installed in Hancock Hall at Virginia Tech. The successful completion of the facility allows us to intensively investigate the feasibility of this relatively new manufacturing technique for thermoplastic composites. Although we had designed the on-line consolidation system with simplification in mind, there still are five controllable processing parameters involved in the system, namely the heater temperature, heater air flow rate, mandrel speed, roller pressure, and distance between nozzle and nippoint. Therefore, systematic evaluation of the processing parameters becomes inevitable. The following chapter addresses this issue.

4 Statistical Investigation of the Processing Window for the On-Line Consolidation System

4.1 Introduction

The motivation for using the statistical method was to study the impact of individual processing parameters and to establish the processing window for a given material system. In contrast to randomly selected processing conditions or to conducting one-factor-at-a-time studies, a carefully planned experimental design for studying the impact of all variables and their interactions will be more cost-effective [73].

In this chapter, all processing parameters involved in the on-line consolidation system described in Chapter 3 are discussed. Two statistical experimental designs are applied to characterize the processing window for the present design. The first set of experiments, a three-factor Box-Behnken design, focuses on determining the nippoint temperature and then a two-factor central composite design places special emphasis on the impact of winding speed and nippoint temperature on the composite quality.

Interlaminar shear strength and void content of the consolidated parts are adapted as the key quality indicators. Finally, a processing widow is constructed for the present system design and important observations are summarized.

4.2 Processing Parameters

In the present design, there are five separately controllable parameters involved in the system namely, winding speed, pressure of compact roller, nozzle temperature, distance between nozzle and nippoint, and air pressure for the heater. The preliminary observations and physical limitations on the processing parameters are as follows:

- Air pressure for the heater can be varied from 0 kPa (0 psi) to about 103 kPa (15 psi). The higher the air pressure, the more air flows through the heater. While the heater will burn out in a short period of time when no air passes through the coils, the life of the heater will also be shortened drastically if air pressure exceeds the manufacturer's recommended 55.2 kPa (8 psi). To prevent burning of the electrical coils inside the air heater, a pressure switch was installed. This device ensures that the heater will not be turned on accidentally without sufficient airflow.

- The distance between the nozzle and the nippoint as shown in Figure 3.1, can be changed freely. However, in general, longer distances yield lower nippoint temperatures and larger heating areas. The profile of the nozzle also plays an important role in determining the heating area. The nozzle

that came directly from the heater manufacturer has a round opening of merely 3.175 mm (1/8 in) in diameter. Therefore, an important guideline for choosing the distance between the nozzle and nippoint is that it should be long enough to cover the entire width of the towpreg, i.e. 6.35 mm (1/4 in).

- Nozzle temperature is controlled by a PID temperature controller and can go as high as 760°C (1400°F) with less than a 1 percent margin of error.

- Since the compressed air for the pneumatic cylinder comes through an in-wall outlet in our laboratory, we are limited on the maximum pressure of the compressed air available through the building. Fortunately, the pressure required to consolidate the molten towpreg is far less than that needed in hot-press consolidation. Throughout the initial winding stage, air pressures for the compact roller ranging from 207 kPa (30 psi) to about 414 kPa (60 psi) were found to be sufficient.

- Through the control panel, winding speed can be easily adjusted from 0 to 100 percent of the full winding capacity. However, since the winding speed for on-line consolidation requires that the winder operate at lower end of the machine capacity where the winding speed cannot be accurately controlled. Thus, the time needed for the entire winding process is recorded and used to calculate the actual winding speed.

Observations from initial experiments showed that the nippoint temperature can be several hundred degrees Celsius lower than the nozzle temperature and is very sensitive to the following three system parameters:

nozzle temperature, air flow rate in heater and distance between nippoint and nozzle. Meanwhile, we found that using nippoint temperature to construct the processing window has two major advantages. First, it is more realistic since nippoint temperature is the actual temperature that the towpregs are subjected to. Second, it is more concise because, by using nippoint temperature to represent three of the system parameters, the system parameters are simplified from five down to three, i.e. winding speed, roller pressure, and actual nippoint temperature.

In the following sections, we investigate the impact that air flow rate, distance between nozzle and nippoint, and nozzle temperature have on the actual nippoint temperature using a three-factor Box-Behnken design. Then a central composite design is applied to study the processing window for the present on-line consolidation system.

4.3 Study of Nippoint Temperature

As stated previously, actual nippoint temperature can vary due to the selected nozzle temperature, air flow rate, and distance between nozzle and nippoint. In order to investigate individual impact of these three parameters and their interaction on the nippoint temperature, a three-factor, Box-Behnken design is conducted. There are fifteen possible factor-level combinations in this experimental design. The three-factor Box-Behnken design is shown in Figure 4.1 and a randomized design is given in Table 4.1.

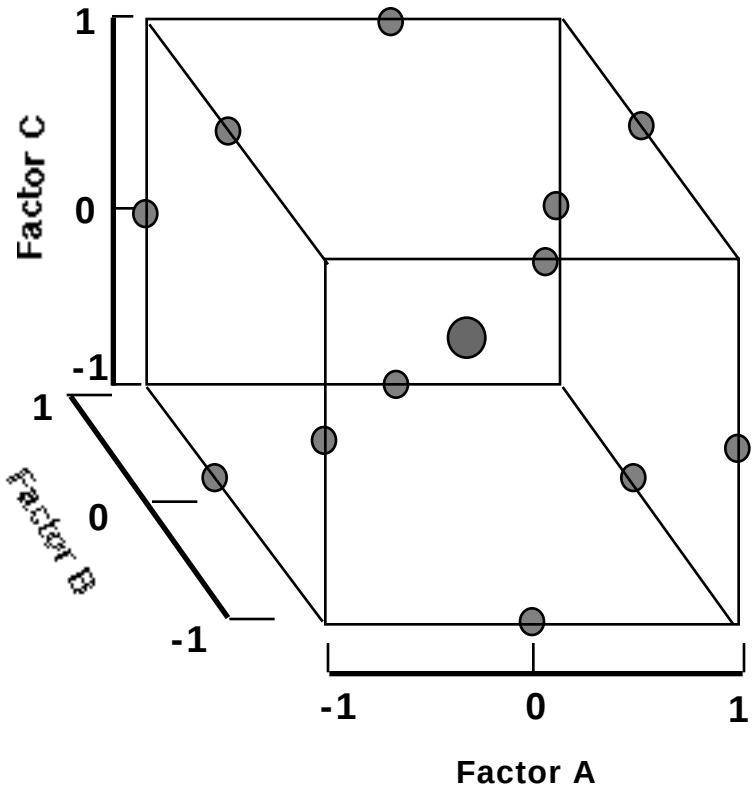

Figure 4.1 The three-factor Box-Behnken design.

Table 4.1 Randomized testing sequence of the three-factor Box-Behnken design.

Run	Distance	Air Pressure	Nozzle Temperature
1	0	0	0
2	+	+	0
3	+	0	+
4	0	0	0
5	0	+	-
6	0	-	+
7	0	-	-
8	-	0	+
9	-	+	0
10	-	-	0
11	+	-	0
12	0	+	+
13	0	0	0
14	-	0	-
15	+	0	-

The high (+), midpoint (0), and low (-) value represent the experimental variables and are listed as the following:

- Distance between nozzle to nippoint varies from 12.7 mm (0.5 in), 19.1 mm (0.75 in) to 25.4 mm (1.0 in),
- Air pressure is from 27.6 kPa (4 psi), 55.2 kPa (8 psi) and 82.7 kPa (12 psi), and
- Nozzle temperature of hot air heater is set at 538°C (1000°F), 593°C (1100°F) and 649°C (1200°F).

The nippoint temperature was measured by a K-type, air-probe thermocouple for each factor-level combination. The experimental results are shown in Table 4.2.

Now, more in-depth analysis is required to further interpret the results. First of all, the response, i.e. nippoint temperature, is written as

$$Y = b_0 + b_1 D + b_2 P + b_3 T + b_4 D^2 + b_5 P^2 + b_6 T^2 + b_7 DP + b_8 PT + b_9 TD \quad (4.1)$$

where D is the distance from nozzle to nippoint, P is the heater air pressure, and T is nozzle temperature.

The coefficients, $b_0 - b_9$, are calculated from a second-order linear regression analysis for three independent variables and are given in Table 4.3.

Since the calculated nippoint temperature is used to represent three system parameters in the following section, we have to verify how well the predictions from the statistical model compare to the data. We randomly

Table 4.2 Experimental results of the three-factor Box-Behnken design.

Run	Distance mm (inch)	Air Pressure kPa (psi)	Nozzle Temperature °C (°F)	Nippoint Temperature °C (°F)
1	19.1 (0.75)	55.2 (8)	593 (1100)	**490 (914.2)**
2	25.4 (1.0)	82.7 (12)	593 (1100)	**440 (824.0)**
3	25.4 (1.0)	55.2 (8)	649 (1200)	**419 (915.0)**
4	19.1 (0.75)	55.2 (8)	593 (1100)	**485 (904.7)**
5	19.1 (0.75)	82.7 (12)	538 (1000)	**423 (794.2)**
6	19.1 (0.75)	27.6 (4)	649 (1200)	**555 (1031.4)**
7	19.1 (0.75)	27.6 (4)	538 (1000)	**459 (858.2)**
8	12.7 (0.5)	55.2 (8)	649 (1200)	**597 (1107.2)**
9	12.7 (0.5)	82.7 (12)	593 (1100)	**511 (952.5)**
10	12.7 (0.5)	27.6 (4)	593 (1100)	**517 (962.4)**
11	25.4 (1.0)	27.6 (4)	593 (1100)	**444 (831.2)**
12	19.1 (0.75)	82.7 (12)	649 (1200)	**530 (985.2)**
13	19.1 (0.75)	55.2 (8)	593 (1100)	**488 (910.5)**
14	12.7 (0.5)	55.2 (8)	538 (1000)	**449 (840.4)**
15	25.4 (1.0)	55.2 (8)	538 (1000)	**401 (754.0)**

Table 4.3 Regression analysis coefficient.

b_0	***Constant***	138.14
b_1	***D***	26.682
b_2	***P***	-1.151
b_3	***T***	-0.3427
b_4	***D x D***	-0.209
b_5	***P x P***	-0.002
b_6	***T x T***	0.0017
b_7	***D x P***	0.002
b_8	***D x T***	-0.0417
b_9	***P x T***	0.0016

choose different combinations of parameters over the entire domain and measure the nippoint temperature for each case. The overall deviations between the predictions from statistical model and the measured nippoint temperatures were less than three percents. Figure 4.2 shows the results with a distance between nippoint and nozzle equal to 12.7 mm (0.5 in).

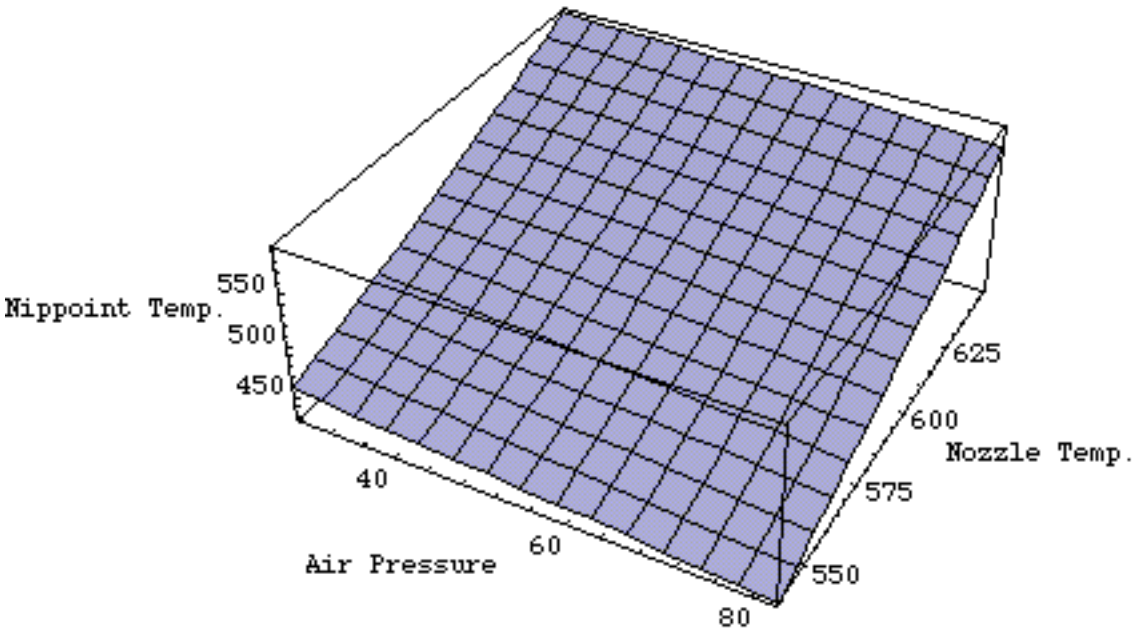

Figure 4.2 Result of nippoint temperature with a distance between nippoint and nozzle of 12.7 mm (0.5 inch).

4.4 Processing Window For On-Line Consolidation System

The processing window for the on-line consolidation system is determined by adjusting the three system processing parameters, namely roller pressure, winding speed, and nippoint temperature. To simplify the approach a step further, a fixed roller pressure of 380 kPa (55 psi) was chosen for fabricating all cylinders. It should be noted that we are not presuming that there is no significant impact of pressure on the quality of composite cylinders; a fixed roller pressure is simply a system constraint for the present design. For now, the study is focused on the impact of winding speed and nippoint temperature on composite quality.

First, a two-factor central composite design of experiments was used to define the combination of processing parameters. Second, the density and the thickness of the resulting cylinders are measured and then, as described in the previous section, their void content was calculated. Micrographs taken at cross sections of each consolidated part are used to qualitatively describe the consolidation under a certain processing condition. Differential scanning calorimetry (DSC) was used to measure the degree of crystallinity. Finally, the interlaminar shear strength of consolidated parts was measured.

4.4.1 Central Composite Design

A central composite design of experiments was used to systematically study the processing window and to maximize the quality of composite parts. The total number of test runs in a central composite design is calculated by

$$n = 2^K + 2K + m \tag{4.2}$$

where:

n is the total number of test rums,

K is the number of factors, and

m is the number of center points.

Since only one center point is used, there are nine total test runs required in the two-factor central composite design. Four corner points are located at $(\pm 1, \pm 1)$. The star points are located along coordinate axes and each pair of star points is denoted as follows:

$$\begin{aligned} &(\pm a, \quad 0), \\ &(0, \quad \pm a) \end{aligned} \tag{4.3}$$

where **a** is a constant and can be obtained by $a = (2^K)^{1/4}$.

An illustration of the two-factor central composite design is given in Figure 4.3. The levels for winding speed range from about 4-10 mm/s and the nippoint temperature has a high value of 660°C (1220 °F) and a low value of 493°C (920 °F). Nine composite cylinders, 26-ply thick and 19 mm (0.75 in) wide were fabricated under the prescribed processing conditions given by the experimental design. The winding time ranges from 77 to 172 minutes. In Table 4.4, a randomized design is generated.

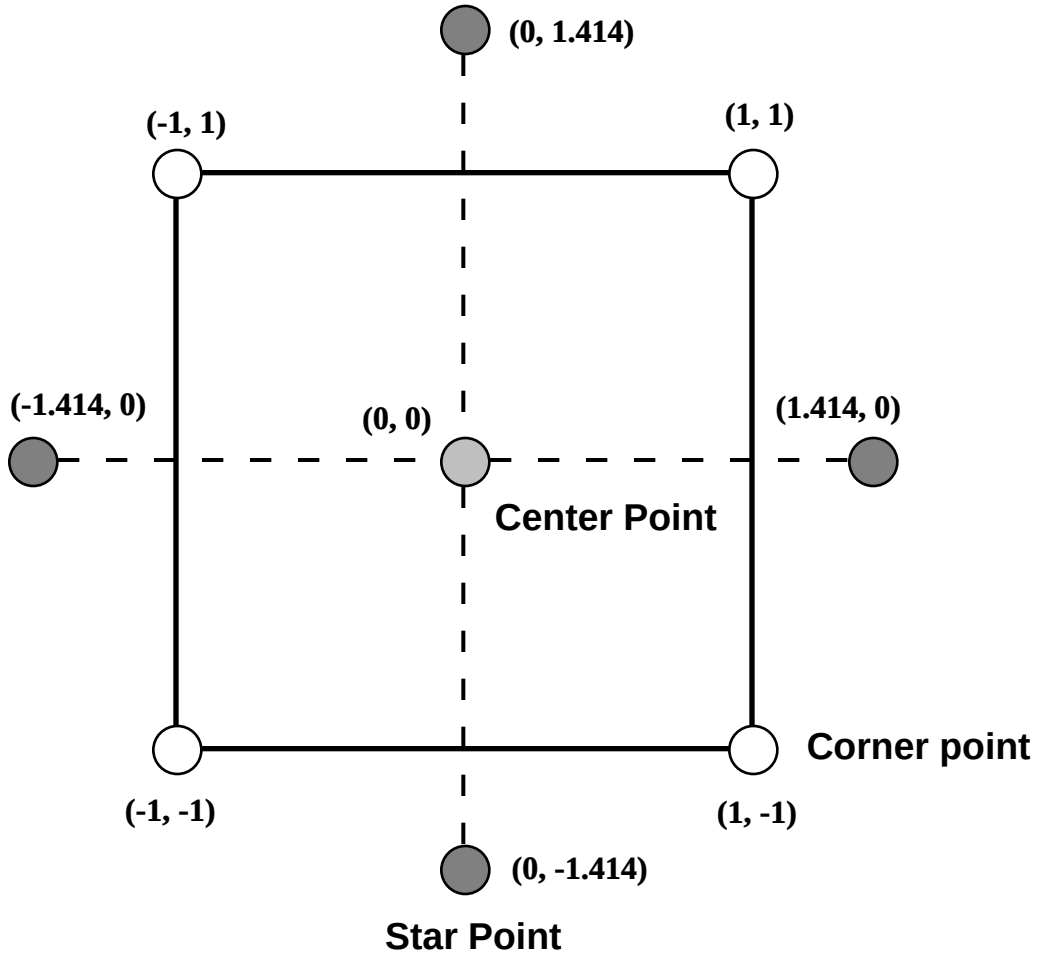

Figure 4.3 Illustration of a two-factor central composite design.

Table 4.4 A randomized two-factor central composite design with only one center point.

Cylinder Number	**1**	**2**	**3**	**4**	**5**	**6**	**7**	**8**	**9**
Factor A	0	1	0	0	-1	1.414	-1.414	-1	1
Factor B	0	-1	1.414	-1.414	-1	0	0	1	1
Nozzle Temperature °C (°F)	635 (1175)	677 (1250)	635 (1175)	635 (1175)	539 (1100)	649 (1281)	576 (1069)	539 (1100)	677 (1250)
Set Winding Speed (%)*	10	6	15	5	6	10	10	14	14
Actual Temperature °C (°F)**	572 (1061)	633 (1172)	573 (1061)	572 (1061)	517 (962)	660 (1220)	496 (924)	517 (962)	633 (1172)
Actual Winding Speed (mm/s)***	6.34	3.71	9.97	3.53	3.71	6.34	6.34	7.91	7.91

* Winding speed enter into the computer for controlling the winding machine.

** Estimated from Equation 4.1 using the coefficients given in Table 4.3.

*** Calculated by dividing the total time required to complete the winding by the total length of towpreg used for winding a 19.1 mm (.75 inch) wide cylinder.

4.4.2 Micrograph Study on Quality of Consolidated Cylinders

The purpose of the optical micrographs taken at cross sections of each composite cylinder is threefold. First, we can visually observe the degree of intimate contact between layers since intimate contact is the necessary condition for good bonding. Second, we can examine whether or not the fibers distribution is uniform. Third, we can observe the size and location of voids, for void content reflects composite quality. As a result, the micrographs give a qualitative description of the composite quality.

Specimens were cut from each composite cylinder and mounted in an epoxy potting compound. Each cross section was carefully polished and analyzed under an optical microscope. Figure 4.4 and Figure 4.5 show results for Cylinder #2 which was manufactured under a nippoint temperature of 633°C (1172°F) and a winding speed of 3.71 mm/s (8.764 in/min.). Virtually no voids are observed at the interply region. Uniform fiber distribution is also achievable under on-line consolidation as shown in Figure 4.5(a). Some of the carbon fibers are even able to migrate into the resin-rich interply area as shown in Figure 4.5(b). No significant fiber waviness confirms that on-line consolidation does have the advantage over the conventional autoclave consolidation where fiber waviness usually occurs (Figure 4.6).

(a)

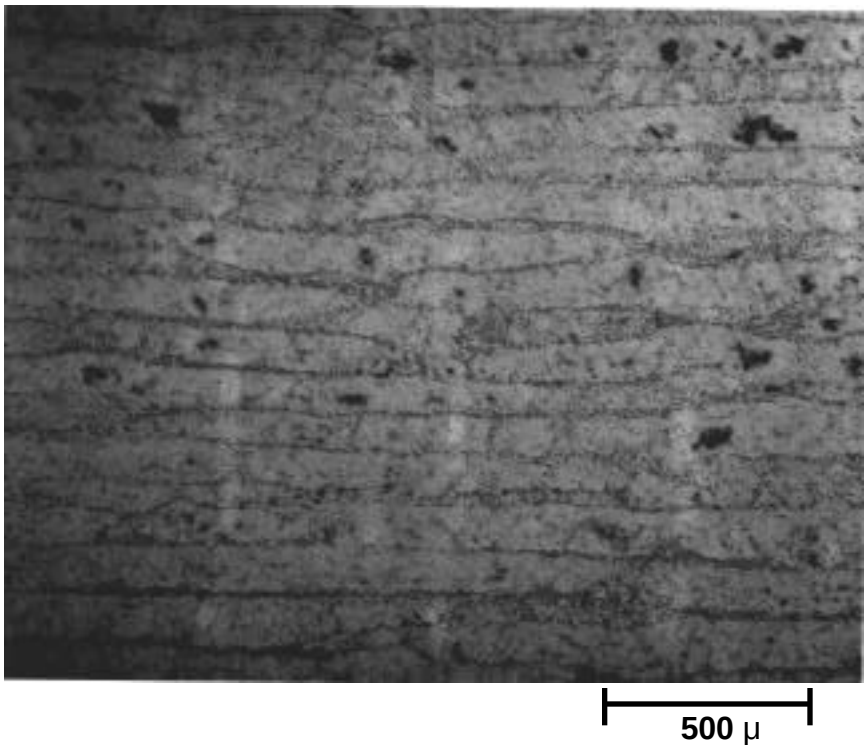

(b)

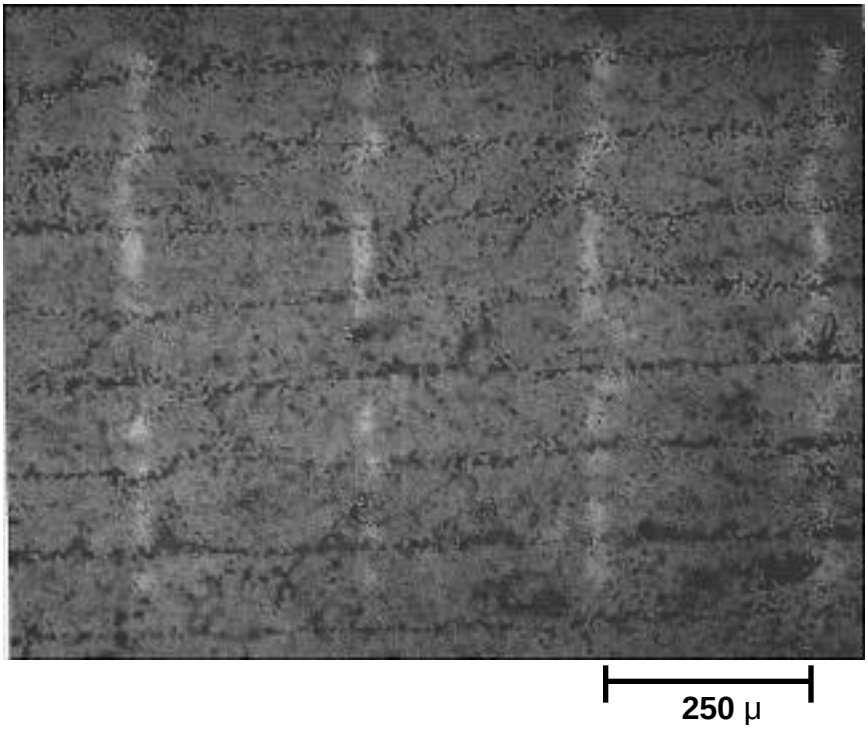

Figure 4.4 Micrographs of cross-section of Cylinder #2.

(a)

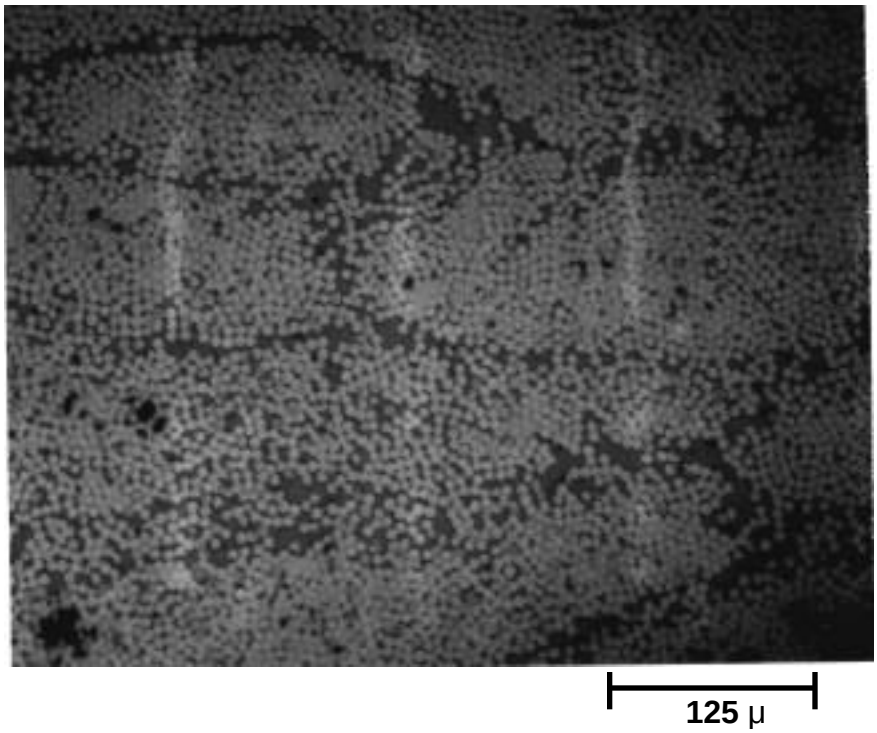

(b)

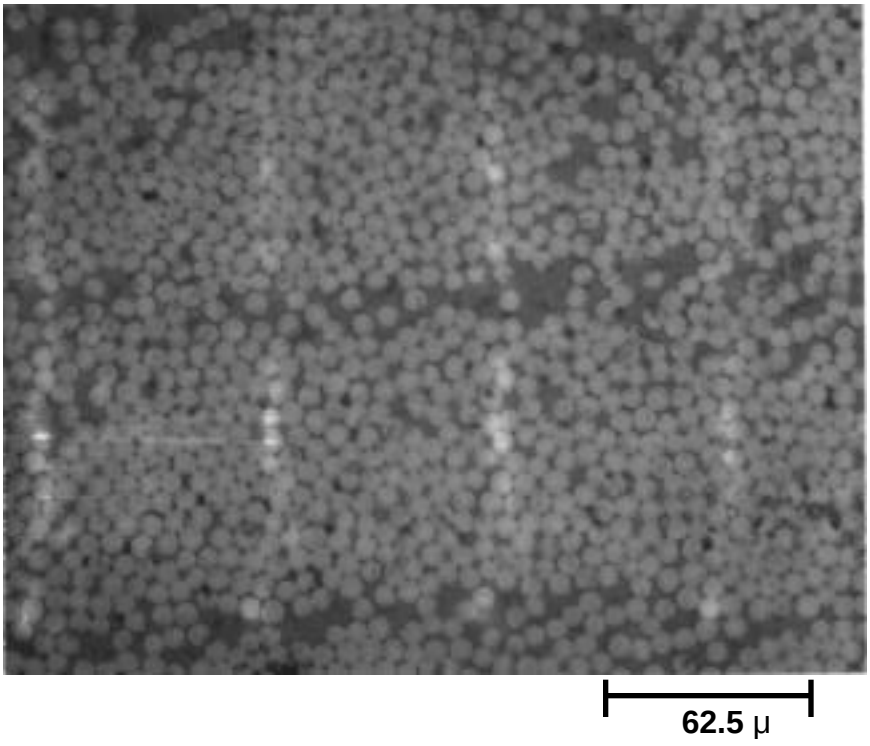

Figure 4.5 Micrographs of cross-section of Cylinder #2.

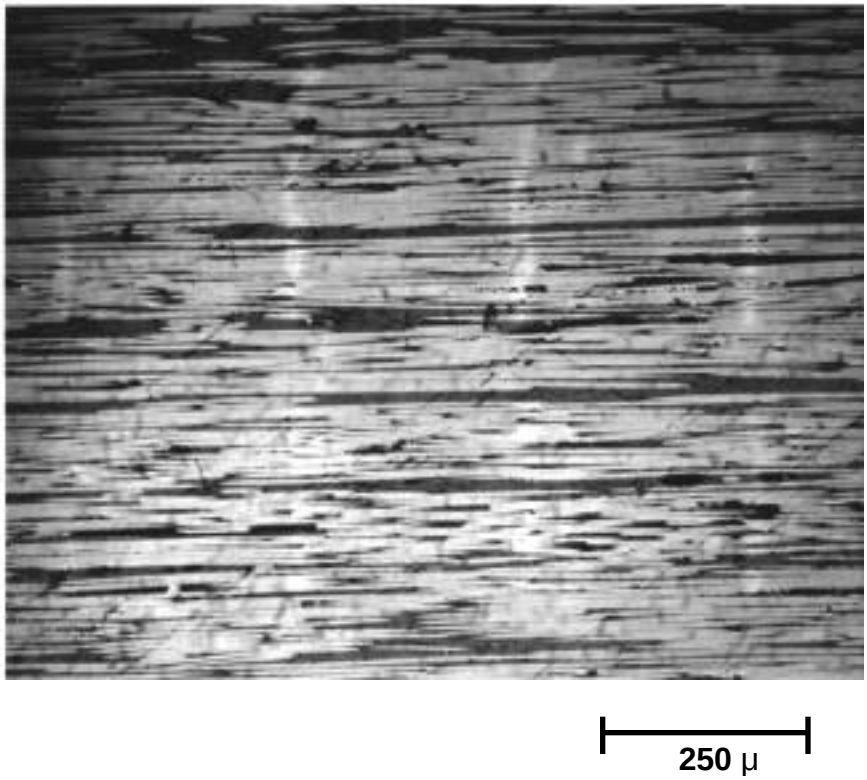

Figure 4.6 Micrograph of cross-section along the circumferential direction of Cylinder #2.

As expected, not all cylinders yield the same high quality. Figure 4.7 to Figure 4.11 are the micrographs of the cross section of all nine cylinders manufactured under conditions as listed in Table 4.4. In the case of Cylinders #3, #7, and #8, large, resin-rich areas exist at almost every interply regions. Under external loading, the resin-rich areas are the most vulnerable due to the lack of surrounding reinforcement. This observation suggests that the specimens from these cylinders may fail much more easily than the specimens cut from a well-consolidated cylinder in which the fiber is distributed more uniformly.

Although some large resin-rich regions were observed in specimens of Cylinders #1 and #9, there exist well-consolidated areas as well. Therefore, the quality of Cylinders #1 and #9 was judged to be better than the quality of the aforementioned cylinders. The overall uniformity of fiber distribution and smaller resin-rich areas observed in the specimens from Cylinders #2, #4, #5, and #6 suggest that the quality of these cylinders is close to ideal.

(a)

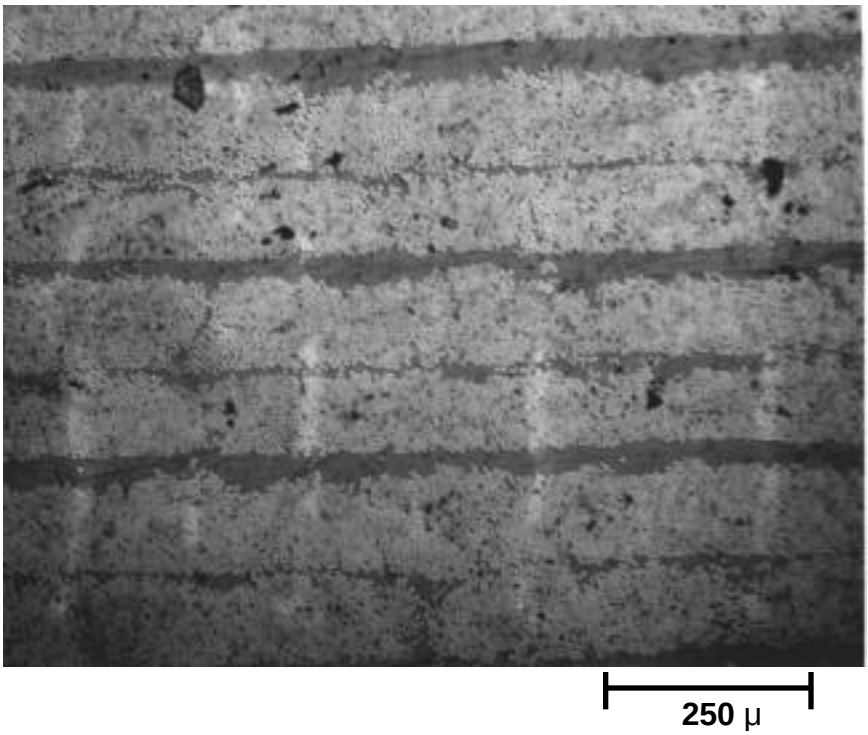

(b)

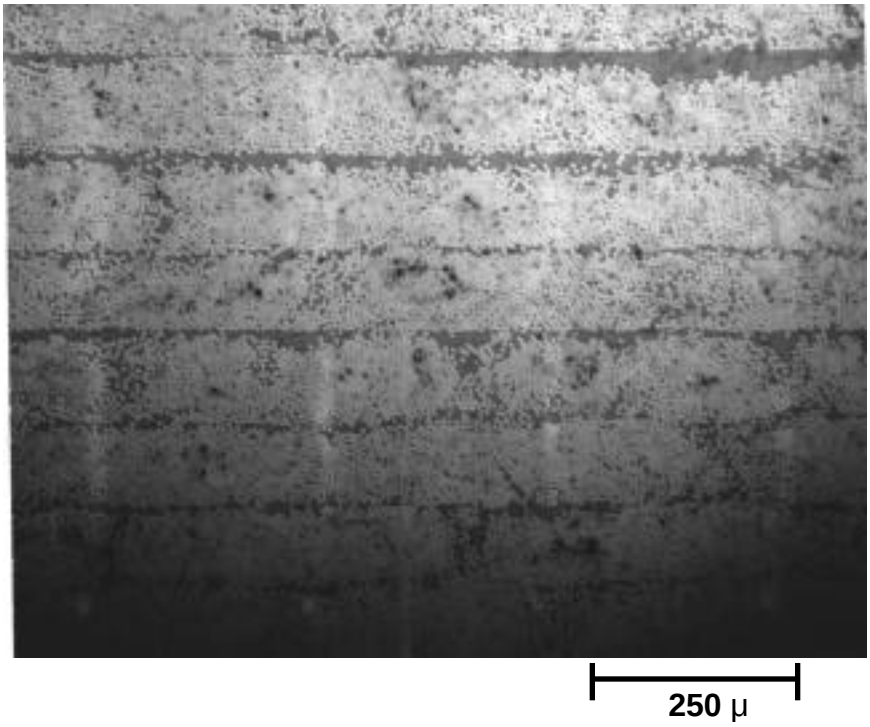

Figure 4.7 Micrographs at cross-section for Cylinders #1(a) and #2(b)

(a)

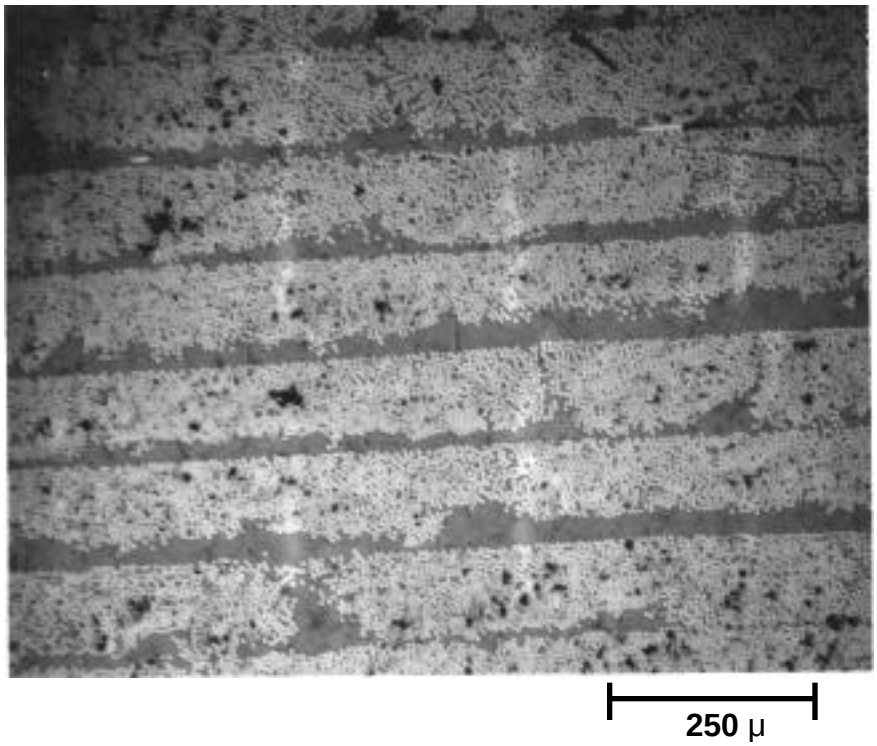

(b)

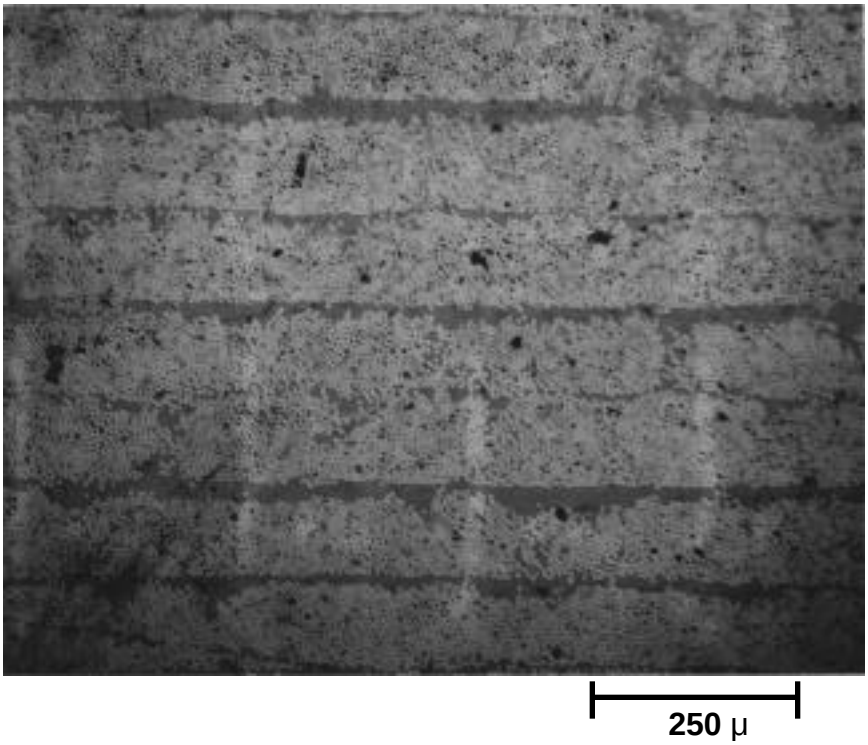

Figure 4.8 Micrographs at cross-section for Cylinders #3(a) and #4(b)

(a)

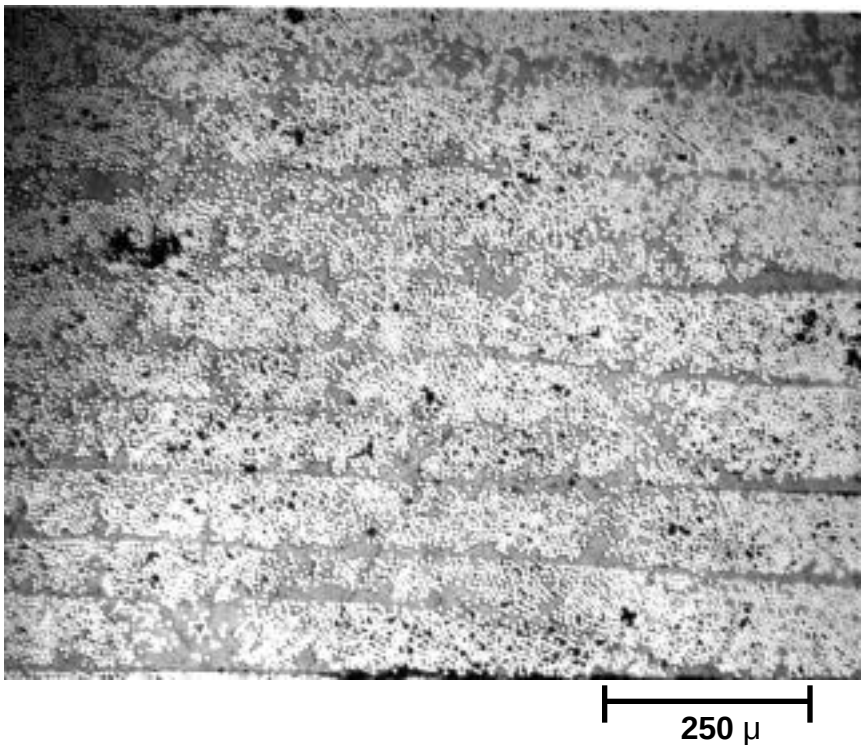

(b)

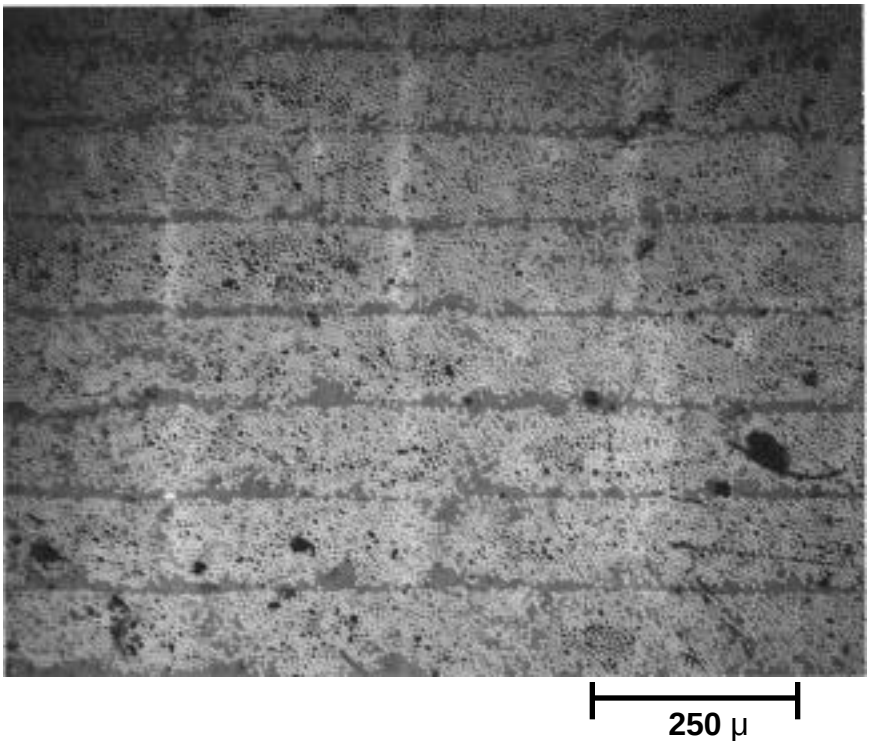

Figure 4.9 Micrographs at cross-section for Cylinders #5(a) and #6(b)

(a)

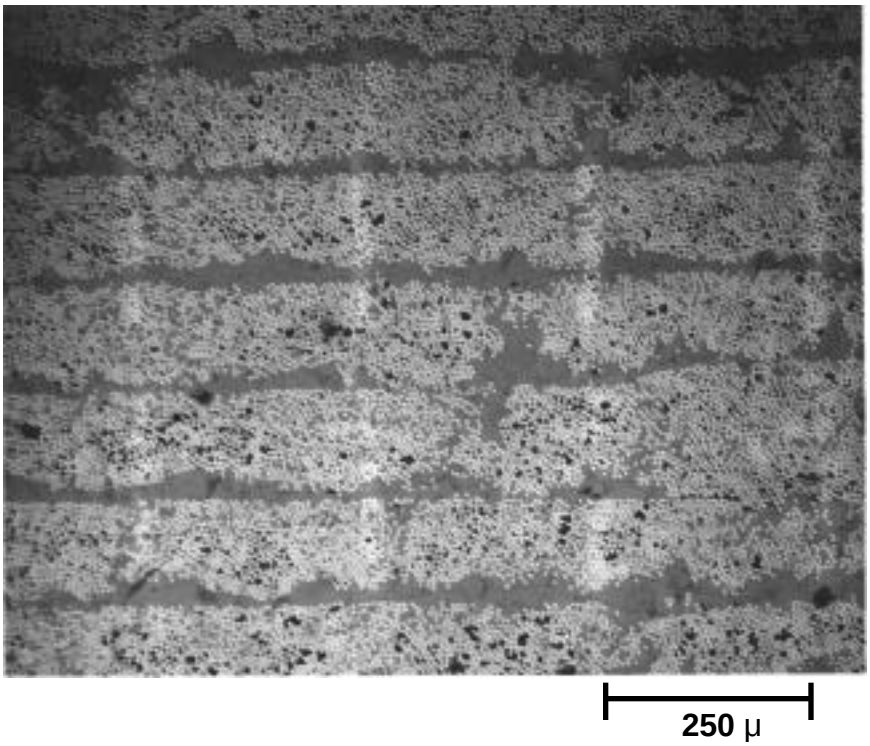

(b)

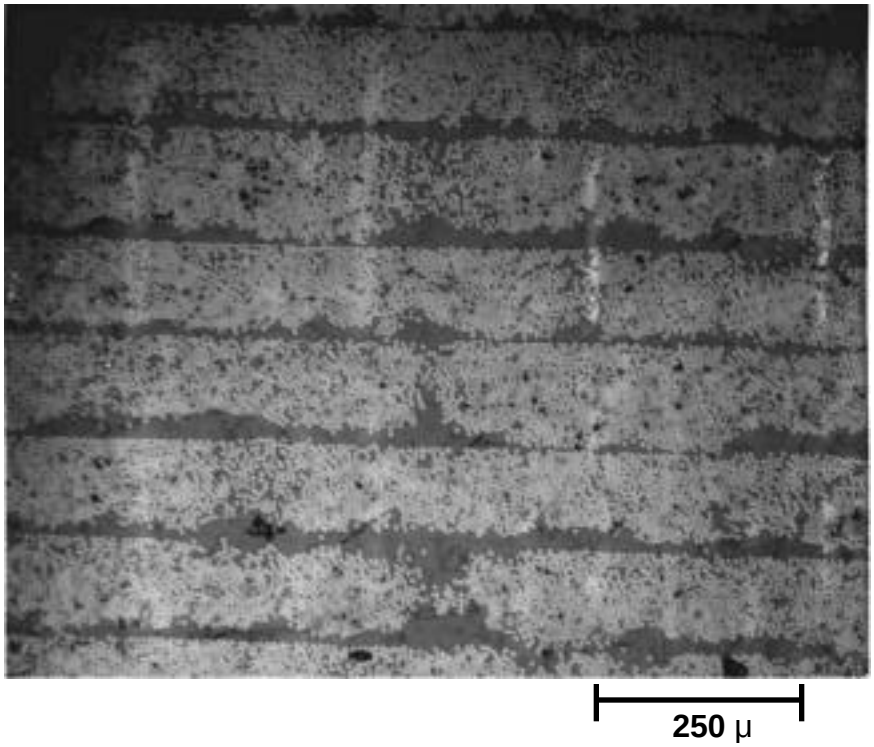

Figure 4.10 Micrographs at cross-section for Cylinders #7(a) and #8(b)

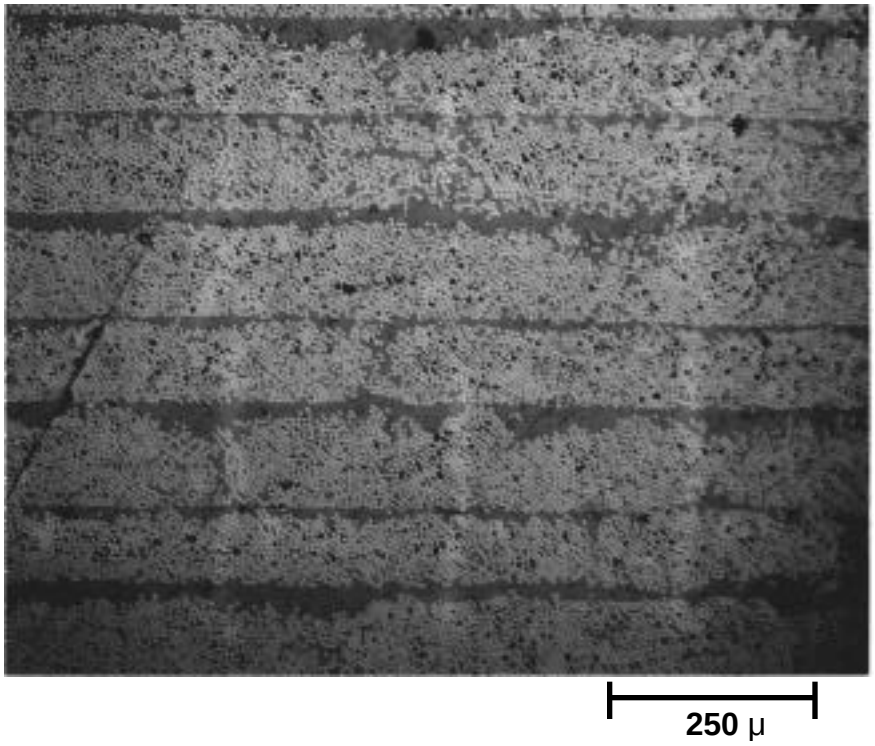

Figure 4.11 Micrograph at cross-section for Cylinder #9

4.4.3 Effect of Processing Parameters on Density and Void Content of Consolidated Cylinders

The ASTM standard D792-91 was used to determine the density of the consolidated composite cylinders made by various processing conditions. Four samples are cut from each cylinder and then put inside a 60°C vacuum oven for about 60 minutes. This procedure eliminates any moisture that might have accumulated during slow-speed cutting in which water was used for cooling. After air-cooling at room temperature for another 60 minutes, the samples are weighted first in the air then in isopropyl alcohol. Figure 4.12 shows the density of the consolidated composite cylinders. It should be noted that the measured density of the towpreg as received does not totally conform to the ASTM standard in which specimen should weigh 1 to 5 gm. Due to the weight constraint, we measured 32 smaller towpreg samples instead. By sampling a larger number, we hope to minimize the error.

Before calculating the void content, we need to determine the theoretical density of a 60% fiber volume fraction, void-free APC-2 composite. Using the material density listed in Table 4.5 and assuming 30% degree of crystallinity in PEEK, we obtain a value of 1589.6 kg/m^3 as the theoretical density of an APC-2 composite. Figure 4.13 shows the calculated void content for each cylinder. Experimental results on density and void content for each cylinder are summarized in Table 4.6.

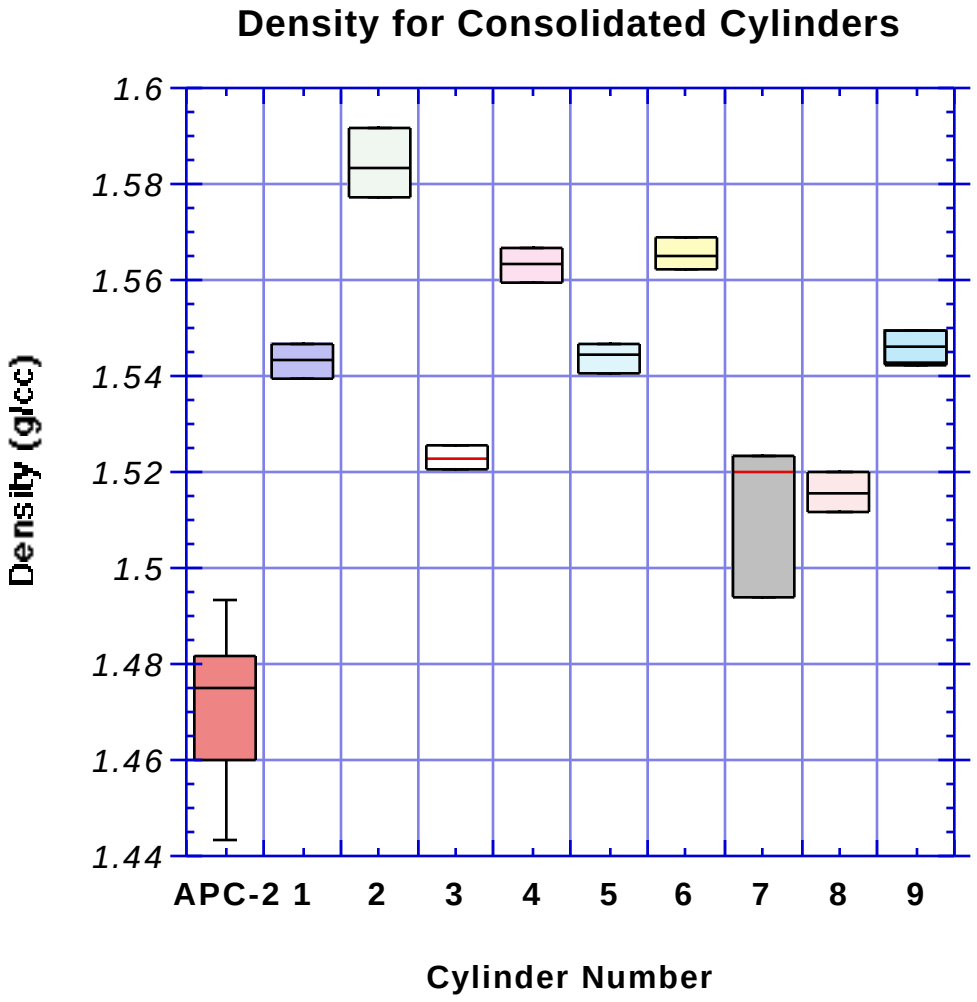

Figure 4.12 Density of the consolidated composite cylinders.

Table 4.5 Material properties for density calculation.

Property	AS-4 Fiber	PEEK	
		Amorphous	Crystallinity
Volume Fraction	60%	40%	
Degree of Crystallinity	NA	NA	30%
Density (kg/m^3)	1780.0	1262.6	1400.6

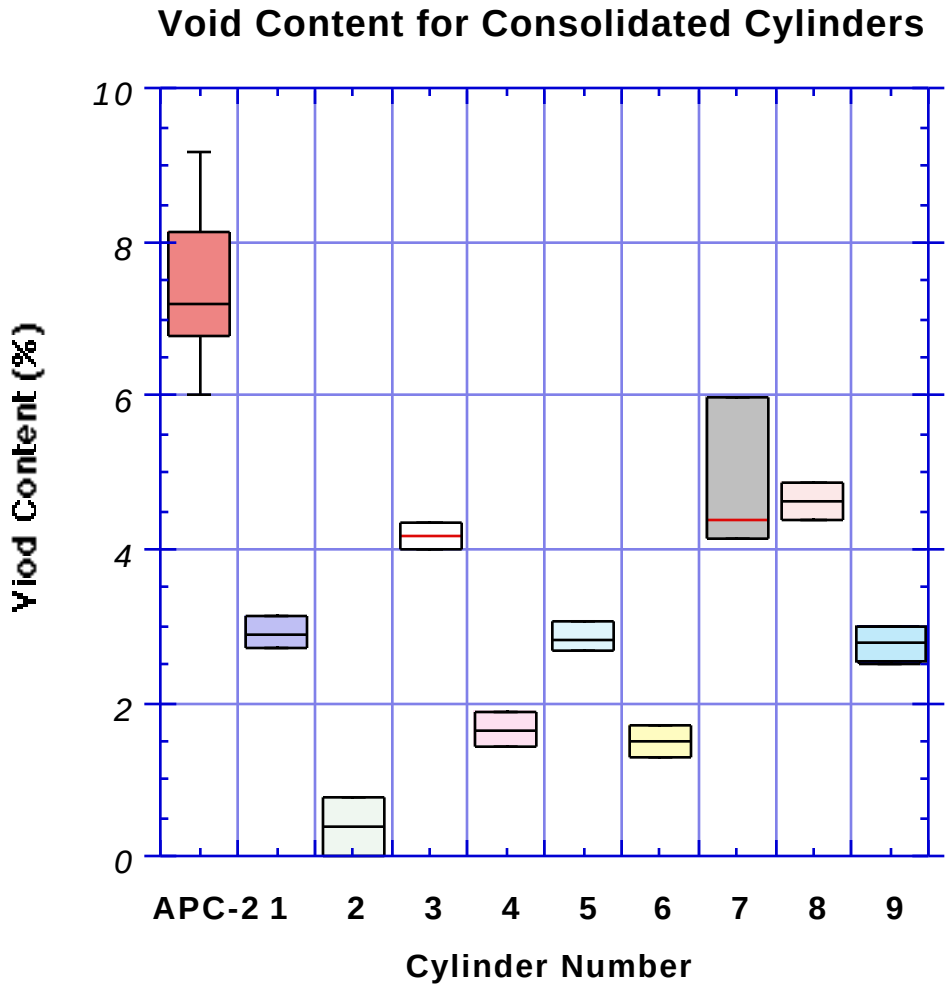

Figure 4.13 The calculated void content for each cylinders.

Table 4.6 Composite density and void content analysis results.

Cylinder	Density (kg/m^3)	Void Content (%)	Thickness mm (inch)	Fiber Volume Fraction (%)	Resin Mass Fraction (%)
1	1543.5	2.90	3.21 (0.126)	58.3	34.3
2	1584.2	0.38	2.90 (0.114)	59.8	33.0
3	1523.3	4.17	3.47 (0.137)	57.5	35.1
4	1563.4	1.65	3.18 (0.125)	59.0	33.7
5	1544.5	2.84	3.25 (0.128)	58.3	34.3
6	1565.2	1.51	3.06 (0.121)	59.1	33.6
7	1517.5	4.72	3.58 (0.141)	57.2	35.4
8	1516.1	4.63	3.60 (0.142)	57.2	35.3
9	1545.6	2.77	3.26 (0.129)	58.3	34.3

4.4.4 Study of Degree of Crystallinity

The crystallization mechanism of a semi-crystalline thermoplastic composite is very complicated. Factors such as molecular weight of polymer, the presence of reinforcement, residence time above melting, and cooling rate affect the polymer's degree of crystallinity. In the on-line consolidation process, the material is experiencing a complicated thermal history which includes rapid melting, and cooling, and possibly annealing. Modeling crystallization under conditions involved in on-line consolidation is outside the scope of the present study. Instead, we simply present the degree of crystallinity of the cylinders processed under different conditions.

The degree of crystallinity determined by the differential scanning calorimetry (DSC) is calculated as follows:

$$C_r = \frac{H_T}{H_U} \tag{4.4}$$

where:

H_T = total heat of crystallization at a given processing condition, J/g

H_U = theoretical ultimate heat of crystallization, J/g.

Figure 4.14 shows a typical heat flow vs. temperature plot obtained by DSC. Using the total area under the baseline as denoted in Figure 4.14 and H_U = 130 J/g for PEEK polymer [63], the degree of crystallinity for cylinder #4 is 32.7%. It should be noted that the polymer weight, a requirement for obtaining H_T in the DSC, is calculated by multiplying the weight of the composite sample by the resin mass fraction given in Table 4.6

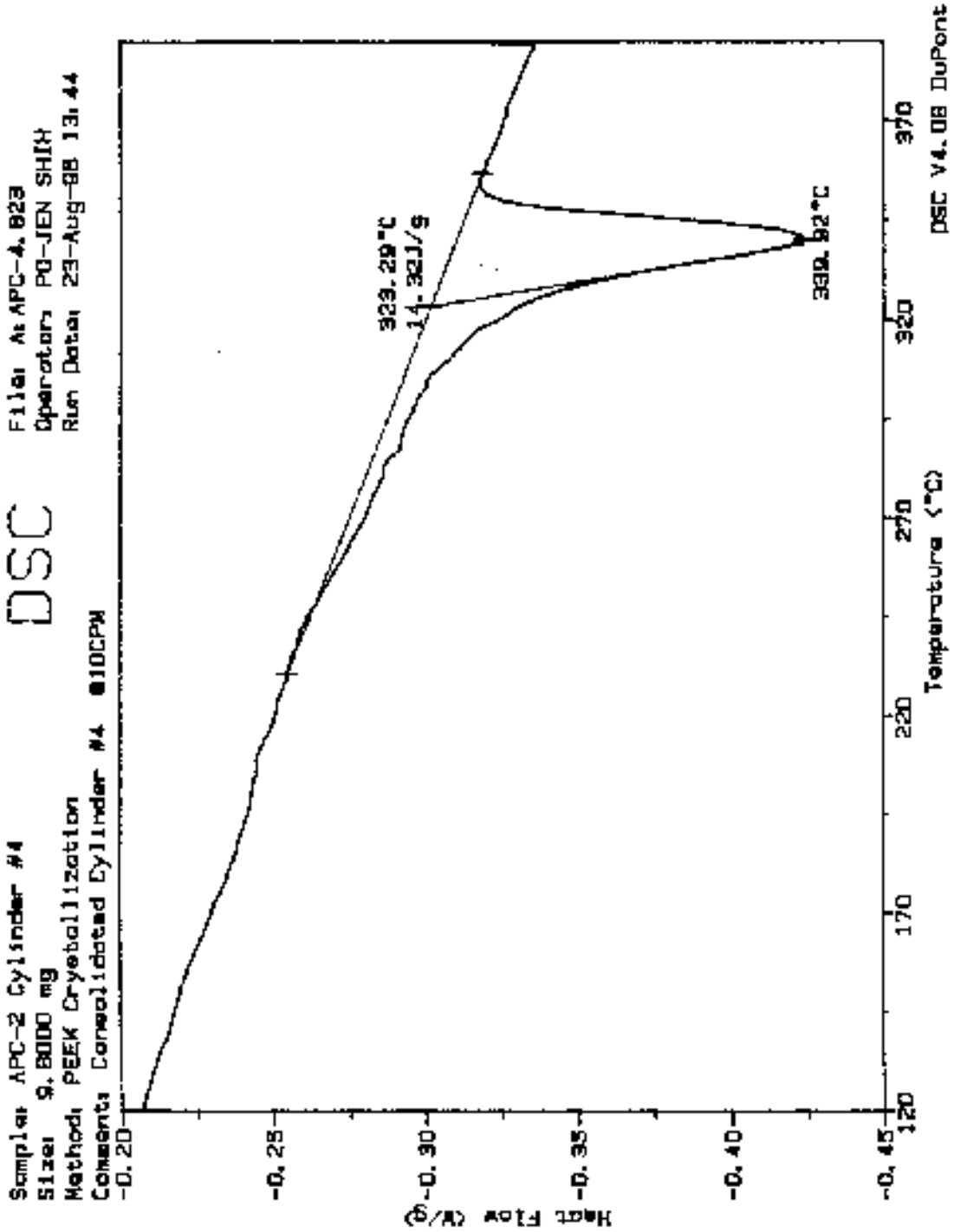

Figure 4.14 A typical DSC plot of heat flow vs. temperature, Cylinder #4.

The DSC measurements at a heating rate of 10°C/min. were conducted on samples from each cylinder and the APC-2 towpreg. Figure 4.15 shows the DSC results for the APC-2 towpreg. The existence of an exothermic region right after the glass transition temperature indicates that the towpreg was quenched from melt. Note that the exothermic region was not observed in any of the samples from consolidated cylinders. This observation suggests that either the cooling rates under various conditions involved in on-line consolidation were not as high as the cooling rates under quenched conditions or that the annealing does take place during winding when the hot-air heater revisits the same spot while winding the very next layer onto the substrate.

Finally, Table 4.7 summarizes the resulting degree of crystallinity under each processing condition. The degree of crystallinity ranges from about 26 % to 34%. Again, the data shown here is for reference only. We have made no effort to correlate the degree of crystallinity of consolidated cylinders to the processing conditions in which the composite cylinder was made.

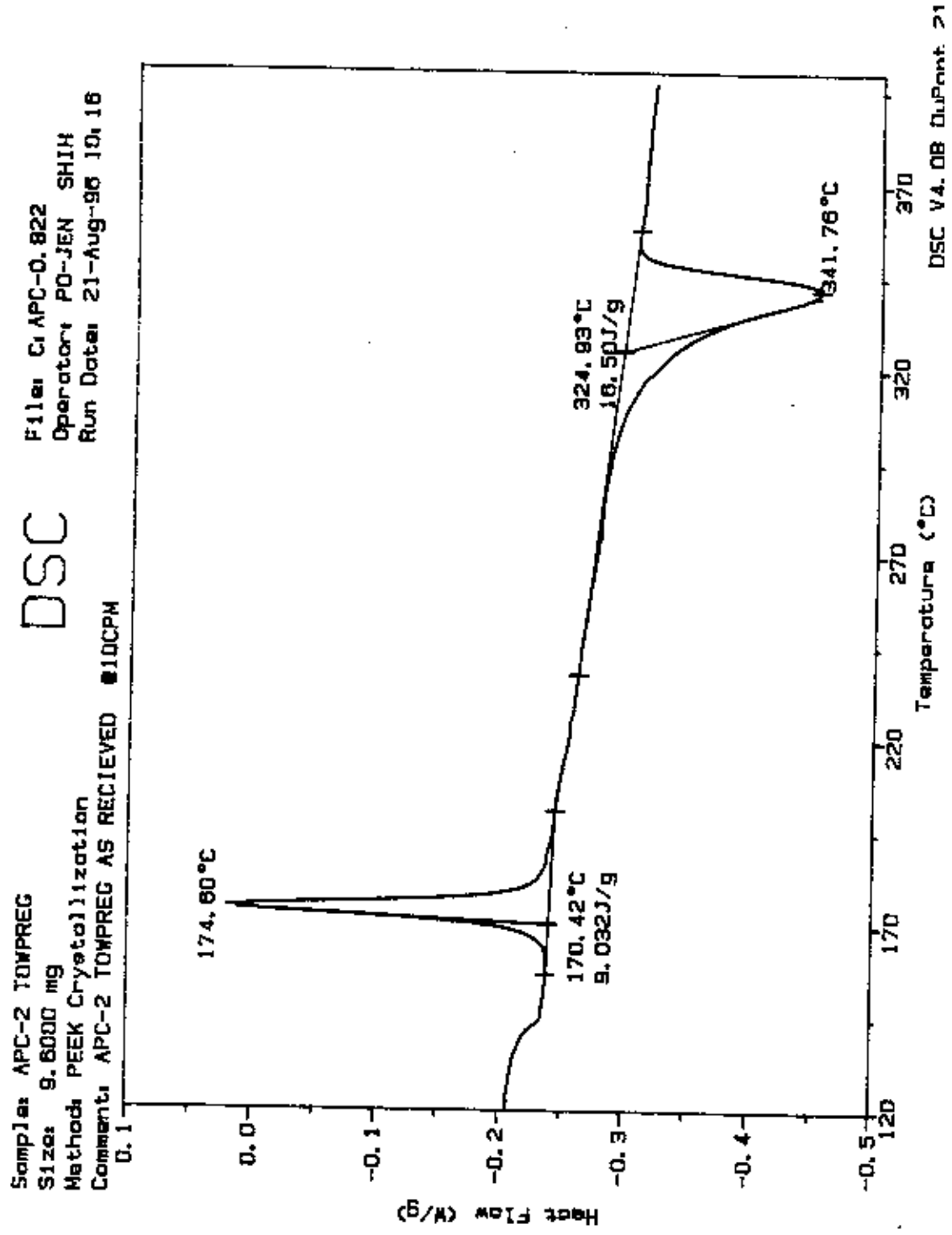

Figure 4.15 A typical DSC plot for towpreg as received.

Table 4.7 The degree of crystallinity for consolidated cylinders.

Cylinder	APC-2 weight (mg)	Onset Temperature (°C)	Melting Temperature (°C)	H_T (J/g)	Degree of Crystallinity (%)
1	10.0	323.99	340.85	13.31	32.8
2	10.0	324.36	339.64	12.61	29.4
3	9.8	323.10	341.05	12.60	29.0
4	9.8	323.29	339.92	13.42	32.7
5	13.3	323.74	340.83	14.995	33.6
6	15.2	324.48	341.28	12.73	29.2
7	14.3	323.76	341.93	13.99	30.4
8	9.8	323.14	340.89	12.18	26.5
9	9.9	323.52	341.06	12.19	27.4
Towpreg	9.6	324.93	341.76	7.47	15.1

4.5 Effect of Processing Parameters on Interlaminar Shear Strength

After investigating the impact of processing parameters on the density, void content and degree of crystallinity, the next logical step is to conduct interlaminar shear strength (ILSS) tests that give a quantitative description of the bonding quality of the resulting cylinders. Figure 4.16 shows data obtained from three specimens of Cylinder #6. The first-ply failure initiates at similar displacements and the maximum loads are similar. When an individual ply fails, an audible cracking sound is heard followed by a sharp decrease in load. The damaged laminate continues to carry loading until the next failure occurs. With only two exceptions, most of the specimens follow this pattern. The specimens from Cylinder #7 and #8 have slightly different load-displacement curves. As shown in Figure 4.17 and Figure 4.18, premature failure occurs in these specimens well before the maximum loading is reached. Specimens from these two cylinders failed differently from the specimens from other cylinders. In addition to the pure shear failure at midplane, the first few layers from inner section of the specimens were totally debonded. The interply bonding between the first few layers was much weaker than bonding between the other layers of the specimens.

Figure 4.19 shows the interlaminar shear strength of all cylinders. It is noted that the small circle in the box plot indicates a data point which is far away from the statistical average.

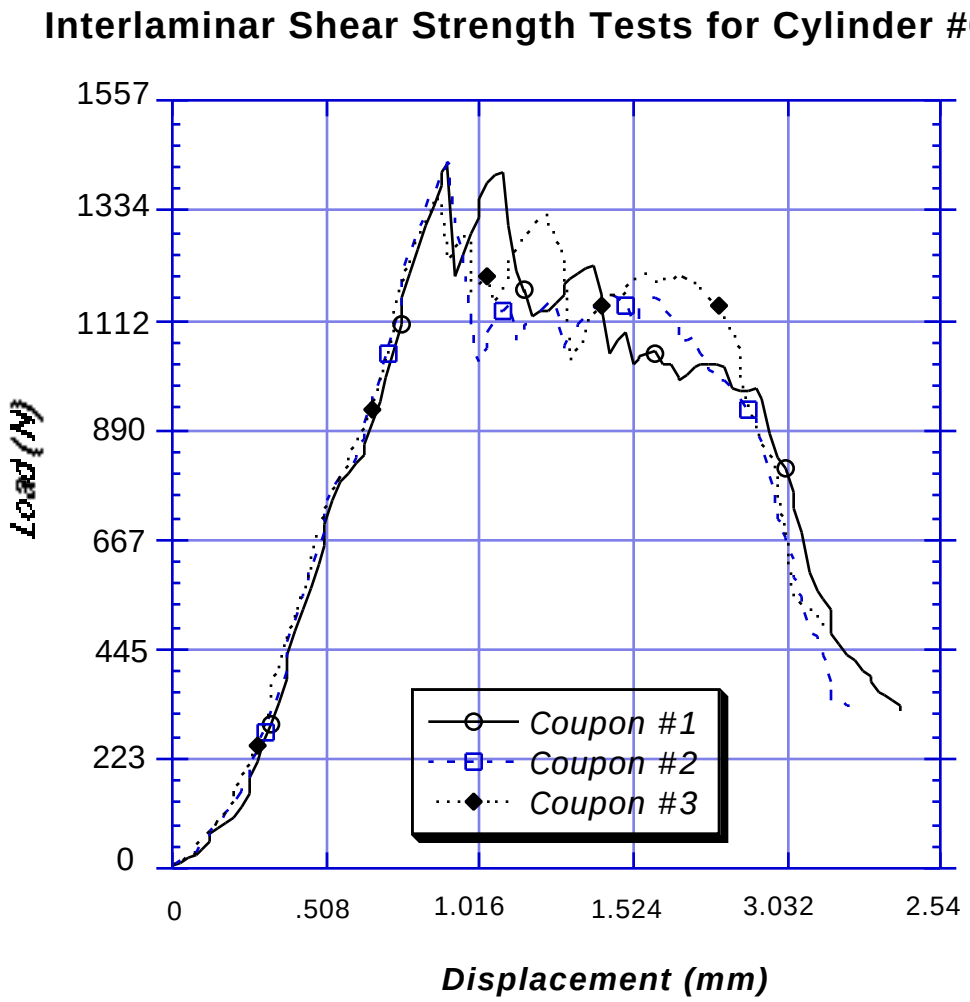

Figure 4.16 Load-displacement curve for Cylinder #6.

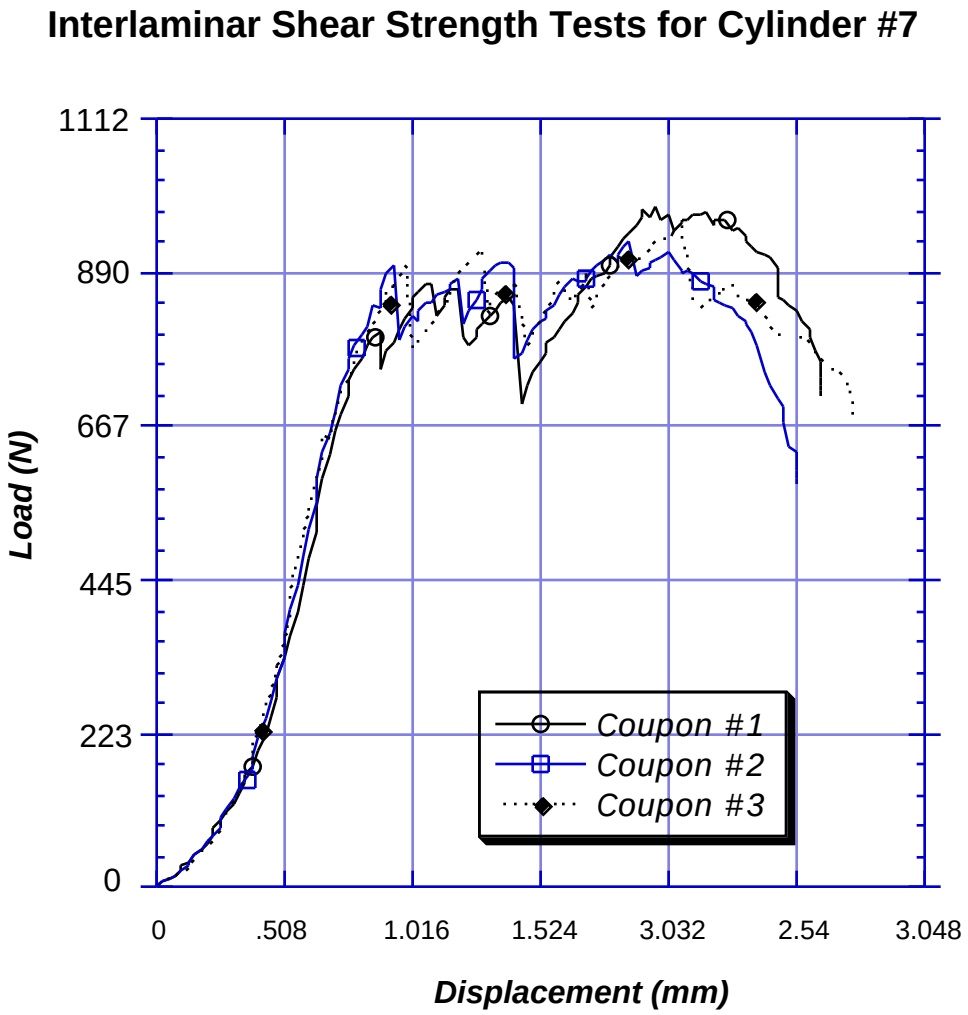

Figure 4.17 Load-displacement curve for Cylinder #7.

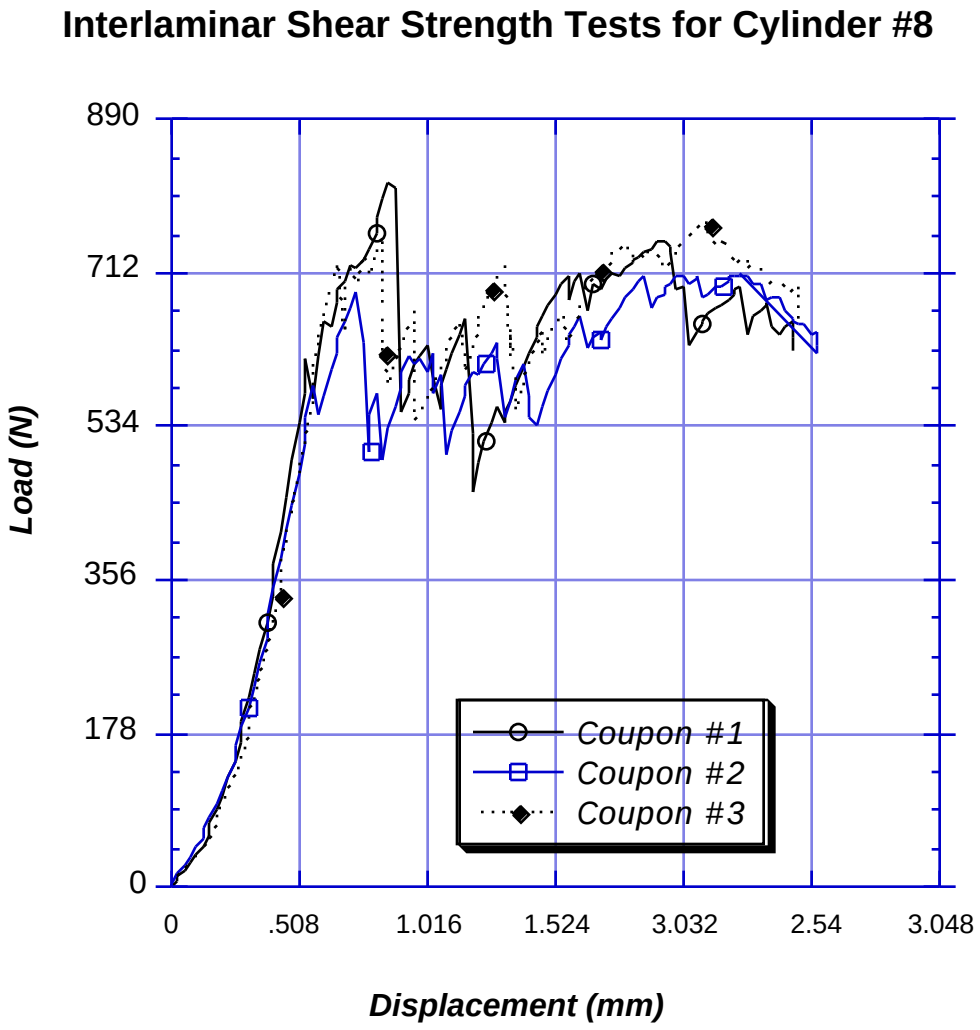

Figure 4.18 Load-displacement curve for Cylinder #8.

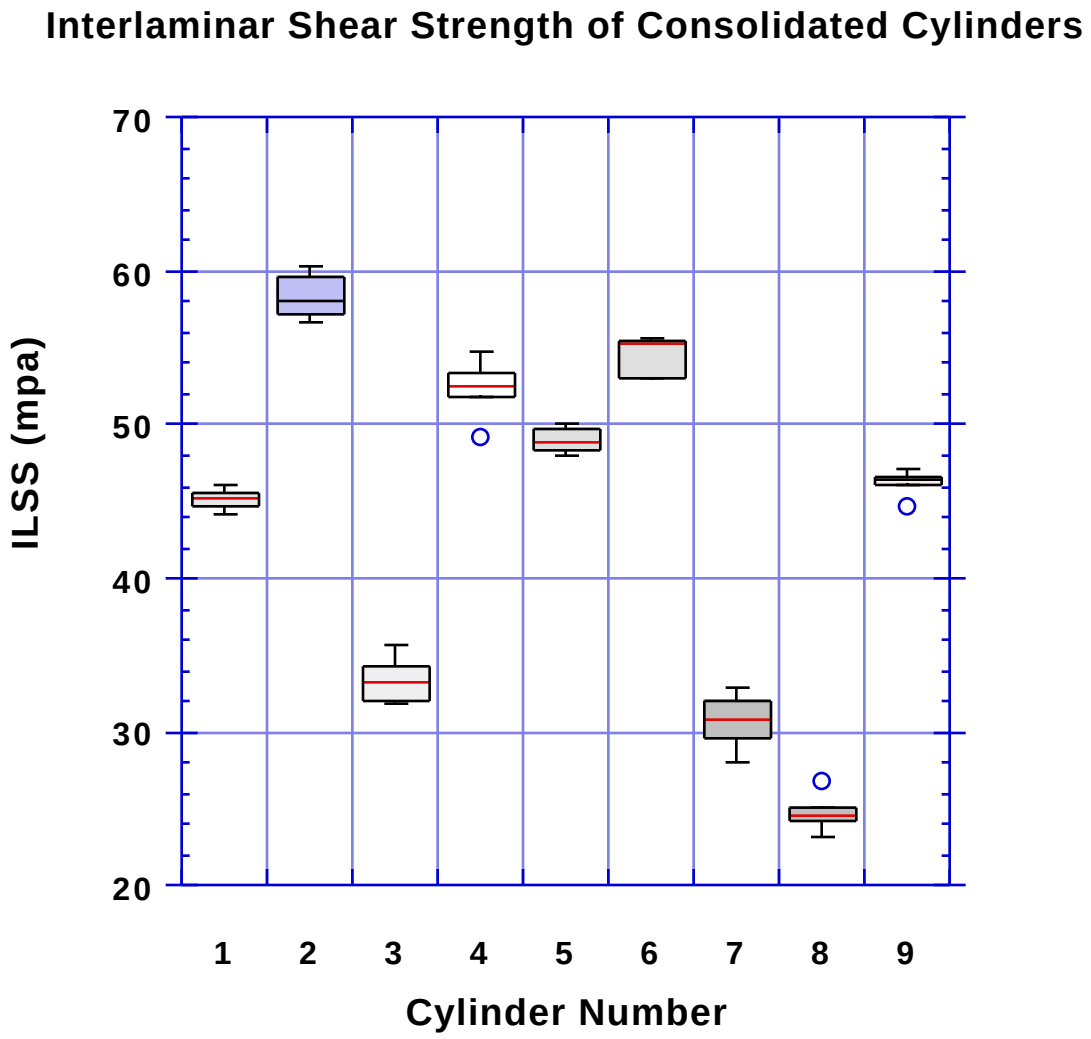

Figure 4.19 Interlaminar shear strength of all cylinders.

For APC-2 composites, an interlaminar shear strength of 71.8 MPa (10.4 ksi) has been reported by using manufacturer recommended processing conditions, i.e. 380°C for 5 minutes under a hot press loading at 1380 kPa (200 psi) [64]. The average ILSS obtained from Cylinder #2 is about 80% of the ILSS of flat compression molded composite laminates. Therefore, we consider the present design of the on-line consolidation system an acceptable one.

After measuring the interlaminar shear strength (ILSS) for all cylinders, the next step is to study the impact of nippoint temperature and winding speed on the ILSS of the composites. For this we use MINITAB®, a statistical computer software package. Figure 4.20 shows the effects of changing nippoint temperature and changing winding speed. We can see that the nippoint temperature has the biggest effect. While higher nippoint temperature yields better composites, the ILSS does not always increase when lowering winding speed. This means that, within the temperature range investigated, we can make a composite cylinder with higher ILSS by simply raising the nippoint temperature. This may also mean that the thermal degradation of polymer is not too severe under high temperature as long as the dwelling time during winding remains brief. However, the issue of thermal degradation under conditions of on-line consolidation requires a more in-depth investigation and was not addressed in the present study.

In order to study how ILSS varies under various processing conditions, a response surface using a two factor central composite design was constructed. A second order linear regression model can be written as follows:

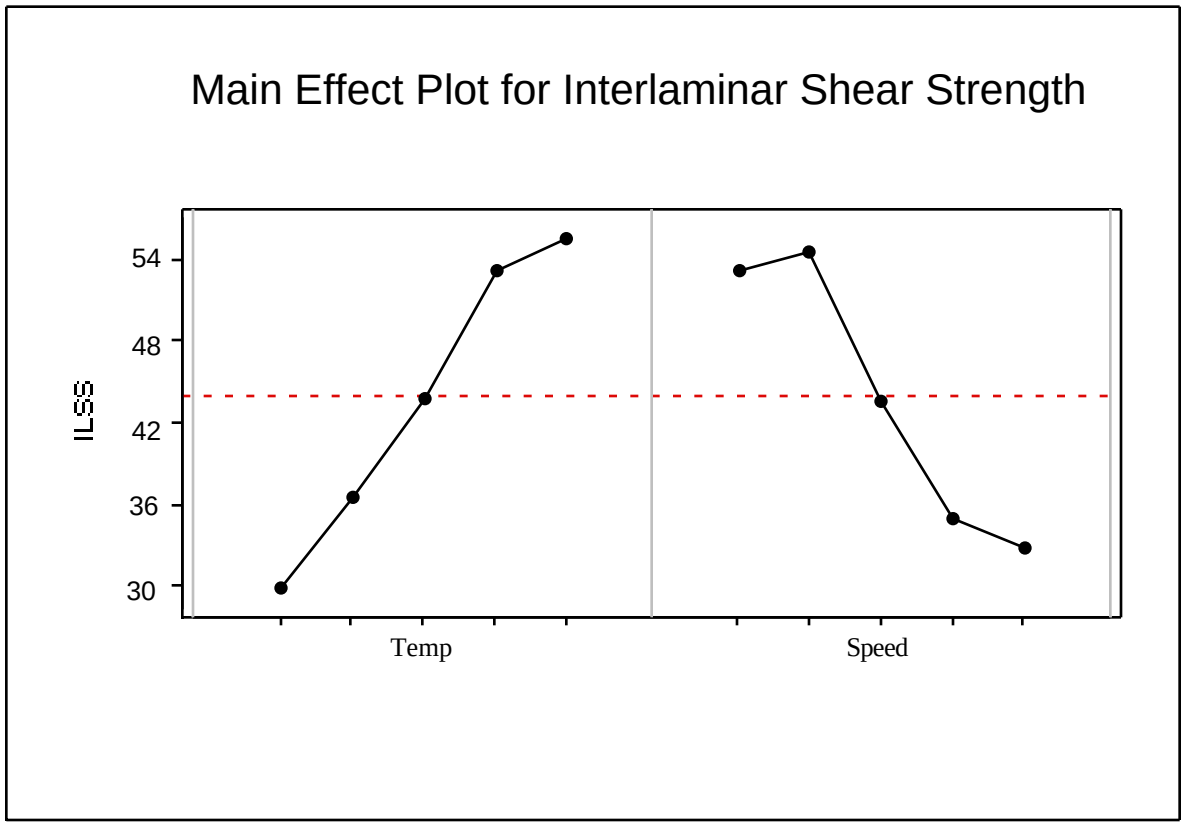

Figure 4.20 Main effect plot for interlaminar shear strength of all cylinders.

$$ILSS = -14.9207 + 0.31192\ NT - 19.663\ WS - 0.000278\ NT^2 + 0.1643\ WS^2 + 0.0244\ NT \times WS \quad (4.5)$$

where:

ILSS = interlaminar shear strength, MPa,

NT = nippoint temperature, x 100°C,

WS = winding speed, mm/s.

Figure 4.21 shows the impact of nippoint temperature and winding speed on the interlaminar shear strength of consolidated composite cylinders. The black dots in Figure 4.21 indicate data points. Overall, the correlation of model to experiment is acceptable. In general, higher nippoint temperature and lower winding speed yield higher ILSS. For convenience, a contour plot of the response is given in Figure 4.22. If the highest strength is desired, we can wind the cylinder at a lower speed and a higher temperature. However, if productivity is a concern, winding the cylinder at a higher speed and at a higher nippoint temperature will not sacrifice too much strength. It should be noted that all observations made here are good only for the range investigated for each variable and cannot be used to explicitly study the ILSS response outside this range.

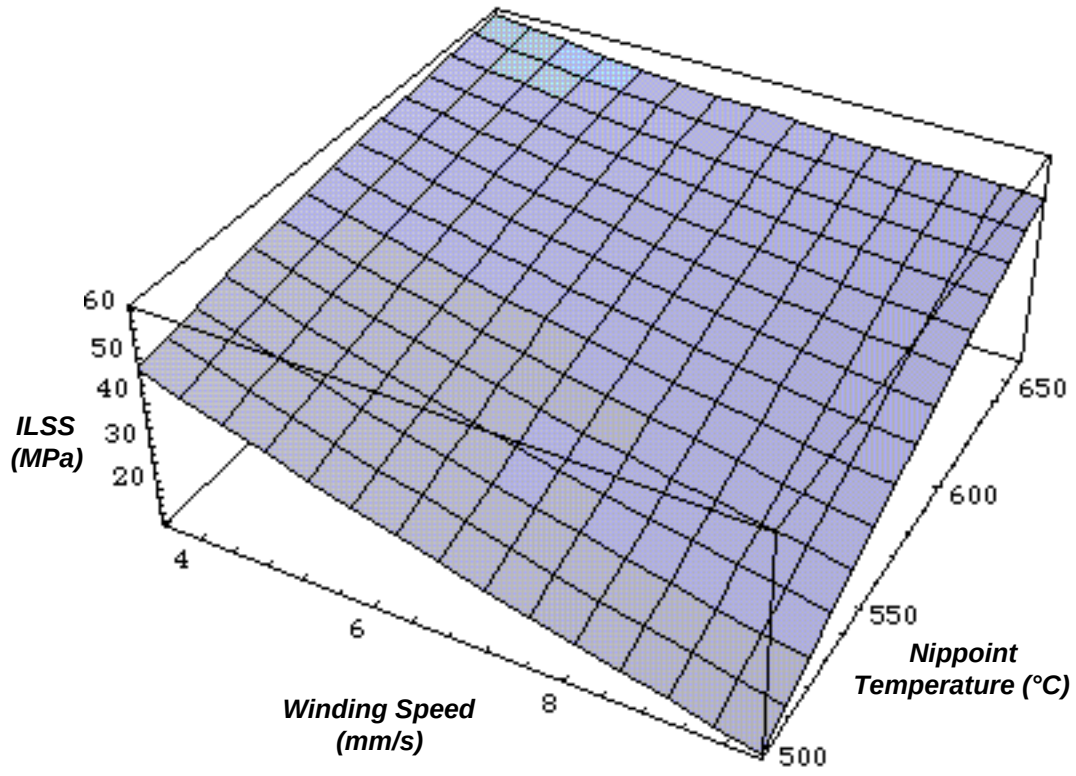

Figure 4.21 Impact of nippoint temperature and winding speed on the interlaminar shear strength.

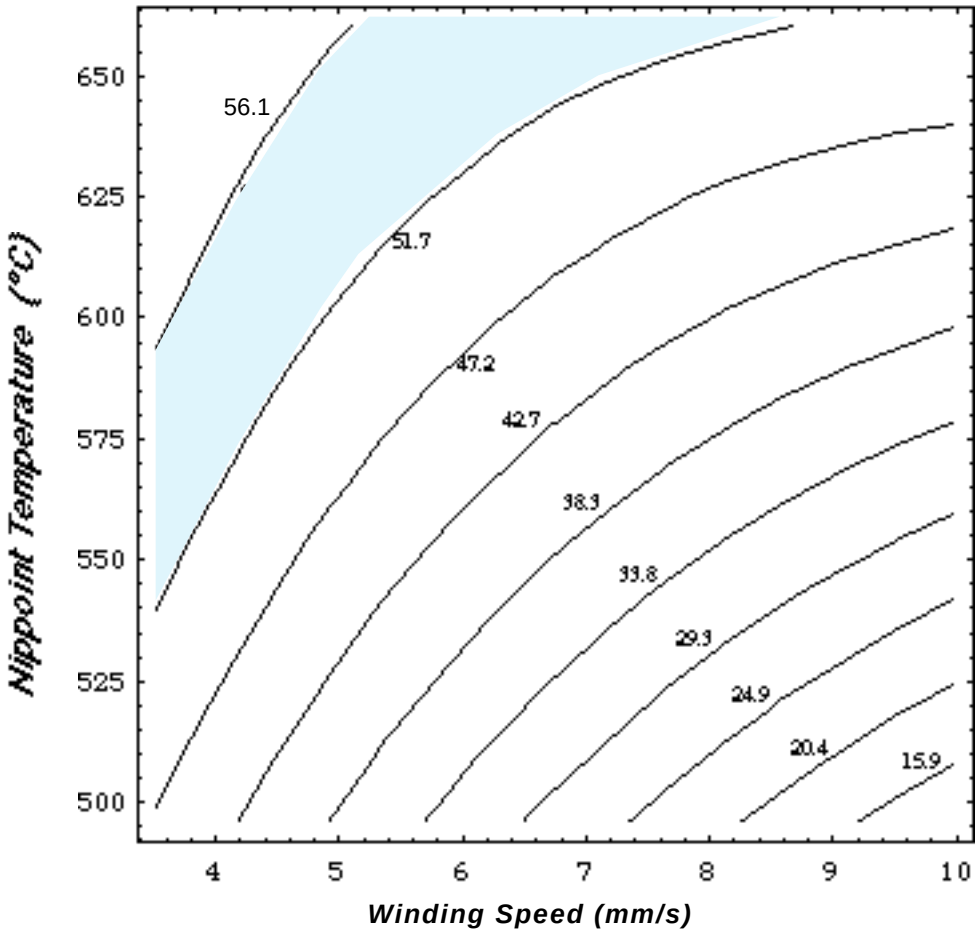

Figure 4.22 Response contour for interlaminar shear strength study.

4.6 Summary

Experimental results prove that the present on-line consolidation system is a viable design for manufacturing composite parts. The bonding strength as well as the overall quality of consolidated parts compare well with those produced by compression molding consolidation. The main disadvantages of the present system design, from the practical point of view, is the winding speed and hence the productivity is very low. However, for research purposes, the present design is well equipped to thoroughly investigate the fundamentals involved in the on-line consolidation process.

The design of experiments allows us to statistically study the impact of the processing parameters. The nippoint temperature and winding speed have the greatest impact on the overall quality of the consolidated composite parts. Micrographs of the cross-section of the composite cylinders reveal the resin flow mechanism. The degree of crystallinity of the consolidated cylinders under different processing conditions was measured by differential scanning calorimetry (DSC). However, the non-isothermal crystallization behavior of APC-2 composites was not investigated. Void content tests assure us that consolidating the thermoplastic prepreg layer by layer helps to squeeze out the air entrapped in the raw materials. Finally, observations indicate that the local temperature distribution and thermal history resulting from the nippoint temperature and winding speed are the factors that determine the quality of consolidated parts.

5 In-Situ Measurement System

5.1 Introduction

In order to investigate the maximum temperature and heating area achievable with a single hot-air heater design, an in-situ measurement system was constructed to acquire thermal data during the winding process. This approach allowed us to study the rapid temperature change around the nippoint where the towpreg and composite substrate meet and to continuously monitor the temperature distribution inside the composite cylinders. In the next section, we discuss the equipment used in the in-situ measurement system.

5.2 Equipment

The in-situ measurements were achieved by a Litton Poly-Scientific AC4598 slip ring assembly which was installed between thermocouples and the data acquisition (DAQ) system. The slip ring has 18 conductors and thus is able to record nine channels of data simultaneously during winding. It is

mounted on an elongated shaft attached to the mandrel as shown in Figure 5.1.

Because of the rapid temperature change involved in the on-line consolidation process, a real time data acquisition system with a high sampling rate is required. A PC-based data acquisition system by National Instruments was selected for this purpose. The DAQ system consists of four major components, namely SCXI signal conditioning modules, DAQ board, LabVIEW software, and a computer. Figure 5.2 shows a photograph of the DAQ system.

An experimental composite ring was manufactured with eight K-type, fast-responding thermocouples installed in various position inside the ring. Figure 5.3 schematically shows the position of each thermocouple. An Infra-red temperature sensor were also installed on the consolidation head to measure the surface temperature of the composite ring.

During winding, signals picked up by the thermocouples were sent through the slip ring, amplified by the SCXI modules, transferred from analog to digital format through the DAQ board, and finally stored as a text file on the computer hard disk.

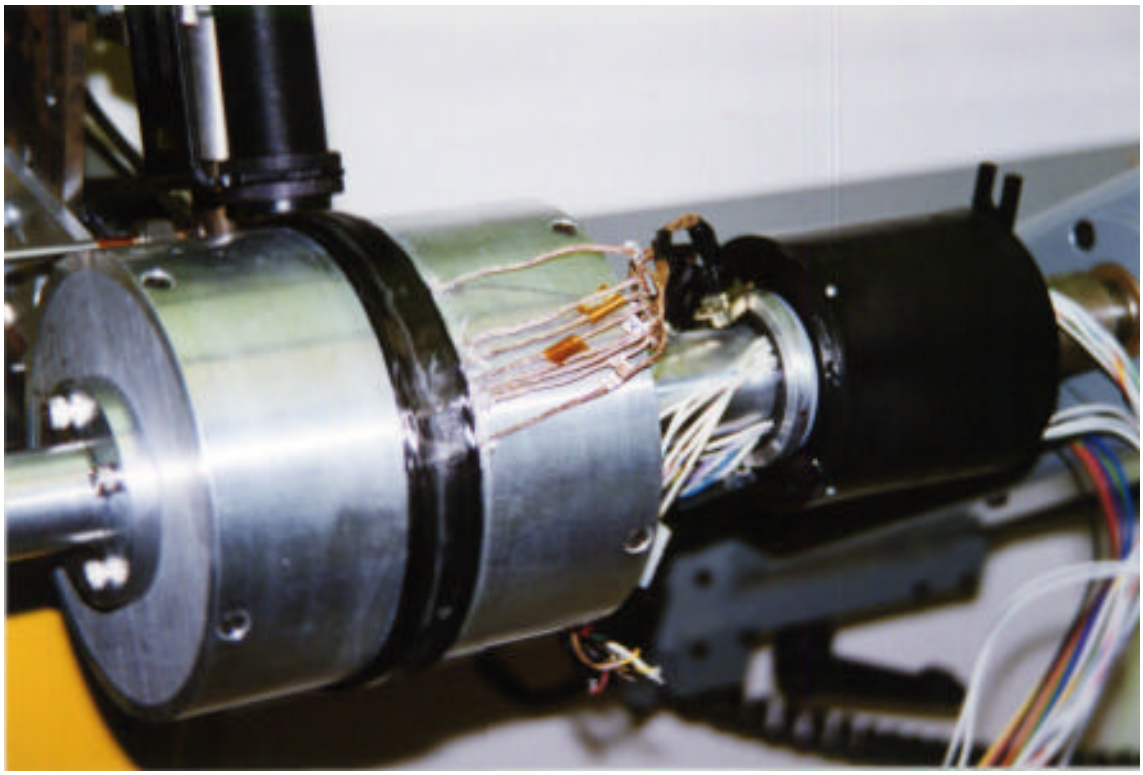

Figure 5.1 Photograph of the slip ring assembly.

Figure 5.2 Photograph of the DAQ system.

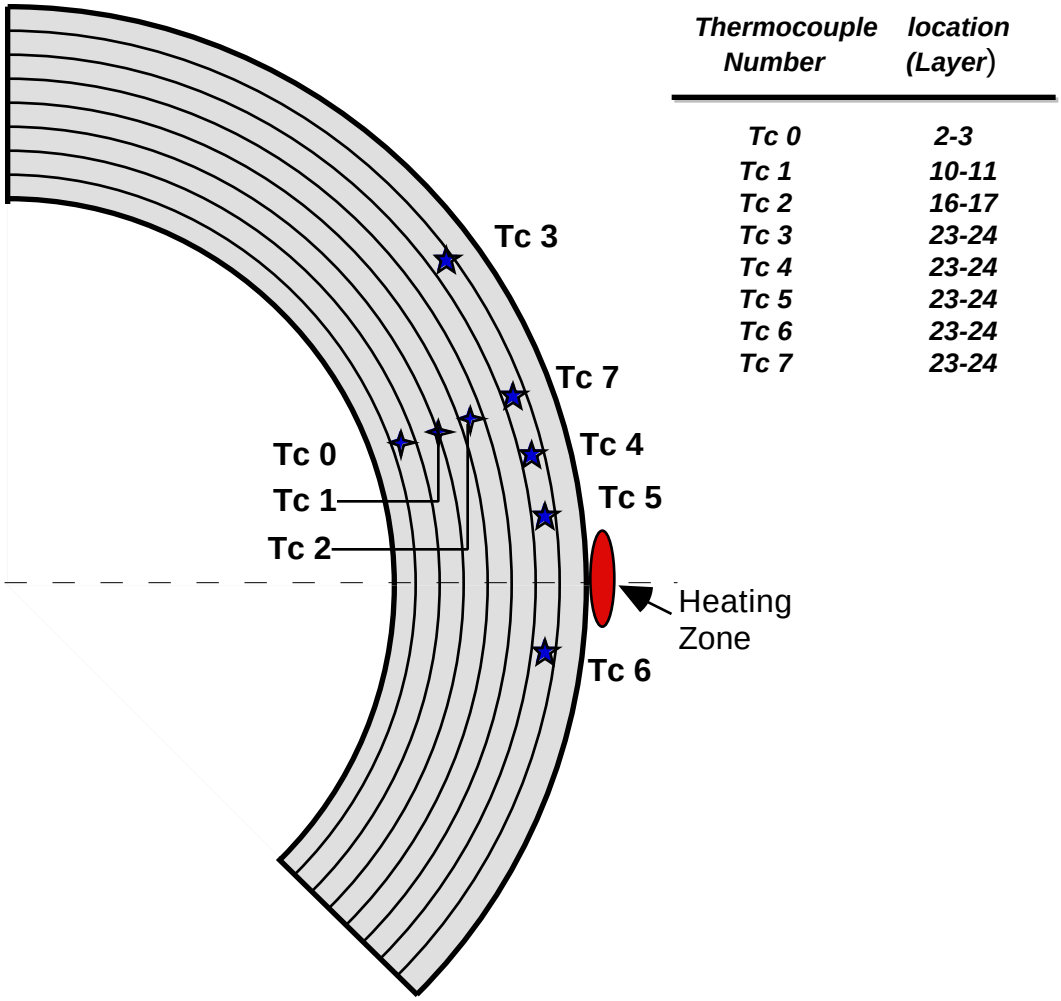

Figure 5.3 Locations of thermocouples installed in the composite ring.

5.3 Results

The in-situ measurement system was used to investigate the temperature distribution through the thickness and along the circumferential direction during winding. Two types of experiments were conducted. First, the hot-air heater was aimed at the stationary mandrel and between thermocouples Tc 5 and Tc 6 as indicated in Figure 5.3, to measure the maximum temperature achievable when the nozzle temperature was set to 650°C (1200°F). Figures 5.4 and 5.5 show the temperature distribution through thickness and along the circumferential direction, respectively, for a stationary composite ring. Second, with the nozzle temperature set to 650°C (1200°F) and winding speed to 1.5 rpm, the temperature distribution through thickness was measured as shown in Figure 5.6.

The in-situ measurement system was also used to study the impact of winding speed. As shown in Figure 5.7, temperature is plotted versus time for different mandrel speeds at thermocouple number #7 located between the twentieth and twenty-first layers. It is noted that the winding speed has a great impact on the maximum temperature and the maximum temperatures at three layers beneath surface at all three winding speeds are well below the melting point of APC-2 composites.

After finishing the in-situ temperature measurements, it became clear that the single air heater design could not melt the resin and create a molten zone on the surface of the composite substrate due to energy losses to the

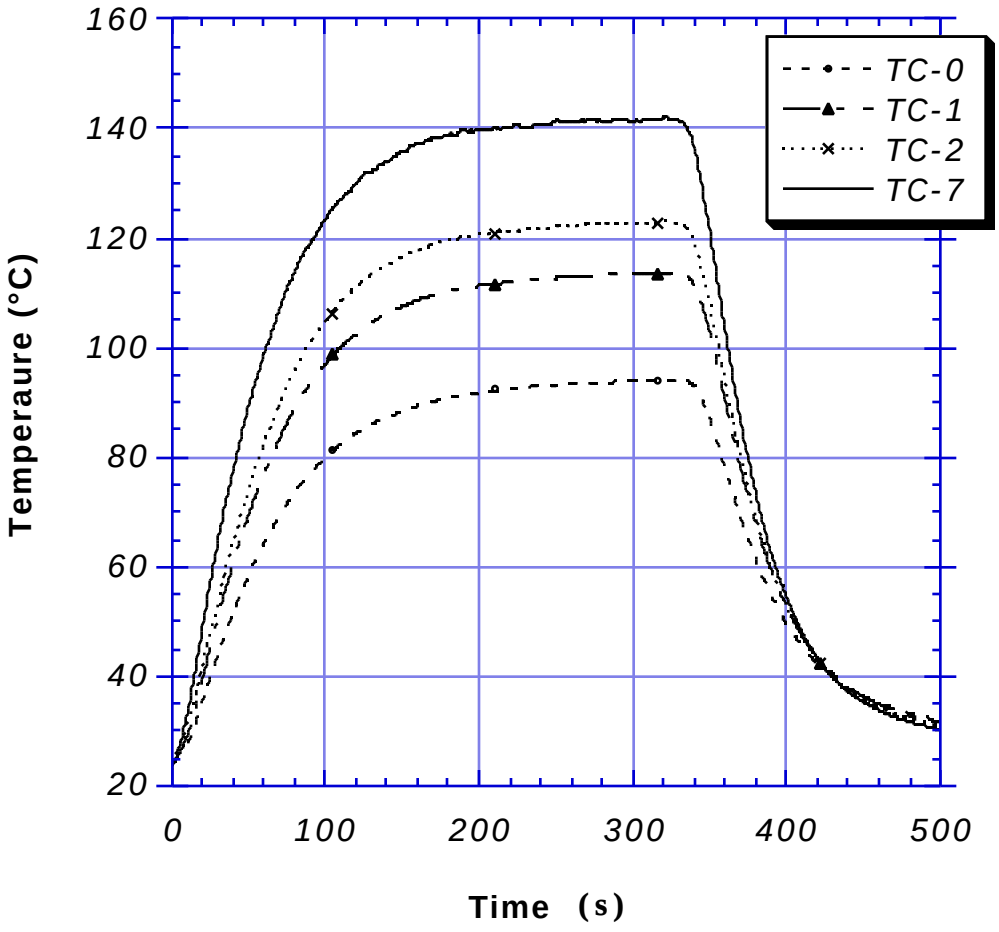

Figure 5.4 Typical temperature distribution through the thickness.

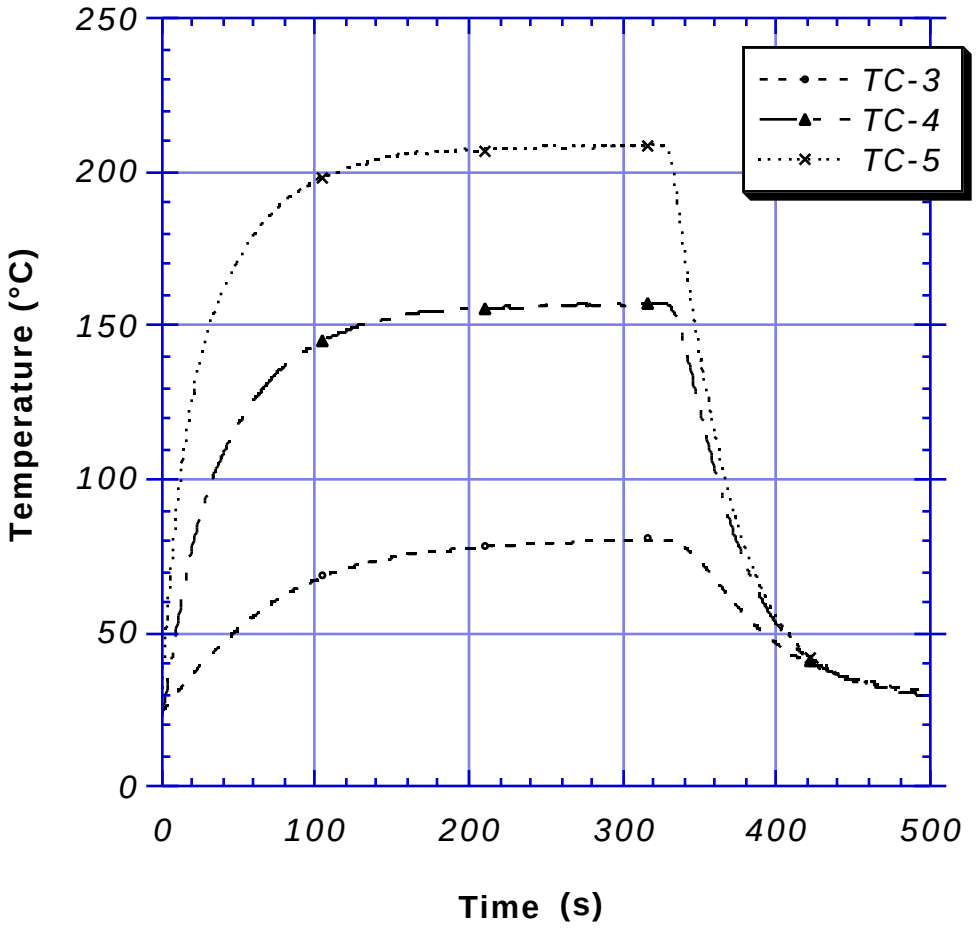

Figure 5.5 Typical temperature distribution along the circumferential direction.

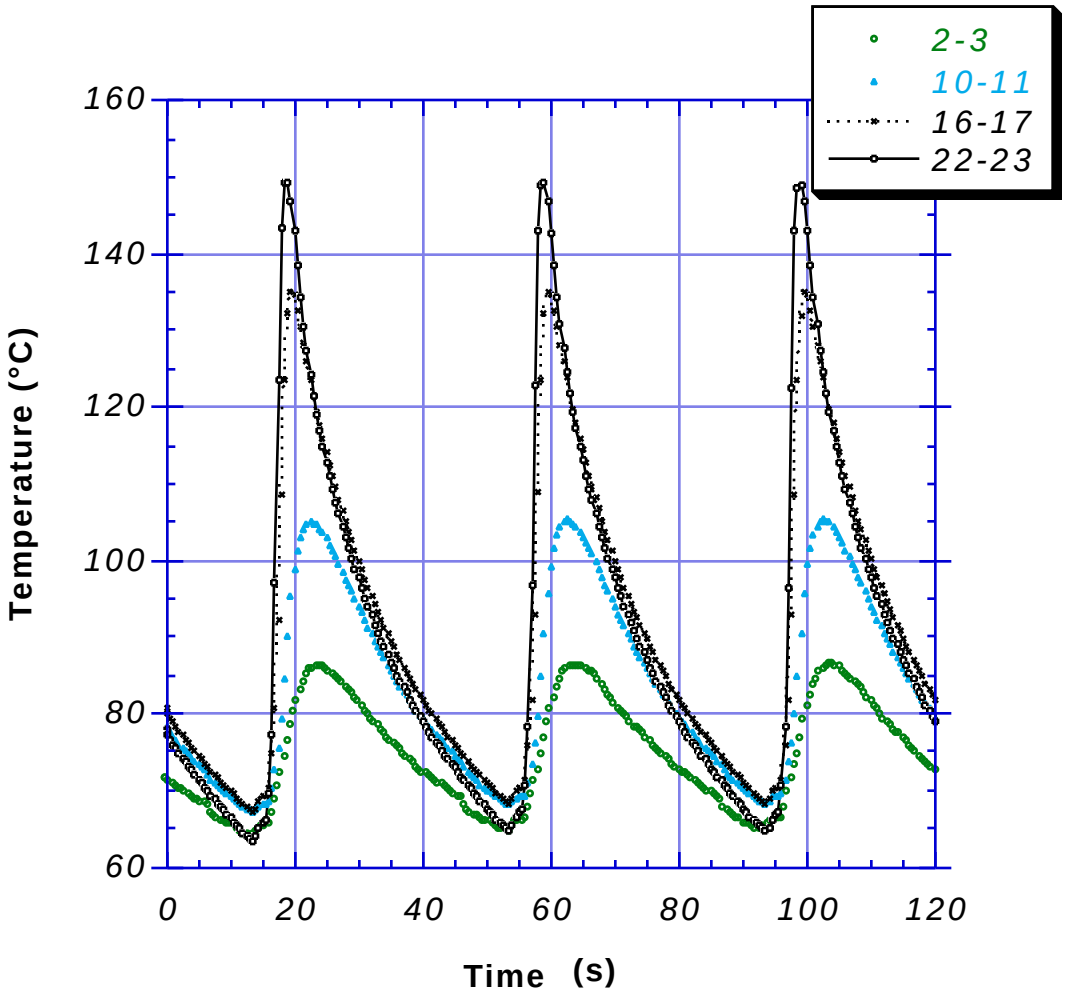

Figure 5.6 Measured temperatures through the thickness during winding. The thermocouples are located between the layers given in the inset.

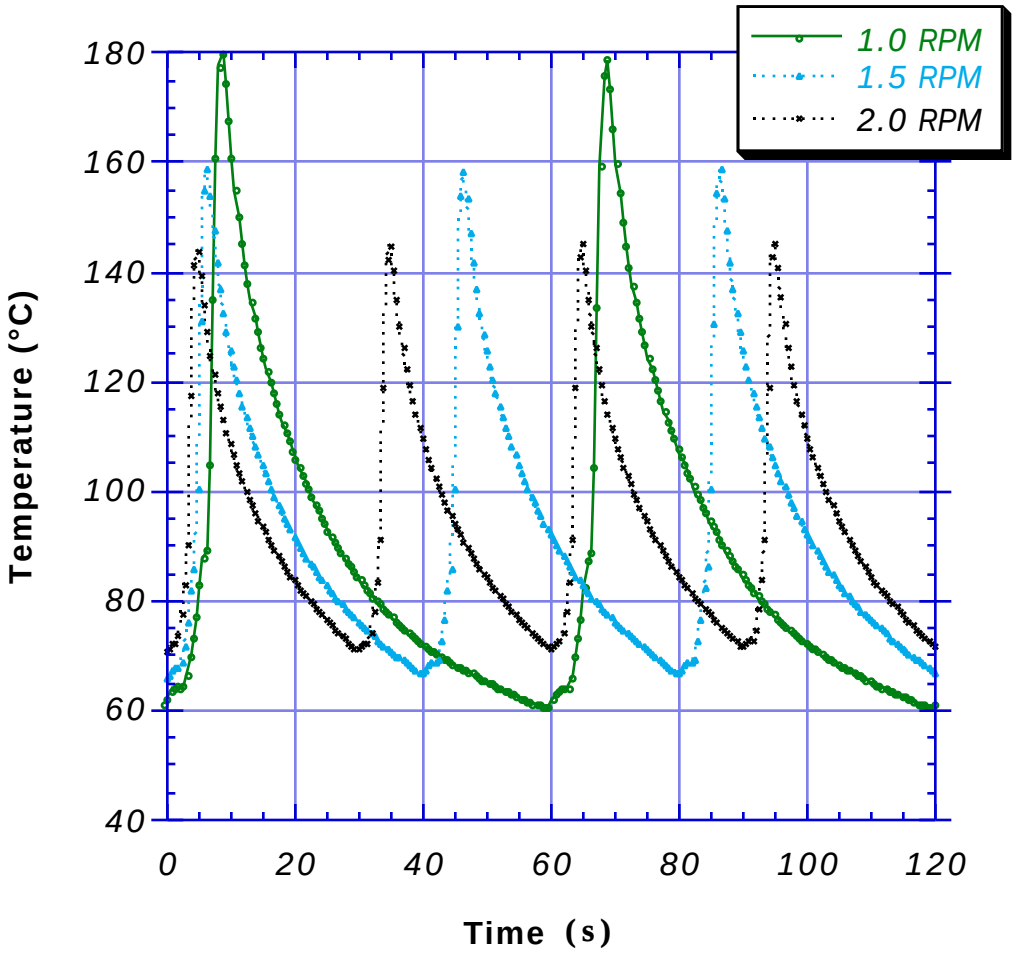

Figure 5.7 The impact of winding speed on the maximum temperature at three layers beneath surface. The winding speeds are denoted in the inset.

mandrel-composite assembly and to the environment. To overcome this obstacle, instead of aiming the heater at the surface of the composite substrate, the heater was focused directly at the towpreg, since the towpreg is much easier to melt thoroughly due to its size. A small area of APC-2 towpreg is melted right before entering the consolidation roller. Then the roller compacts the molten towpreg onto the warm surface of the composite substrate. Intimate contact and bonding between layers are achievable as long as the towpreg is properly melted under a set of particular processing parameters.

Although the in-situ measurement system can easily measure the temperature distribution inside the composite ring, the measurements are valid for only one set of processing conditions. A science-based heat transfer model can be used to quickly determine the temperature distribution in the composite-mandrel assembly for various conditions that might be applied during the on-line consolidation process. In the following chapter, the details of the formulation and construction of the finite element model are presented.

6 On-Line Consolidation Model

6.1 Introduction

The quality of thermoplastic composites depends strongly on their thermal history during processing; therefore it is important to investigate the temperature distribution in the composite during the fabrication process. A comprehensive transient thermal analysis must be developed to simulate the rapid temperature change associated with the manufacturing process. In order to effectively investigate this complicated problem, the present study aims at predicting the temperature distribution in the composite during processing using finite element models based on ABAQUS.

In the following section, we will briefly discuss the fundamental equations involved in transient heat transfer and the finite element formulations in ABAQUS. Then, the finite element model for thermal analysis is constructed and used to predict the temperature field. Once the temperature distribution and thermal history are obtained, the last step is to estimate the formation of process induced thermal stresses using thermal stress analysis.

6.2 Transient Heat Transfer Model Development

6.2.1 Mathematical Formulation

Consider a focused heat source, aiming at the interface between incoming towpreg and the composite substrate, as shown in Figure 6.1. There are five different components included in the domain of interest, namely the compaction roller, mandrel, APC-2 towpreg, composite cylinder, and release cloth. A small area of the outer surface of the composite substrate and towpreg are heated by the focused heat source and the heat is propagated away from the heating area. The outer surfaces of the substrate and towpreg are subjected to free convection and radiation. The free convection and radiation are responsible for heat losses at the surface of the composite cylinder.

The overall thermal energy balance must be maintained at all times. In other words, the net rate of heat entering across the control surface plus the rate of energy generated in the control volume must be equal to the rate of increase of internal energy of the control volume. The Lagrangian formulation of the energy balance equation for an arbitrary control volume can be expressed as follows:

$$\int_{\Gamma} \boldsymbol{q}\, d\Gamma + \int_{\Omega} \boldsymbol{r}\, d\Omega = \int_{\Omega} \rho\, \dot{\boldsymbol{U}}\, d\Omega \tag{6.1}$$

where:

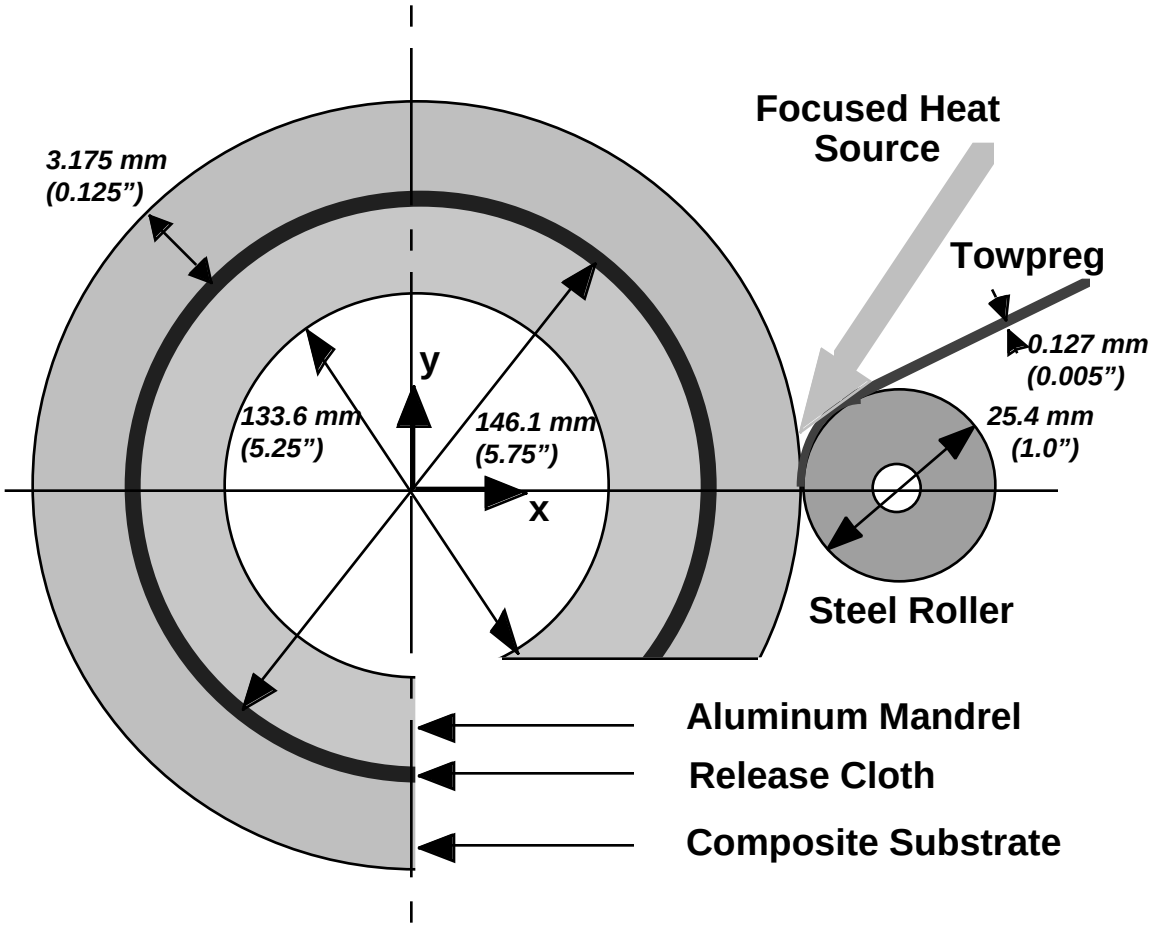

Figure 6.1 Geometry of the transient heat transfer problem.

$\int_\Gamma \boldsymbol{q}\, d\Gamma$ = surface flux term, $\boldsymbol{q}$ positive into the body,

$\int_\Omega \boldsymbol{r}\, d\Omega$ = volumetric flux term (source),

$\int_\Omega \rho \dot{\boldsymbol{U}}\, d\Omega$ = storage term,

$\boldsymbol{q}$ is the heat flux per unit of current area crossing surface Γ from surrounding into the body (scalar quantity), ρ is material's density, $\boldsymbol{r}$ is internal heat generation per unit volume, and $\dot{\boldsymbol{U}}$ is the rate of change of internal energy per unit mass per time.

The governing equations, derived in Appendix A, are given by

$$-\frac{\partial}{\partial \tilde{\boldsymbol{x}}} \cdot \tilde{\boldsymbol{q}} + \boldsymbol{r} - \rho \dot{\boldsymbol{U}} = \boldsymbol{0} \qquad \text{(A.5)}$$

in matrix form and

$$(\boldsymbol{K}_{ij}\boldsymbol{T}_{,j})_{,i} + \boldsymbol{r} = \boldsymbol{C}_p \rho \dot{\boldsymbol{T}} \qquad \text{on domain } \Omega \qquad \text{(A.9)}$$

in tensor form where $\tilde{\boldsymbol{q}}$ is the heat flux vector, $\boldsymbol{K}_{ij}$ is thermal conductivity, $\boldsymbol{T}$ is temperature, $\boldsymbol{C}_p$ is the specific heat capacity, $\boldsymbol{t}$ is time and $\dot{\boldsymbol{T}} = \frac{\partial \boldsymbol{T}}{\partial \boldsymbol{t}}$.

The boundary conditions can be summarized as:

- along the inner surface of the mandrel, the temperature is prescribed,
- throughout the contact surface, i.e. the heat affected zone, heat-flux is prescribed,
- along the unheated boundary, heat dissipation due to convection and radiation are prescribed.

6.2.2 Finite Element Formulation in ABAQUS for Transient Heat Transfer Problem

The derivation in this section is based on the User's Manual, the Theory Manual and the example Problems Manual for the ABAQUS finite element software package [74-76]. The starting point in the finite element formulation for transient heat transfer analysis is the differential form of energy equation. The equation, as derived in Appendix A, is

$$\rho \dot{\boldsymbol{U}} = -\frac{\partial}{\partial \tilde{\boldsymbol{x}}} \cdot \tilde{\boldsymbol{q}} + \boldsymbol{r} \tag{6.2}$$

Next, an equivalent variational form of the thermal energy balance equation is obtained by multiplying Eq (6.2) by an arbitrary variational temperature field, $\delta \boldsymbol{T}$ and integrating the equation over the domain or volume Ω.

$$\int_{\Omega} \rho \dot{\boldsymbol{U}}\, \delta \boldsymbol{T}\, d\Omega = -\int_{\Omega} \left(\frac{\partial}{\partial \tilde{\boldsymbol{x}}} \cdot \tilde{\boldsymbol{q}}\right) \delta \boldsymbol{T}\, d\Omega + \int_{\Omega} \boldsymbol{r}\, \delta \boldsymbol{T}\, d\Omega \tag{6.3}$$

Applying the chain rule to the first term on the right hand side of Eq (6.3) yields

$$\int_{\Omega} \rho \dot{\boldsymbol{U}}\, \delta \boldsymbol{T}\, d\Omega = \int_{\Omega} \left[-\frac{\partial}{\partial \tilde{\boldsymbol{x}}} \cdot (\tilde{\boldsymbol{q}}\, \delta \boldsymbol{T}) + \tilde{\boldsymbol{q}} \cdot \frac{\partial}{\partial \tilde{\boldsymbol{x}}} (\delta \boldsymbol{T}) \right] d\Omega + \int_{\Omega} \boldsymbol{r}\, \delta \boldsymbol{T}\, d\Omega . \tag{6.4}$$

If we apply the divergence theorem to the first term on the right hand side and transform a volume integral to a surface integral, we can rewrite the Eq. (6.4) as

$$\int_{\Omega} \rho \dot{\boldsymbol{U}}\, \delta \boldsymbol{T}\, d\Omega - \int_{\Omega} \frac{\partial \delta \boldsymbol{T}}{\partial \tilde{\boldsymbol{x}}} \cdot \tilde{\boldsymbol{q}}\, d\Omega = -\int_{\Gamma} \tilde{\boldsymbol{q}} \cdot \tilde{\boldsymbol{n}}\, \delta \boldsymbol{T}\, d\Gamma + \int_{\Omega} \boldsymbol{r}\, \delta \boldsymbol{T}\, d\Omega \tag{6.5}$$

or

$$\int_\Omega \rho\, \dot{\boldsymbol{U}}\, \delta \boldsymbol{T}\, d\Omega - \int_\Omega \frac{\partial \delta \boldsymbol{T}}{\partial \tilde{\boldsymbol{x}}} \cdot \tilde{\boldsymbol{q}}\, d\Omega = \int_\Gamma \boldsymbol{q}\, \delta \boldsymbol{T}\, d\Gamma + \int_\Omega \boldsymbol{r}\, \delta \boldsymbol{T}\, d\Omega \tag{6.6}$$

where $\boldsymbol{q} = -\tilde{\boldsymbol{q}} \cdot \tilde{\boldsymbol{n}}$ is the heat flux per unit of current area crossing surface Γ from the surroundings into the body (scalar quantity).

This is one of the weak forms of the energy balance equation. An alternative form can be obtained by substituting the Fourier's heat conduction law, i.e. $\tilde{\boldsymbol{q}} = -\bar{\bar{\boldsymbol{k}}} \cdot \frac{\partial \boldsymbol{T}}{\partial \tilde{\boldsymbol{x}}}$, into Eq. (6.5):

$$\int_\Omega \rho\, \dot{\boldsymbol{U}}\, \delta \boldsymbol{T}\, d\Omega + \int_\Omega \frac{\partial \delta \boldsymbol{T}}{\partial \tilde{\boldsymbol{x}}} \cdot \bar{\bar{\boldsymbol{k}}} \cdot \frac{\partial \boldsymbol{T}}{\partial \tilde{\boldsymbol{x}}}\, d\Omega = \int_\Gamma \boldsymbol{q}\, \delta \boldsymbol{T}\, d\Gamma + \int_\Omega \boldsymbol{r}\, \delta \boldsymbol{T}\, d\Omega \tag{6.7}$$

where $\bar{\bar{\boldsymbol{K}}} = \boldsymbol{K}_{ij}$ is the anisotropic thermal conductivity matrix.

Let us now discretize the volume geometrically using finite elements and let the temperature $\boldsymbol{T}$ and the temperature gradient $\frac{\partial \boldsymbol{T}}{\partial \tilde{\boldsymbol{x}}}$ within a finite element be interpolated from nodal temperatures $\bar{\boldsymbol{T}}^N$:

$$\boldsymbol{T} = \boldsymbol{N}^N \bar{\boldsymbol{T}}^N \text{ and } \frac{\partial \boldsymbol{T}}{\partial \tilde{\boldsymbol{x}}} = \frac{\partial \boldsymbol{N}^M}{\partial \tilde{\boldsymbol{x}}} \bar{\boldsymbol{T}}^M \tag{6.8}$$

where $\boldsymbol{N}^M$ and $\boldsymbol{N}^N$ are the interpolation functions or shape functions and the superscripts M and N are the number of nodes.

The standard Galerkin approach states that the variational temperature, $\delta \boldsymbol{T}$, is interpolated with the same functions as temperature. Therefore the variational temperature and the temperature gradient can be written as

$$\delta T = N^N \delta \bar{T}^N \text{ and } \frac{\partial \delta T}{\partial \tilde{x}} = \frac{\partial N^N}{\partial \tilde{x}} \delta \bar{T}^N . \tag{6.9}$$

In ABAQUS, the function N^N can be in linear or parabolic polynomial product forms for one-, two-, and three-dimensional elements, as well as for axisymmetric elements.

We shall now introduce this interpolation into the heat balance equation and obtain the approximation as follows:

$$\delta \bar{T}^N \left\{ \int_\Omega N^N \rho \dot{U} \, d\Omega + \int_\Omega \frac{\partial N^N}{\partial \tilde{x}} \cdot \bar{\bar{k}} \cdot \frac{\partial N^M}{\partial \tilde{x}} \, d\Omega \, \bar{T}^M - \int_\Gamma q \, N^N d\Gamma - \int_\Omega r N^N d\Omega \right\} = 0 . \tag{6.10}$$

Since the variational quantities $\delta \bar{T}^N$ are arbitrary, the equation inside the parenthesis must be identically equal to zero, or

$$\int_\Omega N^N \rho \dot{U} \, d\Omega + \int_\Omega \frac{\partial N^N}{\partial \tilde{x}} \cdot \bar{\bar{k}} \cdot \frac{\partial N^M}{\partial \tilde{x}} \, d\Omega \, \bar{T}^M = \int_\Gamma q \, N^N d\Gamma + \int_\Omega r \, N^N d\Omega . \tag{6.11}$$

If $\dot{U}$ is replaced by Eq. (A.7), Eq.(6.10) can be written as

$$\begin{aligned} &\int_\Omega N^N \rho C_p N^M \dot{\bar{T}}^M d\Omega + \int_\Omega \frac{\partial N^N}{\partial \tilde{x}} \cdot \bar{\bar{k}} \cdot \frac{\partial N^M}{\partial \tilde{x}} \, d\Omega \, \bar{T}^M \\ &= \int_\Gamma q \, N^N d\Gamma + \int_\Omega r \, N^N d\Omega \end{aligned} \tag{6.12}$$

where C_p is the specific heat of the material.

The approximate heat balance can also be expressed in matrix form as

$$\left[C^e\right]\left\{\dot{T}^e\right\} + \left[K^e\right]\left\{T^e\right\} = \left\{Q^e\right\} \tag{6.13}$$

or of the form as

$$C^e_{MN}(T^e)\dot{T}^e + K^e_{MN}(T^e)T^e = Q^e_N(T^e) \tag{6.14}$$

in which

$\left[C^e\right] = C^e_{MN}(T^e) = \int_\Omega N^N \rho C_p N^M d\Omega$ is the heat capacitance matrix,

$\left[K^e\right] = K^e_{MN}(T^e) = \int_\Omega \frac{\partial N^N}{\partial \tilde{x}} \cdot \bar{\bar{k}} \cdot \frac{\partial N^M}{\partial \tilde{x}} d\Omega$ is the conductivity matrix,

$\left\{Q^e\right\} = Q^e_N(T^e) = \int_\Gamma q\, N^N d\Gamma + \int_\Omega r\, N^N d\Omega$ is the external flux vector,

$\left\{\dot{T}^e\right\}$ is the vector of time rate of nodal temperature change and

$\left\{T^e\right\}$ is the nodal temperature vector.

This set of equations is the basis for the uncoupled, conductive heat transfer analysis. For transient heat transfer problems, the Eq. (6.11) is integrated in time. In ABAQUS, the temporal term is treated by the finite difference method using the backward difference algorithm:

$$\dot{U}_{t+\Delta t} = \frac{(U_{t+\Delta t} - U_t)}{\Delta t}. \tag{6.15}$$

where $U_{t+\Delta t}$ and U_t are the internal energy at $t+\Delta t$ and t, respectively.

Introducing the operator, Eq. (6.15), into the energy balance, Eq. (6.11), yields:

$$\begin{aligned} &\frac{1}{\Delta t}\int_\Omega N^N \rho\,(U_{t+\Delta t} - U_t) d\Omega + \int_\Omega \frac{\partial N^N}{\partial \tilde{x}} \cdot \bar{\bar{k}}\Big|_{t+\Delta t} \cdot \frac{\partial N^M}{\partial \tilde{x}}\, d\Omega\, \bar{T}^M_{t+\Delta t} \\ &-\int_\Gamma q\Big|_{t+\Delta t} N^N d\Gamma - \int_\Omega r\Big|_{t+\Delta t} N^N d\Omega = 0 \end{aligned} \tag{6.16}$$

or

$$\begin{aligned} &\int_\Omega N^N \rho C_p\Big|_{t+\Delta t} N^M \frac{(\bar{T}^M_{t+\Delta t} - \bar{T}^M_t)}{\Delta t} d\Omega + \int_\Omega \frac{\partial N^N}{\partial \tilde{x}} \cdot \bar{\bar{k}}\Big|_{t+\Delta t} \cdot \frac{\partial N^M}{\partial \tilde{x}}\, d\Omega\, \bar{T}^M_{t+\Delta t} \\ &-\int_\Gamma q\Big|_{t+\Delta t} N^N d\Gamma - \int_\Omega r\Big|_{t+\Delta t} N^N d\Omega = 0 \end{aligned}. \tag{6.17}$$

The backward difference scheme is chosen for its unconditional stability and its simplicity of implementation. Therefore, for linear problems, there is no restriction on selecting a time increment. The stability of the operator is important because it allows ABAQUS to analyze problems where the solution is sought over a very long period of time.

ABAQUS can handle the most general nonlinear case in which thermal material properties and boundary conditions depend on temperature. The thermal material properties are defined in the *MATERIAL block of the input file. For example, the thermal conductivity matrix is specified under the command of *CONDUCTIVITY and can be provided as a function of temperature. Referring to Figure 6.2, the orthotropic conductivity matrix for composite materials can be expressed as

$$\begin{bmatrix} K_{XX} & K_{XY} & 0 \\ K_{XY} & K_{YY} & 0 \\ 0 & 0 & K_{ZZ} \end{bmatrix}, \tag{6.18}$$

where

$$K_{XX} = K_{11}Cos^2\theta + K_{22}Sin^2\theta$$
$$K_{YY} = K_{11}Sin^2\theta + K_{22}Cos^2\theta$$
$$K_{ZZ} = K_{22} = K_{33}$$
$$K_{XY} = (K_{11} - K_{22}) \cdot Sin\theta\, Cos\theta = K_{YX}$$

In ABAQUS, the orthotropic conductivity matrix is defined by simply setting the TYPE parameter to ORTHO.

The application of boundary conditions in ABAQUS is also quite straightforward. Prescribed temperatures are imposed at the nodal level and

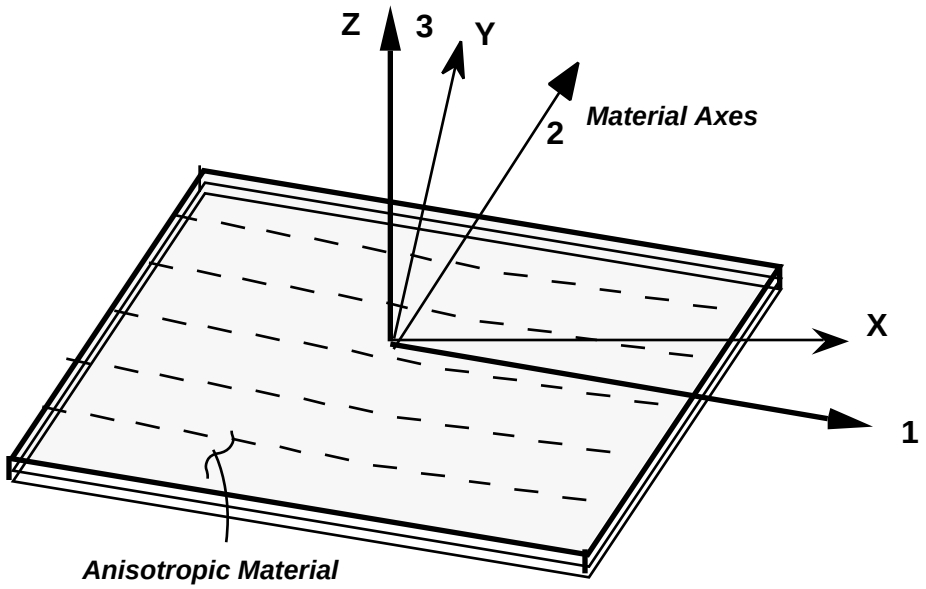

Figure 6.2 Notation for anisotropic conductivity.

can be varied over time by referencing a predefined *AMPLITUDE option. Surface flux, DFLUX, is applied over element edges and can also be varied in time. *FILM is used for applying a convective boundary condition governed by

$$q = -h(T - T_{\infty}) \tag{6.19}$$

where h is the film coefficient.

Note that the film coefficient plays a key role in the heat transfer solution and can be difficult to characterize. Therefore, an experimental calibration is needed to determine the film coefficient. Finally, Newton's method is used to solve the set of nonlinear governing equations as listed in Equation (6.17). By default in ABAQUS, the iterative process is continued until the size of the correction to the approximate solution is less than 1% of the incremental change to the solution for the current time step.

In the following sections, we characterize the film coefficient, h, to simulate the combined effect of radiation and convective boundary conditions associated with hot-air heating. Then we investigate the temperature field during winding. The mandrel rotation is represented by motion of the heater. Finally, the same film coefficient is used to investigate the temperature distribution inside the towpreg before it reaches the nippoint.

6.3 Transient Heat Transfer Finite Element Simulation

6.3.1 Characterization of the Film Coefficient

As stated earlier, a focused hot-air heater is used as the single energy source in the present on-line consolidation system. Since we are interested in the conductive heat transfer problem of the composite-mandrel assembly, the convective heat transfer problem associated with the hot-air heater has been ignored. This means that the temperature distribution inside air flow is neglected and the hot-air heater is treated simply as a convective boundary condition. However, in order to successfully model the transient heat transfer problem involved in on-line consolidation, we must characterize the film coefficient.

Consider a hot-air heater, aiming at the interface between the towpreg and composite substrate with mandrel assembly stationary. The temperature field in the composite cylinder is created by the hot-air heater which in general covers only a small area around the nippoint. The heat then is conducted from the surface into the composite and mandrel. In this case, what is considered is the effective heat flux into the composite-mandrel assembly. In hot-air heating, the effective heat flux can be represented by the actual temperature of hot-air and the film coefficient. The film coefficient depends on the flow conditions on the surface, on the surface properties, on the properties of flow media, and on the temperature difference between the hot-air and the surface of composite cylinder. Therefore, the film coefficient

can be determined only by comparing the numerical solutions with experiments under similar processing conditions.

An ABAQUS finite element model that takes into account all components involved in the on-line consolidation process was constructed. The finite element mesh and the applied boundary conditions are shown in the Figures 6.3 and 6.4. The input parameters for transient heat transfer analysis are given in Table 6.1. The transient temperature field for a stationary heat source is solved by means of the backward time-step method as described in the preceding section. The calculated temperature field and thermal history must now be compared to the experimental data obtained from the in-situ measurement system.

Figure 6.5 shows the thermal history at two positions inside the composite cylinder, as indicated in Figure 6.3. A film coefficient of 260 $w/m^{2}°K$ fits the data the best. Figure 6.6 and Figure 6.7 show the isotherms around the nippoint at four times during the stationary heating process. Note that the heat is not transferred very far away from the heat-affected zone. This means that the energy dissipation to the mandrel and surrounding area is severe; therefore, a heated mandrel and an insulated enclosure for the whole system may be necessary to minimize the heat loss and to achieve higher production rates. Figure 6.8 shows the impact of the film coefficient on the thermal history at position U1, as indicated in Figure 6.3. The larger film coefficient results in a higher temperature beneath the surface of the composite.

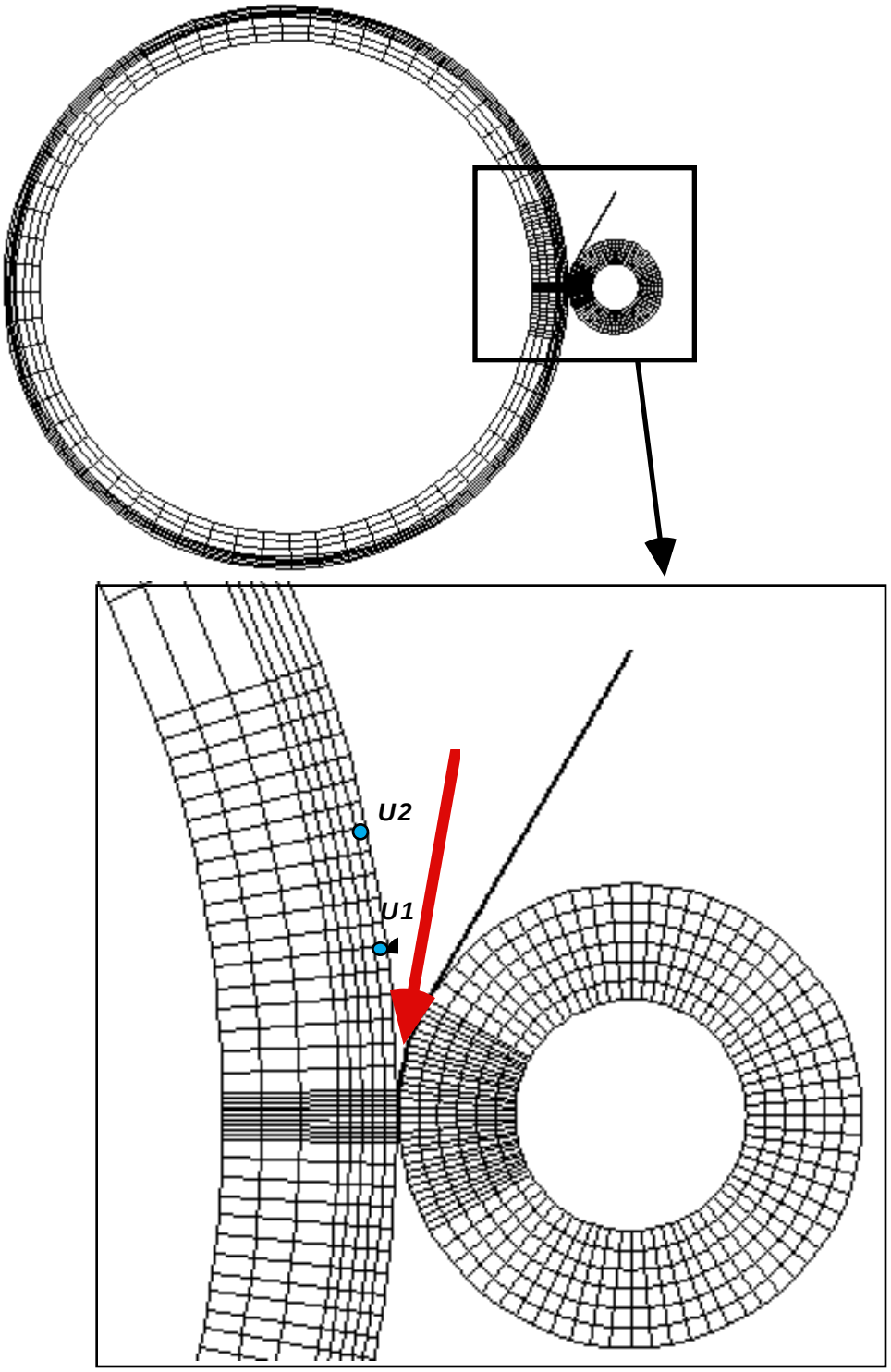

Figure 6.3 Finite element mesh for characterizing the film coefficient.

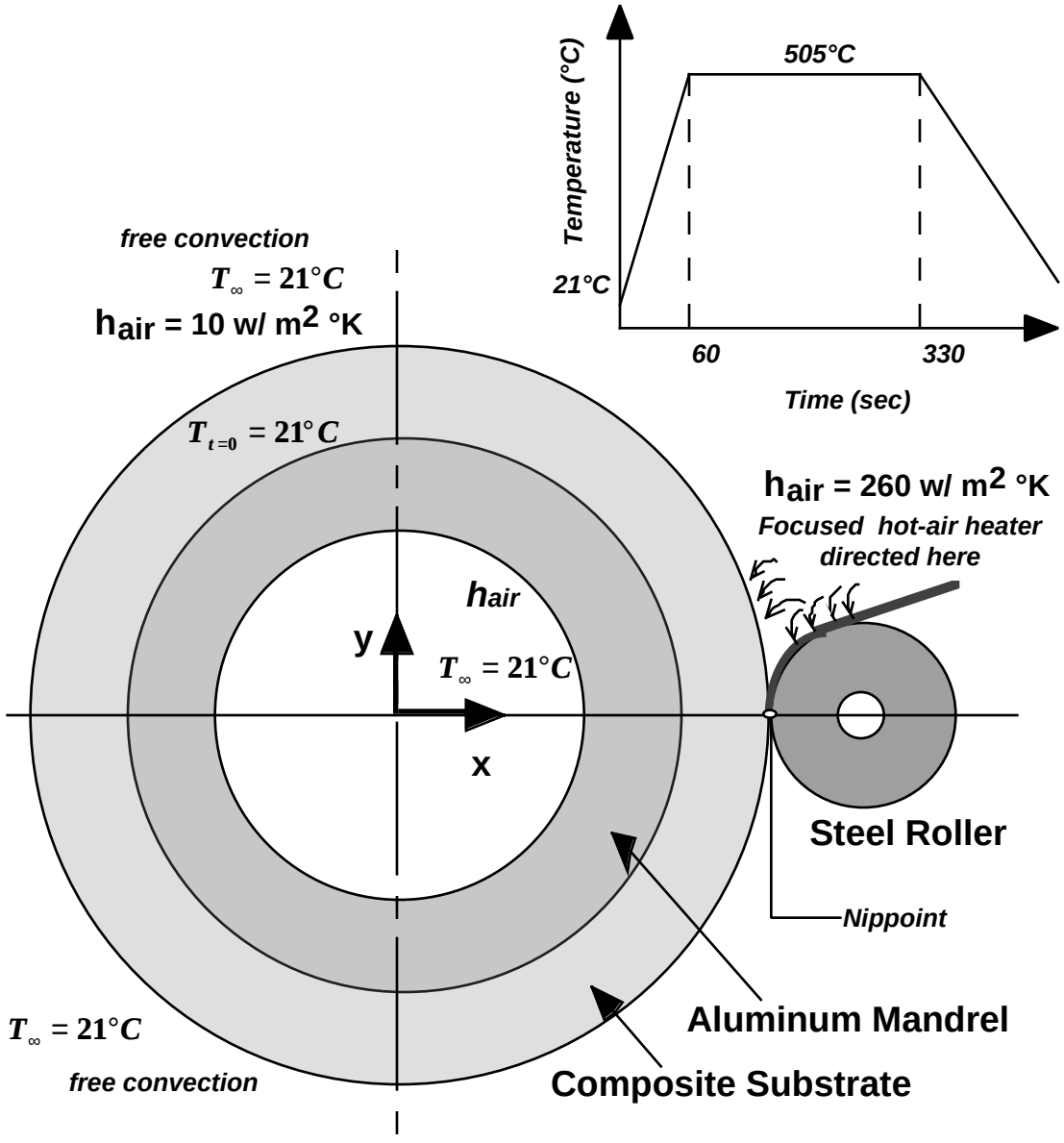

Figure 6.4 Schematic diagram of roller and composite-mandrel assembly and boundary conditions used for characterizing the film coefficient.

Table 6.1 Input parameters for heat transfer calculation.

Properties	APC-2/AS4 [64]	Aluminum	Steel
Density (kg/m^3)	1562	2700	7800
Specific heat ($J/°K$)	1425	905	473
Thermal conductivity, longitudinal ($w/m°K$)	6.0	237	43
Thermal conductivity transverse ($w/m°K$)	0.72	237	43

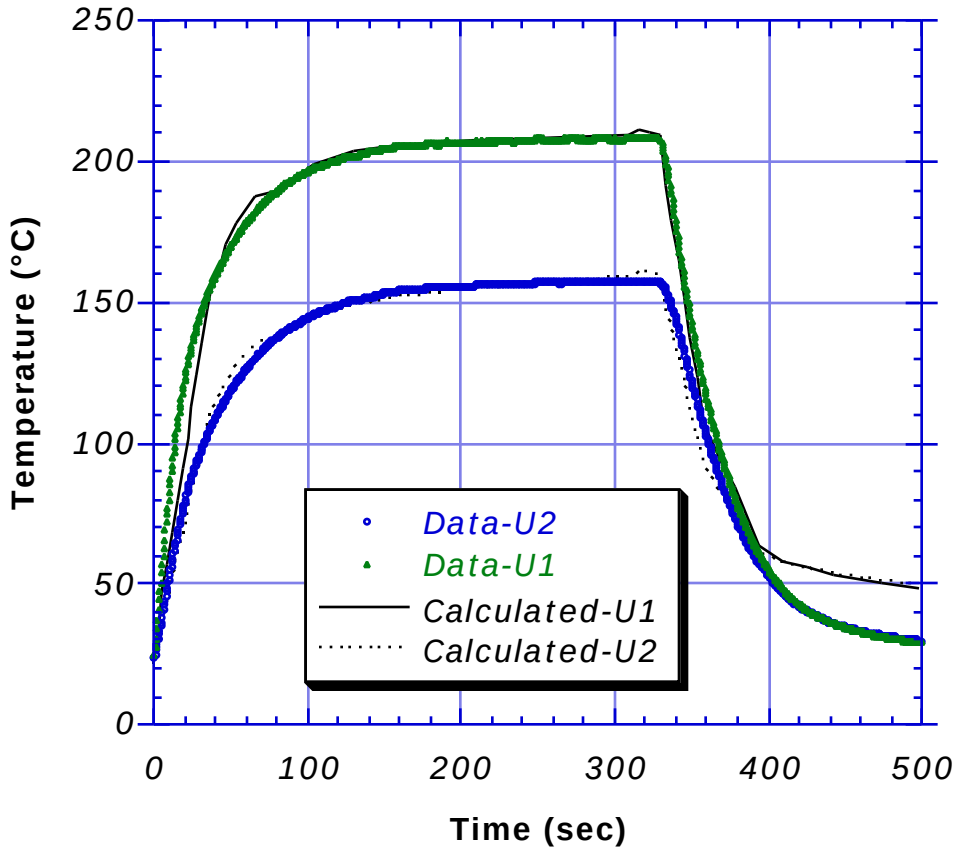

Figure 6.5 Comparison of numerical results (h=260 w / m^2°K) with in-situ measurement data. Locations of U1 and U2 are shown in Figure 6.3.

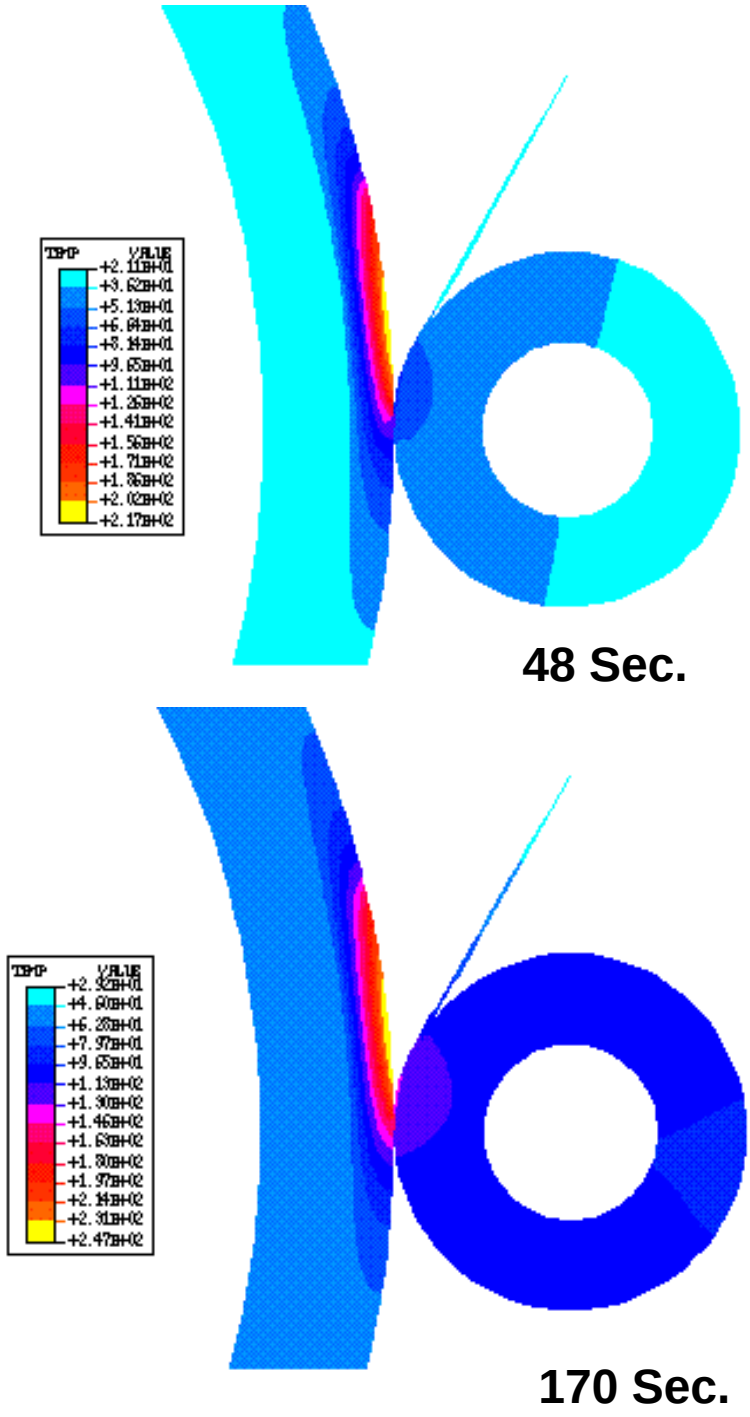

Figure 6.6 Isotherms around the nippoint at two times during the stationary heating process (48 and 170 seconds). Temperatures are in °C.

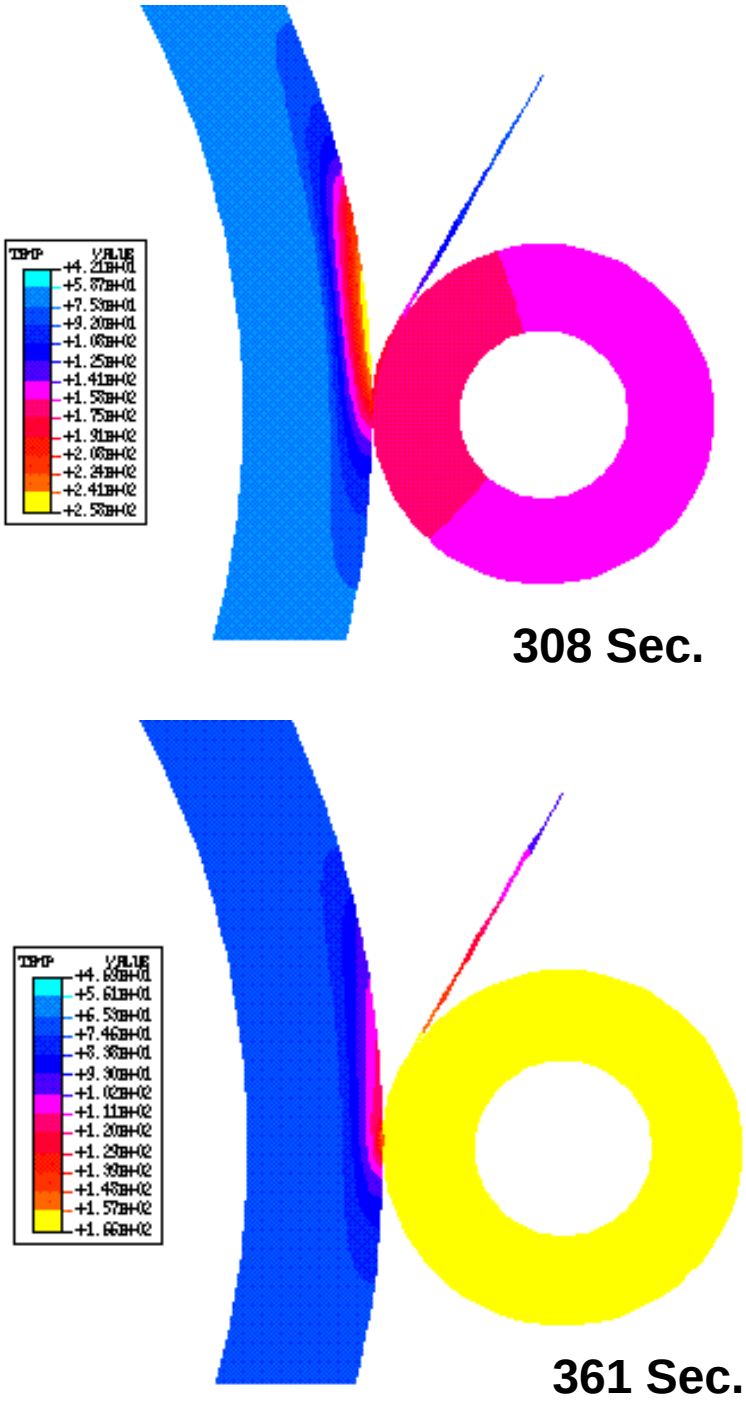

Figure 6.7 Isotherms around the nippoint at two times during the stationary heating process (308 and 361 seconds). Temperatures are in °C.

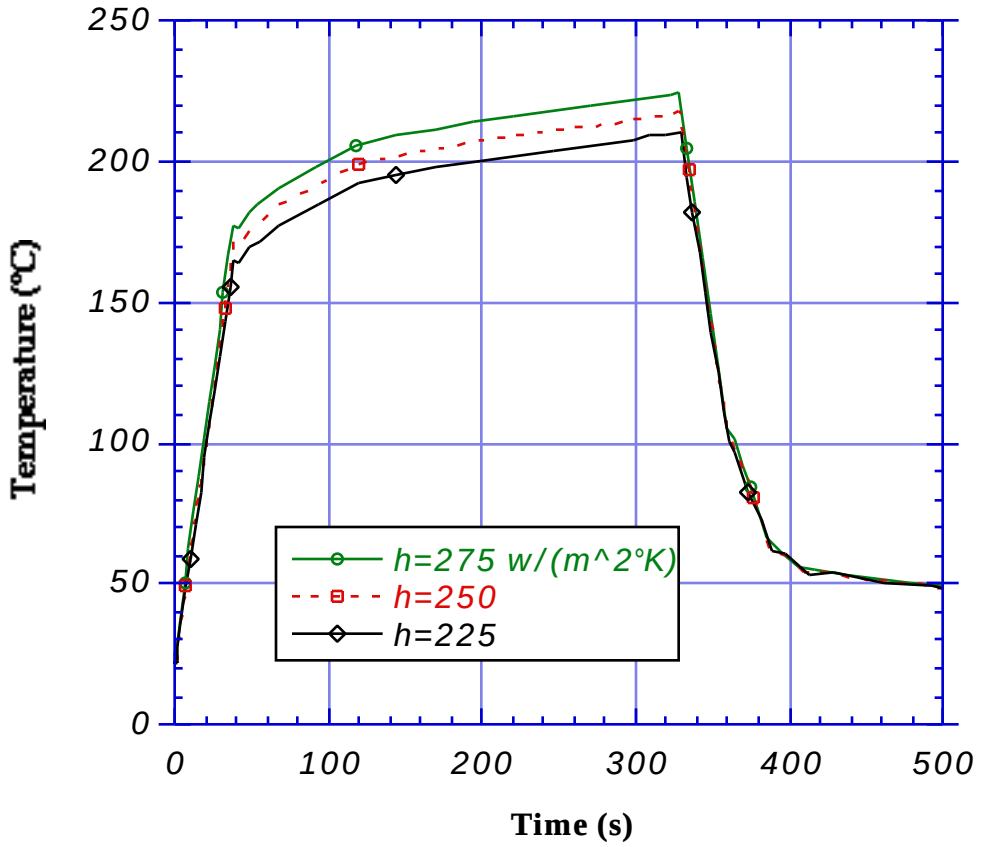

Figure 6.8 The impact of heat transfer coefficient on the thermal history .

6.3.2 Winding Simulation

The next step involved in simulating the on-line consolidation process is to rotate the composite-mandrel assembly at a certain speed. Since ABAQUS uses the Lagrangian description, in which one pays attention to a set of fixed material particles, rotating the finite element mesh that represents the composite-mandrel assembly about a fixed axis is not feasible. In order to simulate the mandrel rotation, we move the hot-air heater counter-clock-wise instead. To be more specific, the focused heat source, modeled by convective boundary condition rotates about the stationery composite-mandrel assembly. The winding speed is modeled by incrementally moving the heat source around the outer surface of the composite cylinder. First, as shown in Figure 6.9, the heat flux $\boldsymbol{q}$ remains in one position for a time period $\Delta \boldsymbol{t}$ and the temperature distribution $\boldsymbol{T^n(\tilde{x})}$ for this step is computed. Second, the flux is moved a distance $\boldsymbol{l}$ and stops there for another time period $\Delta \boldsymbol{t}$. Using the temperature distribution obtained in previous step as the initial boundary condition, the temperature field $\boldsymbol{T^{n+1}(\tilde{x})}$ is then calculated for the current step. The winding speed equals the distance $\boldsymbol{l}$ divided by time period $\Delta \boldsymbol{t}$. Consequently, the mandrel rotation is indirectly modeled by moving the heat source around the mandrel.

Figure 6.10 shows the finite element mesh used in the winding simulation. Through the thickness, the four inner most elements are assigned for the aluminum mandrel and eight outer most elements are assigned for the composite substrate. There are 1440 DC2D4 elements used in

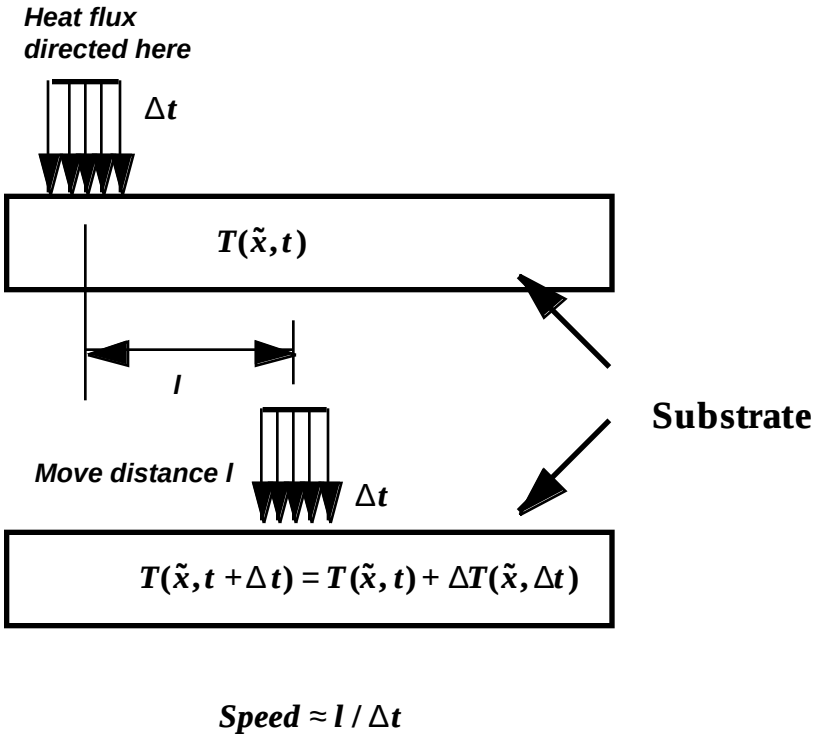

Figure 6.9 Simulation of moving heat source.

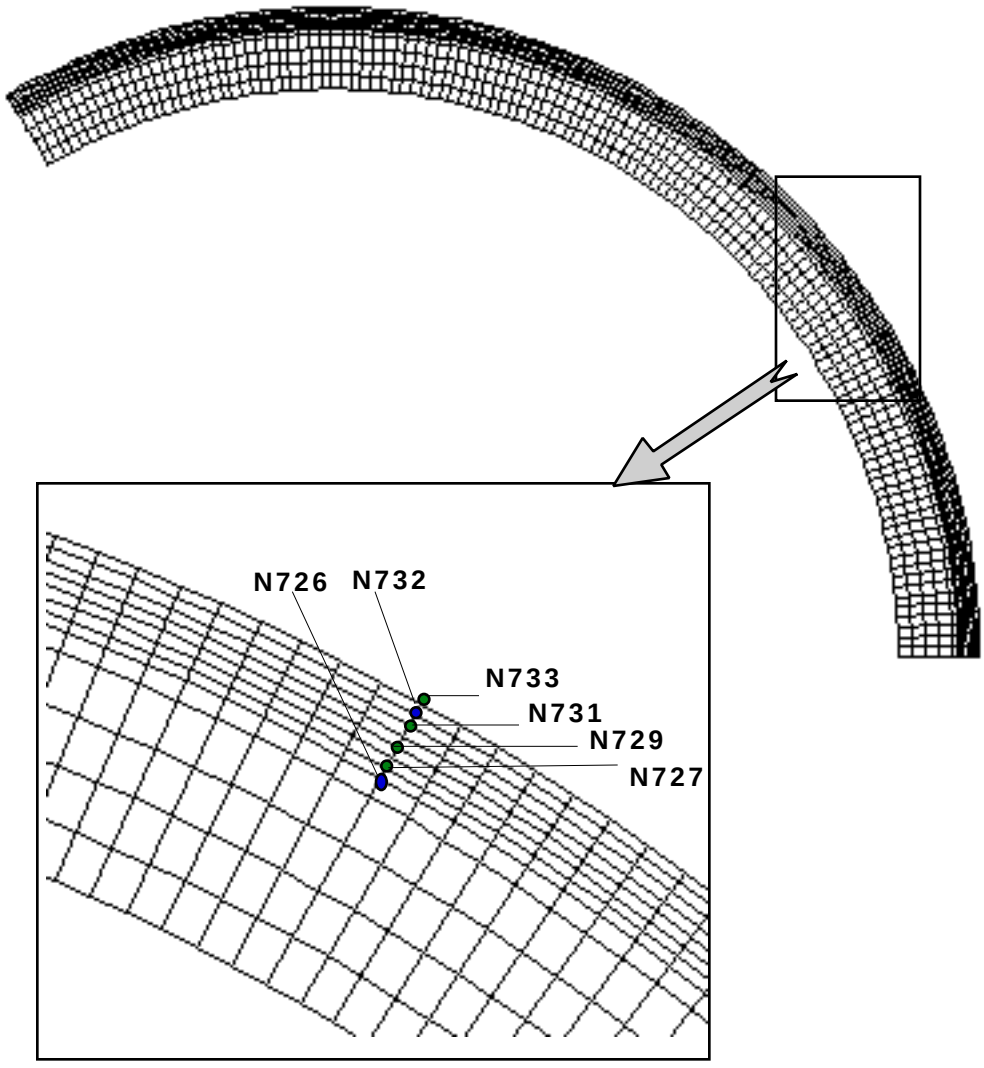

Figure 6.10 The finite element mesh used in the winding simulation.

this simulation. The thermal boundary conditions are indicated in Figure 6.11. From experiments, we noted that the temperature in the heat-affected zone is not uniform. The highest temperature occurs around the nippoint and decreases gradually along the circumferential direction. We use a series of step functions to model the temperature variation in the heat affected zone as shown in Figure 6.11. Fifteen simulation steps, in each of which the boundary conditions move eight degrees counter-clock-wise, are required to completely cover the entire model. Note that the towpreg and steel roller have been neglected and only one-third of the cylinder is considered in the simulation. The reason is twofold. First, since the heater aims simultaneously at the surfaces of both towpreg and composite substrate, we assumed that little energy would propagate across the interface between roller and composite cylinder and consequently would not interfere with the temperature distribution. This allows us to separate the model into two parts, the composite-mandrel assembly and the towpreg-roller assembly. Second, previous simulation results and in-situ measurement data suggested that the heat can neither penetrate deeply into the composite substrate nor transfer far away from the nippoint along the circumferential direction. Therefore, for purposes of simplicity, only one-third of the whole composite-mandrel assembly is modeled.

The thermal history at two positions, as indicated in Figure 6.10, is plotted in Figure 6.12. It is noted that the node N732 is located at about three layers beneath the outer surface of the cylinder and node N726 represents the interface between the third and forth layers above the inner surface of the

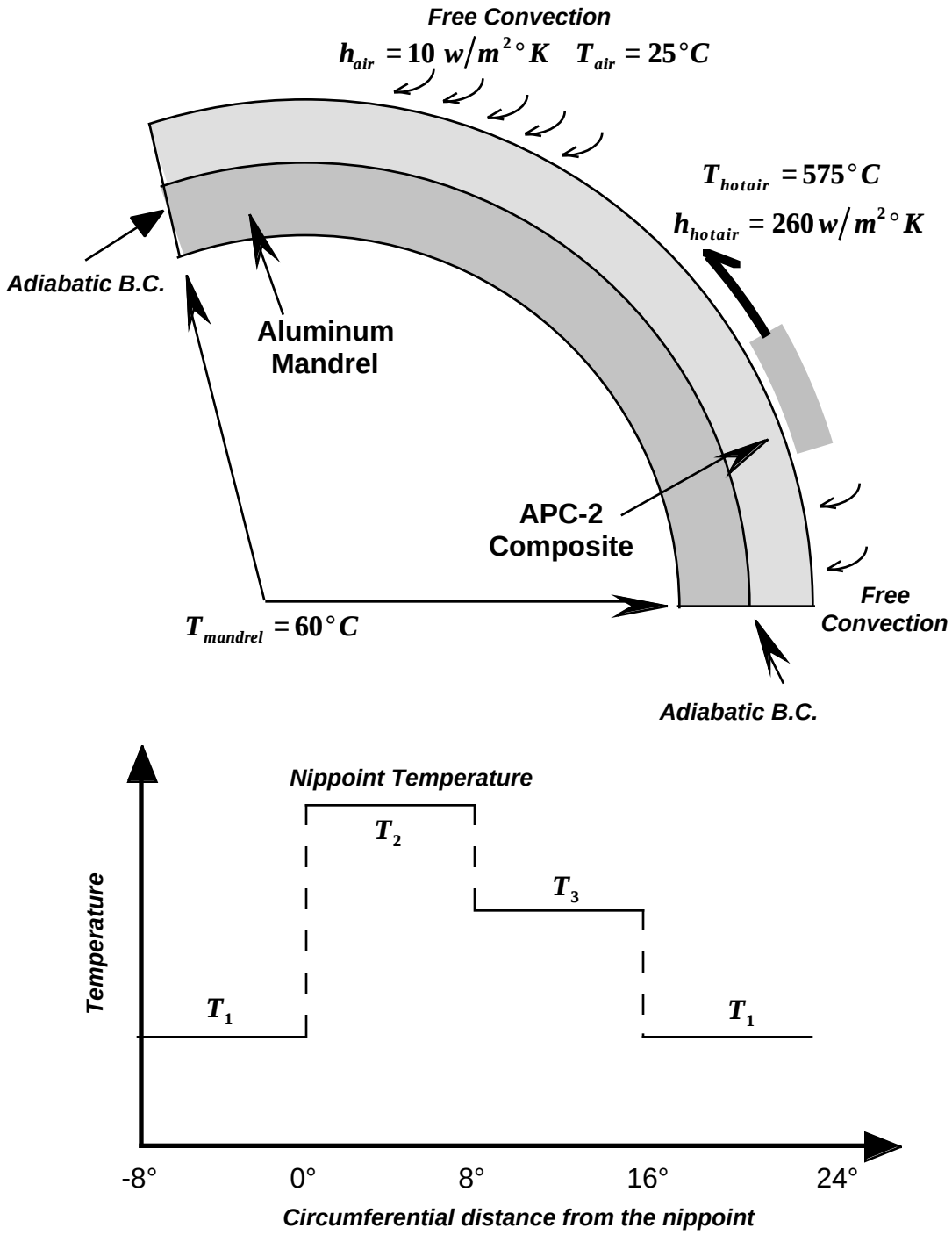

Figure 6.11 Schematic diagram of the boundary conditions of the winding problem.

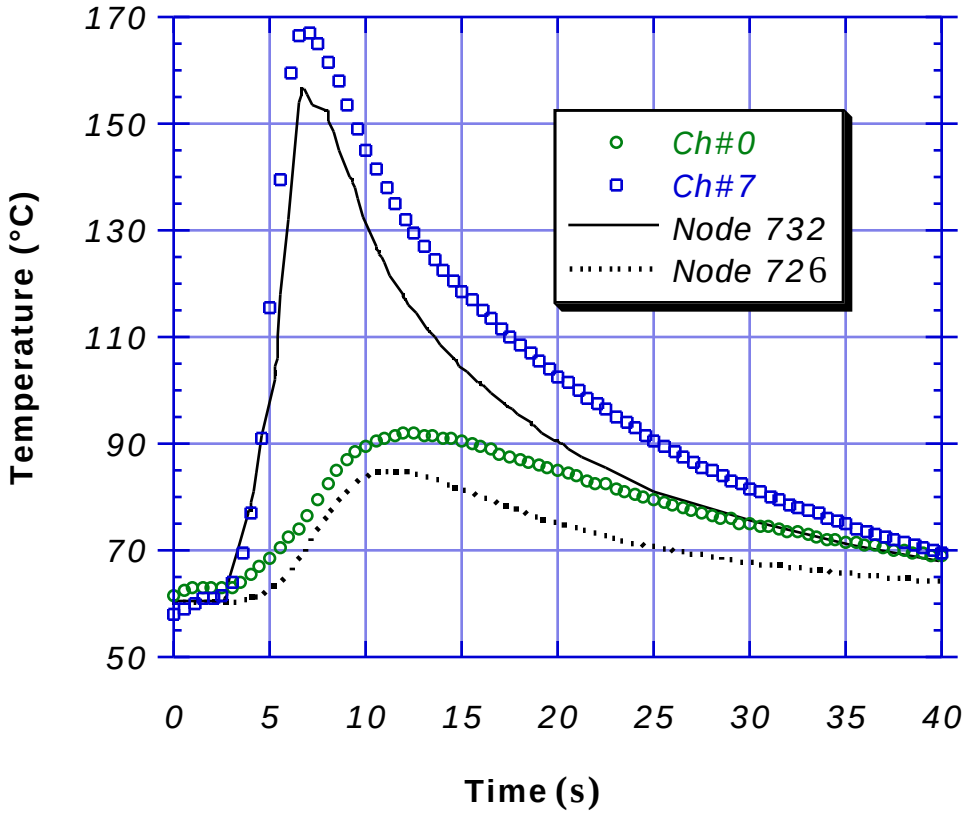

Figure 6.12 Comparison of temperature histories at nodes #732 and #726 (1 rpm).

composite cylinder. The temperature data from thermocouples denoted as Ch#0 and Ch#7 in the Figure 6.12 were compared with the predictions. The location of the thermocouple Ch#0 was in between the second and the third layers above the surface of the mandrel. The thermocouple Ch#7 was installed between the 23rd and 24th layer which is three layers beneath the surface of the composite cylinder. The location of the thermocouples are not perfectly aligned with nodes N732 and N726 (see Figure 6.10). The predictions were about 15% lower than the measured temperatures. Nevertheless the overall prediction captured the transient heating rather well.

The Figure 6.13 and Figure 6.14 show the temperature distribution at various steps during the winding analysis. Note that the cooling takes place immediately after the heat flux moves to the next position on the composite surface. The procedure is continued until all areas in the model are covered. It should be noted that the maximum temperature on the surface of the composite cylinder is well below the melting temperature of PEEK resin composite. In other words, at a winding speed of 1 rpm, the hot-air heater was unable to create a molten zone on the cylinder surface. Naturally, the next question to ask is whether or not the hot-air heater adopted in the present design can create a molten zone at the surface of the composite cylinder. Unfortunately, the answer is no. Even at a much lower winding speed of 1/3 rpm, molten zone was not observed during experiment. The finite element simulation confirms this observation, as shown in Figure 6.15. The maximum temperature reached at the surface of the composite cylinder is about 270°C. Initially, it was planned to create molten surfaces on both

composite substrate and towpreg. The winding simulation model confirms the experimental observation discussed in Section 5.3 that it may be difficult to create a molten zone on the surface of APC-2 composite using a hot-air heater. In order to successfully consolidate the thermoplastic composites using the on-line consolidation technique, the air heater must focus on melting the incoming towpreg as discussed in Section 5.3. In the following section, a finite element model is constructed to predict the temperature distribution on the cross section of the incoming towpreg under various processing conditions.

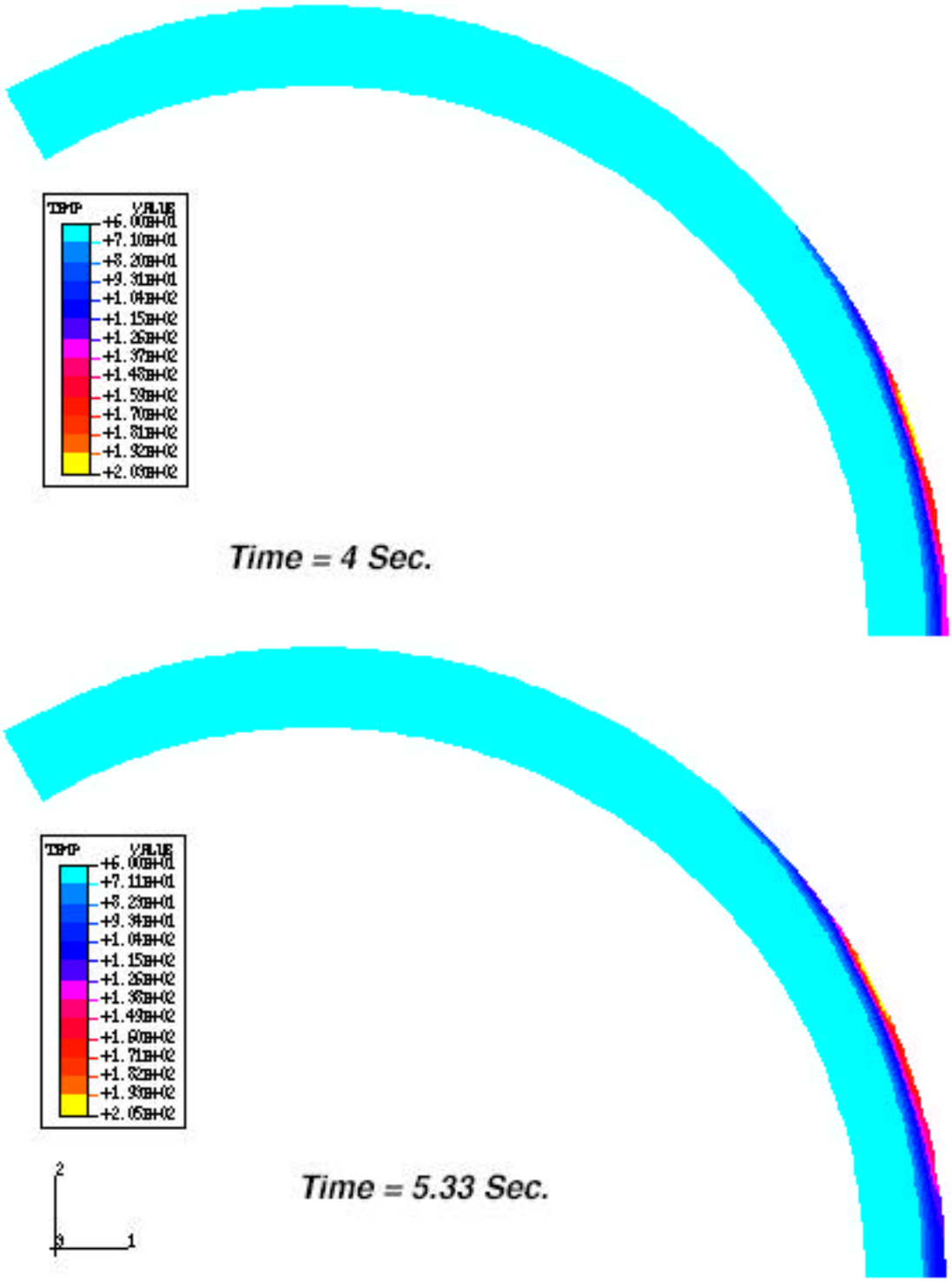

Figure 6.13 Isotherms at two steps during winding analysis (1 rpm). Temperatures are in °C.

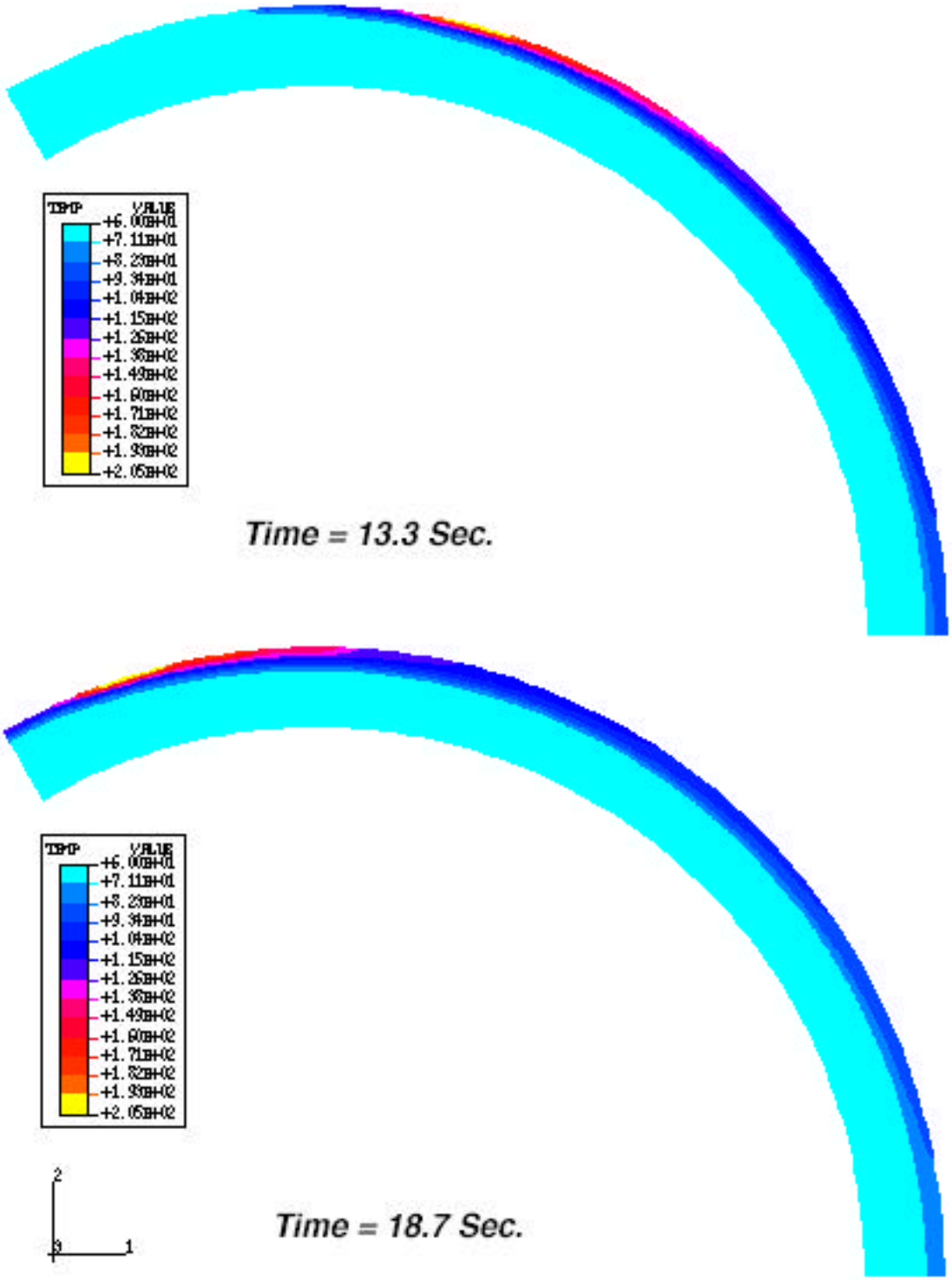

Figure 6.14 Isotherms at two steps during winding analysis (1 rpm). Temperatures are in °C

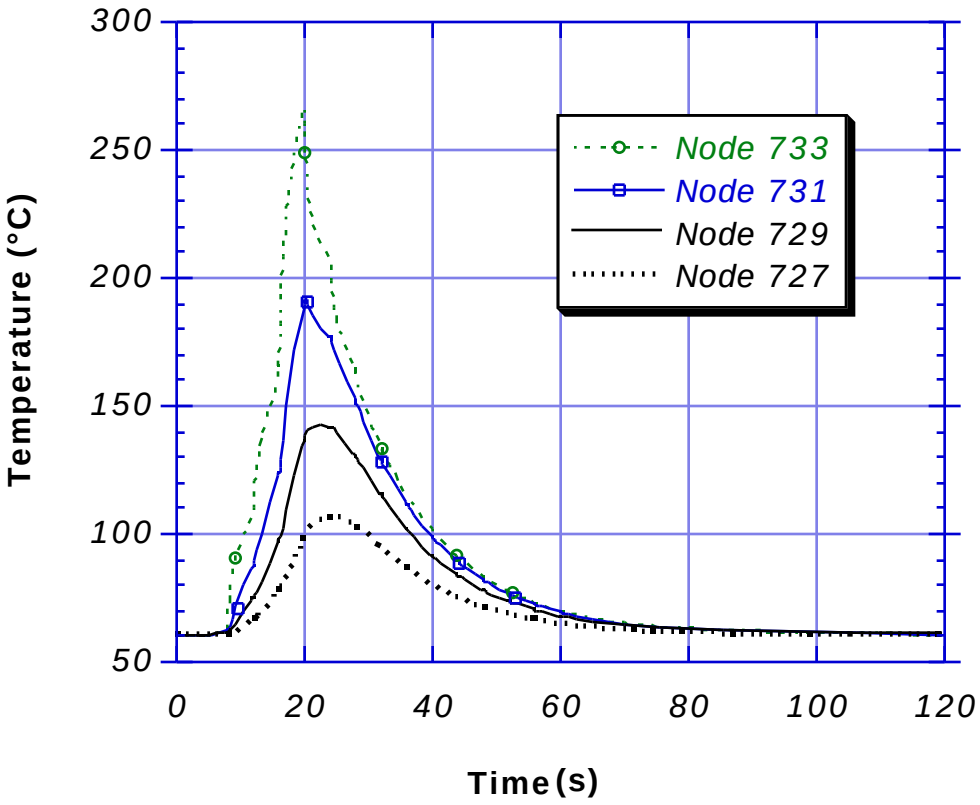

Figure 6.15 Temperature histories at nodes of various elements (1/3 rpm). Nodal locations are shown in Figure 6.10.

6.3.3 Simulation on Heating of Towpreg

We have concluded that the hot-air heater used in the on-line consolidation system was unable to create a molten zone on the surface of the substrate. The next step was to study whether the hot-air heater could melt the resin of incoming towpreg. A two-dimensional ABAQUS finite element program was constructed to solve the transient heat transfer problem of the towpreg. The towpreg is continuously passing the heating zone as shown schematically in Figure 6.16. The thermal boundary conditions for the model are also illustrated in Figure 6.16.

From experimental observation, the size of the heating zone is about 15 mm (0.6 in) or about 70 degrees of the circumference of the 25.4 mm (1 in) compaction roller. Again, the hot-air temperature is also not uniform in this region as we measure the air temperature along the towpreg surface. For simplification, we model this variation by using a two-step approach in which the towpreg is heated at 300°C for the first 5 mm (0.2 in), then at the selected temperature for the last 10 mm (0.4 in). The speed is determined by the time required to pass through the heating zone. Two cases were used for applying the boundary conditions. In the first case, the top surface of the towpreg was heated by the hot air, the edge was subjected to free convection, and the bottom surface was assumed to be adiabatic. Heat is input into the towpreg due to convection. In this simulation, the duration of heating operation ranges from one second to four seconds during which the towpreg is exposed to hot air with temperature ranging from 550°C to 650°C. This heating time corresponds approximately to a winding speed of 0.5 rpm

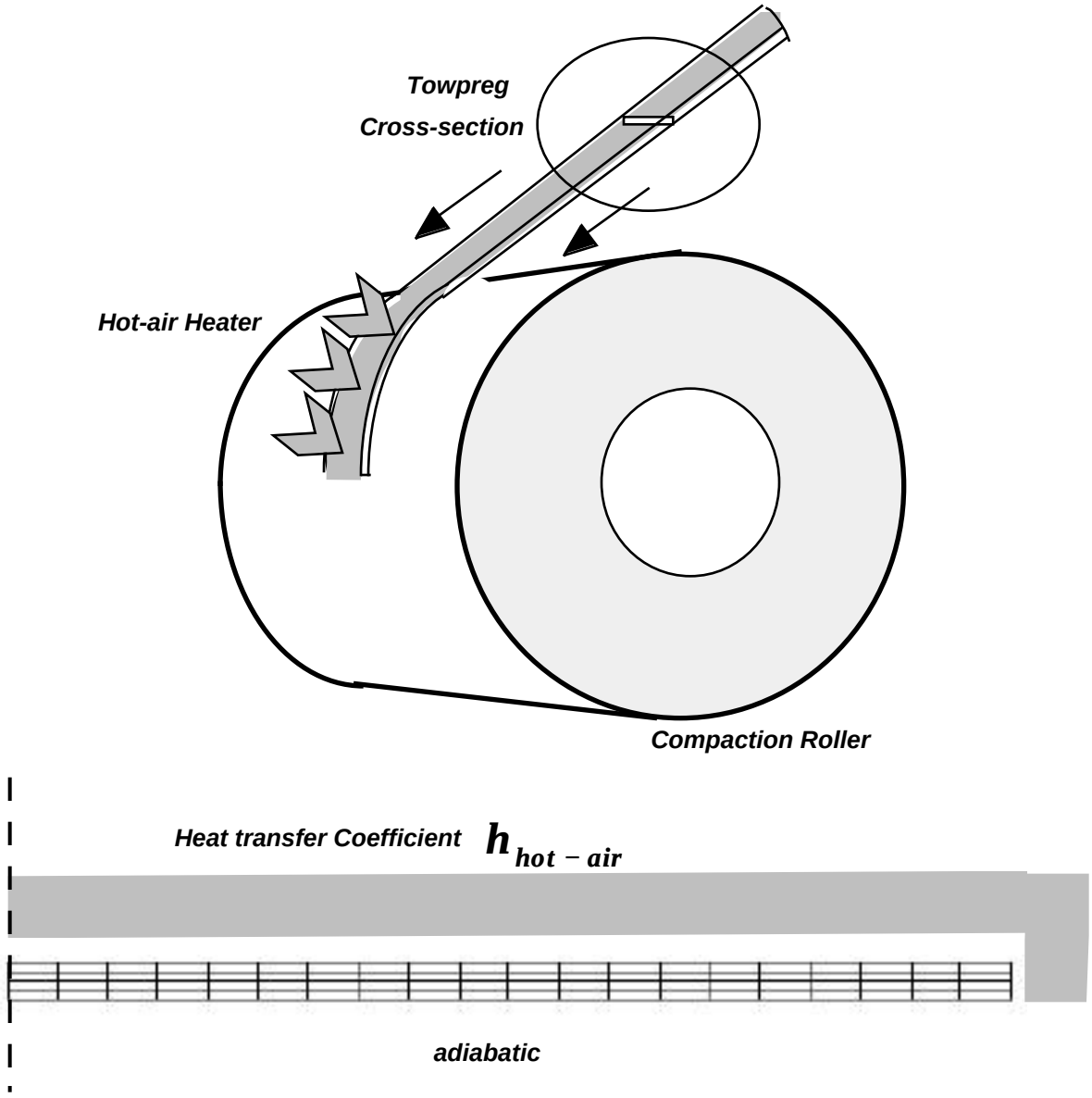

Figure 6.16 Schematic of towpreg heating and finite element mesh for one-half of the cross-section of the towpreg.

(4 mm/s) to 2 rpm (16 mm/s). The second set of boundary conditions allows heat input through the edge of the towpreg. Boundary conditions on the top and bottom surface are identical to the first case. Tables 6.2 and 6.3 show the temperature distribution of towpreg before entering the nippoint for case one and case two, respectively. The actual conditions should lie in between these two cases.

As indicated in the tables, the hot-air heater is able to melt the towpreg under most of the processing conditions. However, some difficulty is encountered at the two extreme conditions-namely, higher speed at lower nippoint temperature and lower speed at higher nippoint temperature. While the former yields insufficient bonding, the latter may cause thermal degradation. This finite element model of towpreg heating can be used to predict the towpreg temperature for various thermoplastic composite systems, and to provide operational limits to avoid insufficient melting and thermal degradation.

Table 6.2 The temperature range of towpreg before entering the nippoint; $h_{top} = 270\ w/m^2 \cdot K$ and $h_{edge} = 10\ w/m^2 \cdot K$.

Nippoint Temperature (°C)	Mandrel RPM (mm/sec)		
	0.5 (4)	1.0 (8)	2 (16)
530	491.7 - 493.4	401.6 - 406.6	278.4 - 287.4
580	538.7 - 540.5	437 - 442	303.3 - 313.4
630	582.8 - 584.8	473.6 - 479.6	327.2 - 338.0

Table 6.3 The temperature range of towpreg before entering the nippoint; $h_{top} = 270\ w/m^2 \cdot K$ and $h_{edge} = 270\ w/m^2 \cdot K$.

Nippoint Temperature (°C)	Mandrel RPM (mm/sec)		
	0.5 (4)	1.0 (8)	2 (16)
530	492.1 - 504.1	401.8 - 435.8	278.7 - 331.3
580	537.7 - 551.1	438.0 - 475.6	303.4 - 361.4
630	583.1 - 598.0	474.2 - 515.4	327.2 - 390.5

6.4 Finite Element Simulation on Thermal Stresses

6.4.1 Introduction

A thermal stress analysis for the on-line consolidation process was developed to predict the fabrication stresses upon completion of processing. For simplification, we consider the composite-mandrel assembly as a solid body during processing. This simplification is acceptable, since viscous flow occurs only at the nippoint where the molten towpreg is continuously consolidated onto the surface of the composite substrate.

In solid bodies, the temperature change is associated with thermal strain via the thermal expansion coefficient. Under linear-elastic analysis, once the temperature distribution has been obtained, the formation of process-induced thermal strains and stresses can be determined.

In the following section, the basic equations of thermoelasticity are presented. Then, a finite element mesh representing the entire composite-mandrel assembly and an ABAQUS finite element program for thermal stress analysis are constructed. For accuracy assessment, the isotropic thermo-physical properties of aluminum are used in the model and the results are compared to the analytical solutions [77-78]. Finally, the calculated thermal history and the temperature dependent thermophysical material properties

are incorporated into the model to predict the process-induced thermal stresses under on-line consolidation conditions.

6.4.2 Mathematical Formulations

The mathematical formulations of thermoelasticity describe the behaviors of the solid bodies under prescribed temperature distributions. Many concepts and equations are identical with those of the theory of elasticity under isothermal conditions. The basic assumptions are stated as follows:

- The deformations are small compared to the thicknesses of consolidated parts.
- Only linear strain-displacement relations are considered.
- Temperature distribution can be determined independently of the deformation of the solid bodies.

With the above assumptions, the process can be considered as an uncoupled thermoelastic problem that consists of three sets of basic equations:

Equilibrium equations $$\sigma_{ji,j} = \mathbf{0}; \tag{6.20}$$

Linear strain-displacement relations $$\varepsilon_{ij} = \boldsymbol{1/2(u_{i,j} + u_{j,i})}; \tag{6.21}$$

Constitutive equations $$\varepsilon_{ij} = \boldsymbol{S_{ijrs}(T)}\sigma_{ij} + \int \alpha_{ij}\boldsymbol{(T)dT} + \varepsilon^{*}; \text{ and} \tag{6.22}$$

where σ_{ij} are the components of the stress tensor, the subscript $(,j)$ denotes partial differentiation with respect to the corresponding axis, ε_{ij} are the components of the strain tensor, $\boldsymbol{u_i}$ are displacements, $\boldsymbol{S_{ijrs}}$ are the fourth

order compliance tensor, T is the temperature, α_{ij} are the coefficients of thermal expansion, ε^* is the shrinkage strain due to crystallization, K_{ij} is the thermal conductivity, Q is the rate of internal heat generation, C is the specific heat capacity, ρ is the materials' density, t is time and $\dot{T}$ is the time rate of temperature change. It is noted that, in the present study, the shrinkage strain due to crystallization, ε^*, is neglected.

In order to study the thermally induced deformation behavior of the composite-mandrel assembly under the prescribed temperature field, the governing equations are solved in a cylindrical coordinate system. Consider a segment of the composite-mandrel assembly as shown in Figure 6.17. The thermally induced stresses are most severe on the $r-\theta$ plane. Hence, all strains and stresses were considered invariant along the axial coordinate, z. For further simplification, the cross-section of the composite-mandrel assembly was modeled as a thin annular disk and the plane stress conditions were applied. The equilibrium equations can be written as follows:

$$\begin{aligned} \frac{\partial \sigma_r}{\partial r} + \frac{1}{r}\frac{\partial \tau_{r\theta}}{\partial \theta} + \frac{\sigma_r - \sigma_\theta}{r} &= 0 \\ \frac{\partial \tau_{r\theta}}{\partial r} + \frac{1}{r}\frac{\partial \sigma_\theta}{\partial \theta} + \frac{2\tau_{r\theta}}{r} &= 0 \end{aligned} \tag{6.23}$$

where σ_r is the normal (radial) stress and σ_θ is the tangential (hoop) stress and $\tau_{r\theta}$ is the shear stress.

In addition, since the winding angle for all cylinders manufactured in the present study is 90°, the simplified form of the stress-strain behavior is

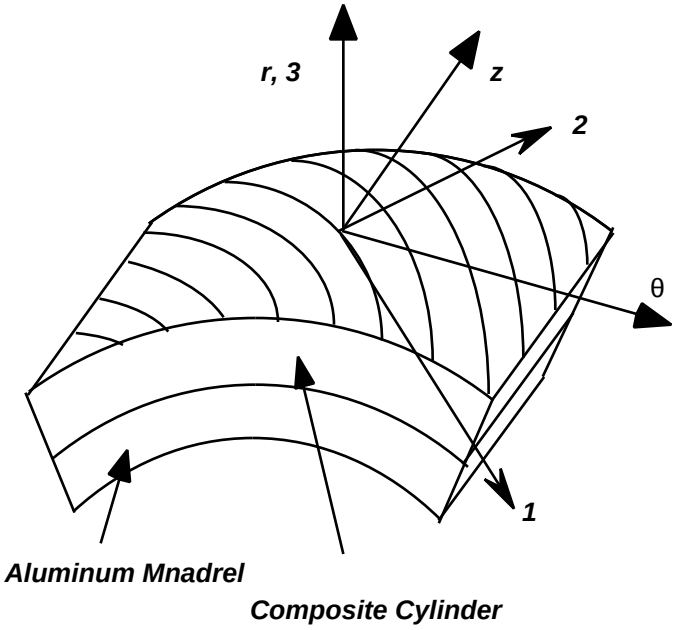

Figure 6.17 Cylindrical coordinate system.

$$\begin{Bmatrix} \sigma_r \\ \sigma_\theta \\ \sigma_z = 0 \\ \tau_{r\theta} \end{Bmatrix} = \begin{bmatrix} C_{11} & C_{12} & C_{13} & 0 \\ C_{12} & C_{22} & C_{23} & 0 \\ C_{13} & C_{23} & C_{33} & 0 \\ 0 & 0 & 0 & C_{66} \end{bmatrix} \begin{Bmatrix} \varepsilon_r - \alpha_r T \\ \varepsilon_\theta - \alpha_\theta T \\ \varepsilon_z - \alpha_z T \\ \gamma_{r\theta} \end{Bmatrix} \tag{6.24}$$

where ε_r is the normal (radial) strain, ε_θ is the tangential (hoop) strain, ε_z is the axial strain, $\gamma_{r\theta}$ is the shear strain, C_{ij} are elastic properties of the materials, α_r is the normal (radial) coefficient of thermal expansion, α_θ is the tangential (hoop) coefficient of thermal expansion and α_z is the axial coefficient of thermal expansion. It should be noted that, under on-line consolidation process conditions, the temperature field T is a function of position and time.

The linear strain-displacement relations take the form

$$\varepsilon_r = \frac{\partial u}{\partial r}; \qquad \varepsilon_\theta = \frac{u}{r} + \frac{1}{r}\frac{\partial v}{\partial \theta}; \qquad \varepsilon_z = \frac{\partial w}{\partial z}$$
$$\gamma_{r\theta} = \frac{1}{2}\left(\frac{1}{r}\frac{\partial u}{\partial \theta} + \frac{\partial v}{\partial r} - \frac{v}{r}\right) \tag{6.25}$$

where u, v, and w represent the components of the displacement vector in the r, θ, and z direction respectively.

The boundary conditions of thermoelastic problems involved in the on-line consolidation process are listed as the following. During the winding stage of the process, the roller pressure is applied on a small portion of the composite cylinder. The traction boundary conditions need to be satisfied at every point on the contact area between roller and composite and are expressed in terms of stress components as follows:

$$\bar{F}_r = \sigma_r n_r + \tau_{r\theta} n_\theta$$
$$\bar{F}_\theta = \tau_{r\theta} n_r + \sigma_r n_\theta \qquad (6.26)$$

where $\bar{F}_r$ and $\bar{F}_\theta$ are the components of the prescribed surface traction in the r and θ directions, and n_r and n_θ are the direction cosines of the outward surface normal. In the present study, the effect of roller pressure is neglected and a zero traction boundary condition is used.

During the final cooling stage, there are no external loads applied to any surface. All deformations correspond to free expansion or contraction of the body. However, displacements interact with each other due to geometric constraints, heterogeneous material properties and non-uniform temperature distribution. To solve these equations, a ABAQUS finite element model which takes into account the temperature dependent material properties and the orientation of the coordinate system was constructed.

6.4.2 Finite Element Approach

In contrast to modeling only a portion of the composite-mandrel assembly in the transient heat transfer analysis of the winding process, the finite element mesh for thermal stress study includes the entire composite-mandrel assembly. Figure 6.18 shows the finite element mesh and a close-up to show details. There are 4320 elements in the model. For thermal analysis, 4-node linear heat transfer quadrilateral elements (DC2D4) were used. For thermal stress analysis, 4-node bilinear plane stress quadrilateral, reduced integration elements (CPS4R) ware used. The thermal boundary conditions are applied separately for the winding stage and the cooling stage.

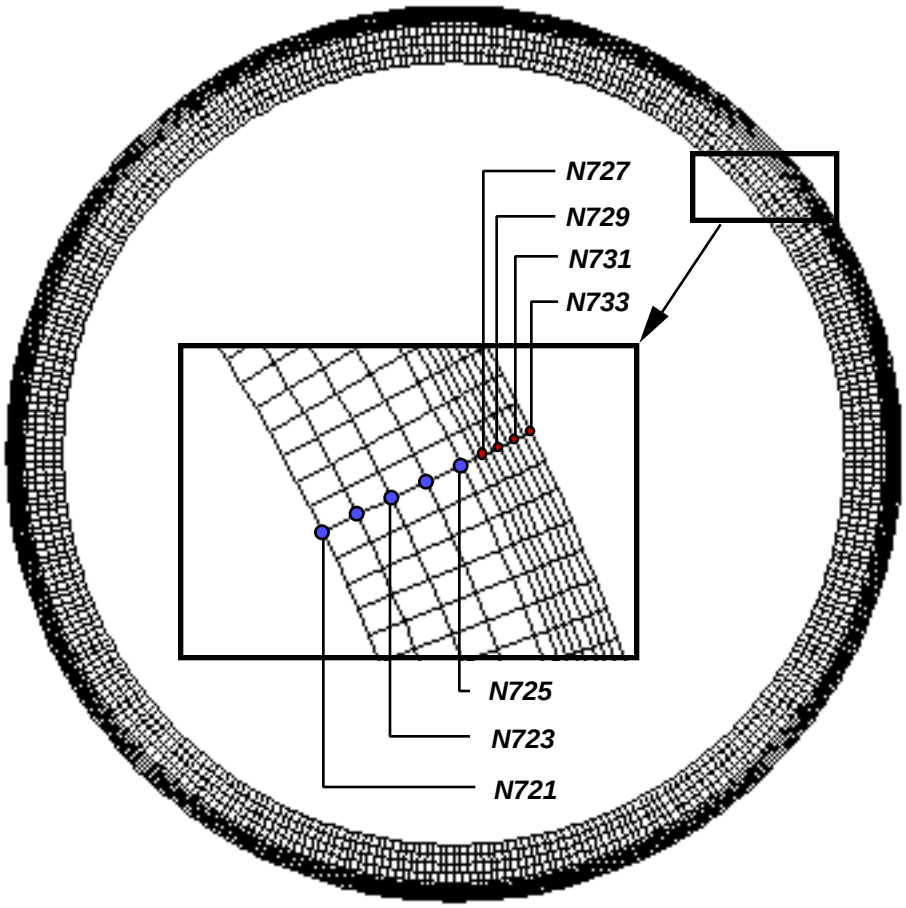

Figure 6.18 Finite element mesh for thermal stresses analysis.

The winding stage boundary conditions are similar to the ones used in winding analysis (Section 6.3.2). The focused heat source move along the composite surface in the hoop direction to simulate the rotation of the mandrel. When the heat source moves away, the cooling stage begins. During cooling, the free convective boundary conditions are applied along the outer surface of the composite cylinder, and a prescribed temperature is specified at every node on the inner surface of the mandrel. Based on experimental observations, it took about 20 minutes for the mandrel to cool down to the room temperature. It is noted that if a controlled cooling rate is preferred, one can easily apply new boundary conditions to simulate a heated mandrel.

The APC-2 is modeled as an orthotropic media with temperature-dependent material properties and the aluminum mandrel as an isotropic solid with constant material properties. The thermophysical properties of APC-2, the aluminum mandrel and the steel roller are given in Table 6.4. The solution scheme of the thermally induced stresses analysis using ABAQUS is shown in Figure 6.19.

Table 6.4 Input parameters for thermal stress analysis.

Properties	APC-2/AS4	Aluminum
Modulus, longitudinal (GPa)	133.8[64]	73
Modulus, transverse (GPa)	8.895[64]	73
Shear modulus (GPa)	5.1[64]	28
Poisson's ratio	0.28[64]	0.3
Thermal expansion coeff. longitudinal ($x10^{-6}$ /°C)	T>Tg 0.6[14] T<Tg - 0.3[14]	23.0
Thermal expansion coeff. transverse ($x10^{-6}$ /°C)	T>Tg 66.0[14] T<Tg 34.3[14]	23.0

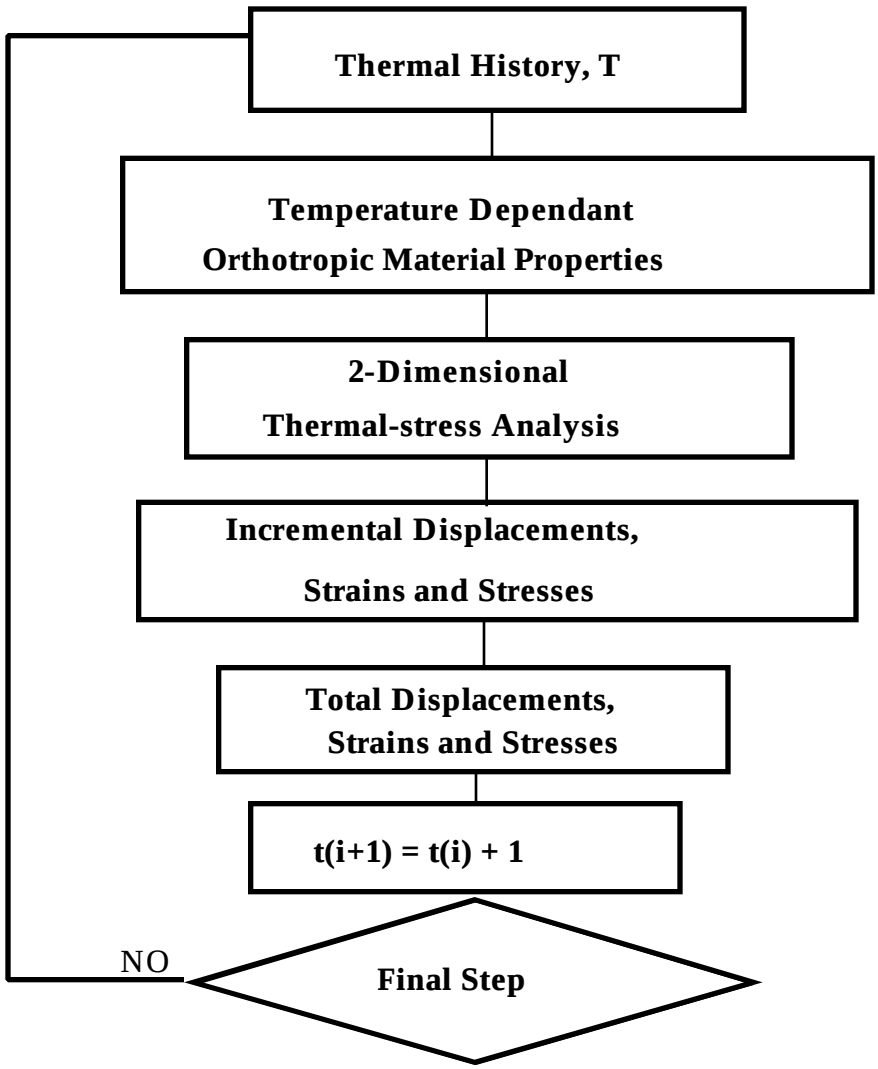

Figure 6.19 Solution scheme of the thermally induced stresses analysis using ABAQUS.

6.4.3 Results

In order to evaluate the accuracy of the results from the finite element simulation, we compare the ABAQUS solution to that of an analytical solution. Consider an circular disk with a concentric circular hole subjected to a radial temperature variation. The temperature on the inner surface of the cylinder, T_{inner} is 25°C and the temperature on the outer surface, T_{outer} is 125°C. The temperature at any distance r from the center is expressed as [77]

$$T = \frac{\Delta T}{\ln(b/a)} \cdot \ln(b/r) \tag{6.27}$$

where b is the outer radius of the cylinder, a is the radius of the hole, and $\Delta T = T_{inner} - T_{outer}$.

For the case of plane stress, the non-zero stress components were given as [78]

$$\sigma_r = \frac{\alpha E}{r^2}\left[\frac{r^2 - a^2}{b^2 - a^2}\int_a^b Tr\,dr - \int_a^r Tr\,dr\right] \tag{6.28}$$

$$\sigma_\theta = \frac{\alpha E}{r^2}\left[\frac{r^2 + a^2}{b^2 - a^2}\int_a^b Tr\,dr + \int_a^r Tr\,dr - Tr^2\right]. \tag{6.29}$$

Substituting Eqn. (6.27) into Eqs. (6.28) and (6.29), the final expressions for the thermal stresses caused by the temperature gradient can be written as

$$\sigma_r = \frac{\alpha E \Delta T}{2\ln(b/a)}\left[-\ln\frac{b}{r} - \frac{a^2}{(b^2 - a^2)}\left(1 - \frac{b^2}{r^2}\right)\ln\frac{b}{a}\right] \tag{6.30}$$

$$\sigma_\theta = \frac{\alpha E \Delta T}{2\ln(b/a)}\left[1 - \ln\frac{b}{r} - \frac{a^2}{(b^2 - a^2)}\left(1 + \frac{b^2}{r^2}\right)\ln\frac{b}{a}\right] \tag{6.31}$$

where α is the coefficient of thermal expansion and E is the Young's modulus of the isotropic material.

For the ABAQUS finite element model, the material properties of aluminum were used throughout the entire model. A steady-state heat transfer model was used to predict the temperature distribution in the composite-mandrel assembly and the calculated temperatures were applied as the thermal boundary conditions to predict the process induced thermal stresses. As shown in Figure 6.20, the temperature simulation compared well. Figure 6.21 and Figure 6.22 show the predictions of thermally induced stresses compared to the analytical solutions. The thermal stress in the hoop direction is tensile at the inner surface and compressive at the outer surface. The ABAQUS finite element solution for thermal stresses agreed with the thermal stresses obtained from the analytical solution. Overall, the sequential ABAQUS finite element models were considered a practical tool for analyzing the heat transfer and thermal stress problem associated with the on-line consolidation process.

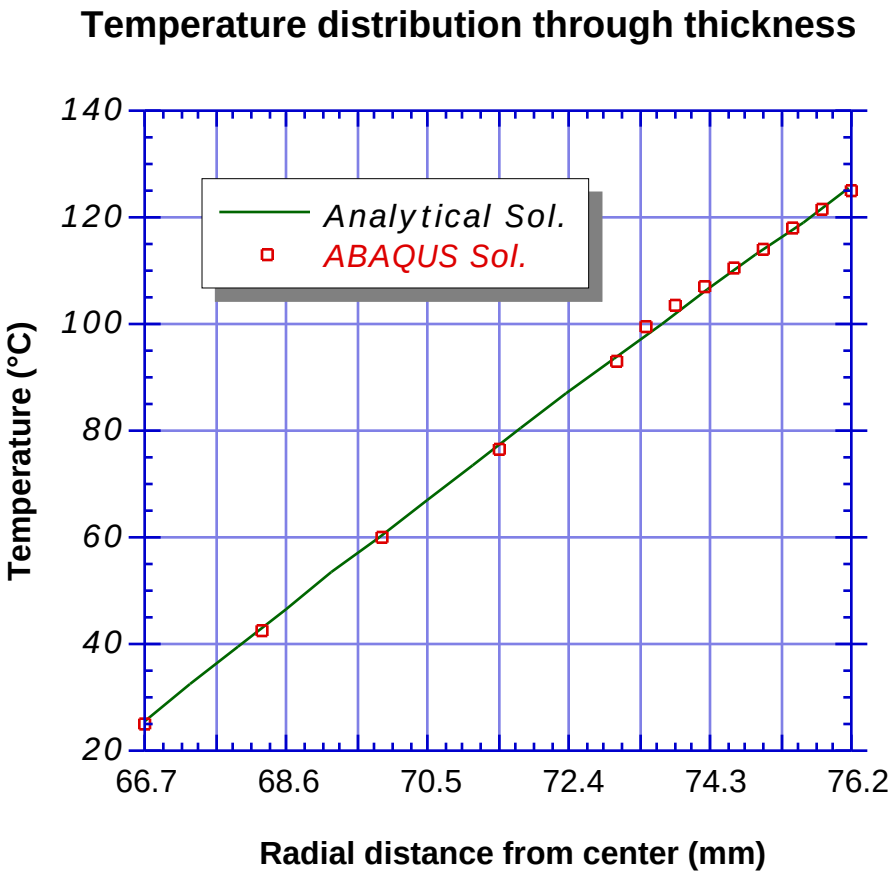

Figure 6.20 Temperature as a function of radial distance from center for hollow isotropic cylinder. Comparison between the ABAQUS finite element solution and analytical solution (Eqn. 6.27).

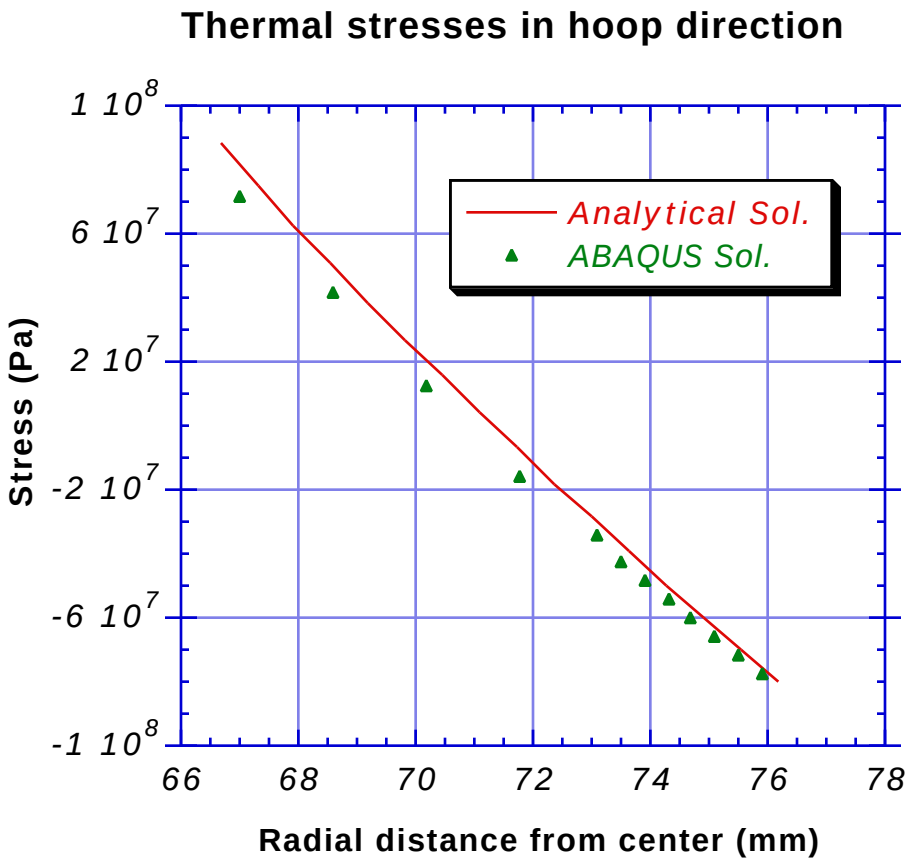

Figure 6.21 Thermally induced hoop stresses as a function of radial distance from center for a hollow isotropic cylinder. The comparison between the ABAQUS finite element solution and analytical solution (Eqn. 6.31).

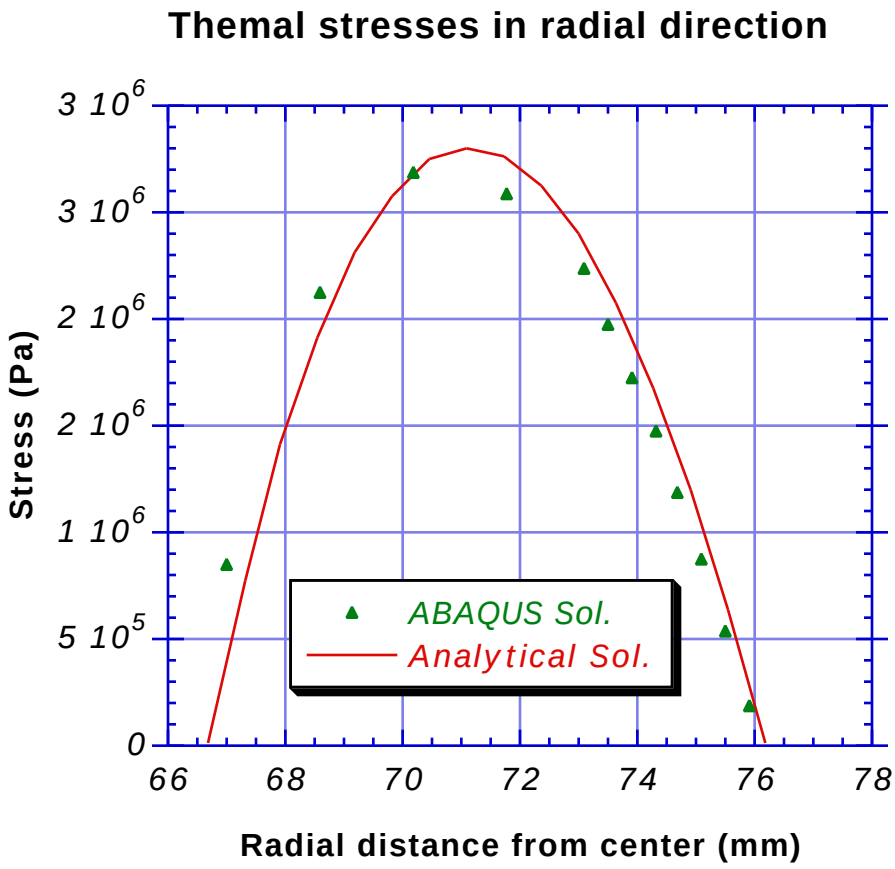

Figure 6.22 Thermally induced radial stresses as a function of radial distance from center for a hollow isotropic cylinder. The comparison between the ABAQUS finite element solution and analytical solution (Eqn. 6.30).

The transient heat transfer and the thermal stress ABAQUS finite element models were used to predict the process-induced thermal stresses in composite-mandrel assembly. The temperature-dependent material properties of APC-2 composite given in Table 6.4 were used in the model. The simulation was performed in two parts. First was the transient heat transfer model followed by the thermal stress model.

The transient heat transfer model has two steps, winding and cooling. During the winding step, only the winding of the last quarter of the outermost layer was simulated. A nodal temperature of 100°C was assigned for every node in the model as the initial condition. Initially, the heat source, located at the three o'clock position, aimed horizontally at the surface of the composite cylinder. Then, the heat source was moved in 8 degrees increment counter-clockwise along the circumference of the cylinder every 1.33 seconds until it arrives at the 12 o'clock position. This motion was equivalent to a winding speed of 1 rpm. The heat source was then moved away and free convective boundary condition was applied along the outer surface of the composite-mandrel assembly. The cooling continued until the entire composite-mandrel assembly reaches room temperature. The cooling step took about 20 minutes based on measurement from experiments. A prescribed boundary condition that takes into account the cooling rate was applied on the inner surface of the mandrel.

For the thermal stress analysis, the thermal histories of all elements are calculated and applied as a predefined field. Since the thermal field is the only driving force for the stress analysis, zero-traction boundary conditions

are applied for entire model. The finite element model was used to simulate the last 1216 seconds which includes winding the last quarter of the final layer and cool down of the part, during which the instantaneous temperature distribution and thermal stresses were calculated at 39 time increments. Figure 6.23 through 6.24 show contour plots of the temperature field at eight times during the winding and cooling process. It is noted that there exists a transient period between winding and cooling stages during which the temperature field changes from highly non-uniform, due to localized heating, to almost uniform through the entire composite-mandrel assembly, as shown in Figures 6.23 (d) and 6.24 (a).

The temperature distribution and thermal stress are presented at one increment from each stage. The first set of results representing the winding stage (time = 13.74 sec) is shown in Figure 6.25 through 6.27. The temperature at the outer surface is about 100°C higher than the temperature at the inner surface. The large temperature gradient causes localized shear stress as shown in Figure 6.26 (a). The radial stresses are negative for entire composite mandrel assembly with slightly non-uniform distribution due to the localized heating (Figure 6.26 (b)). The hoop stresses in the mandrel are compressive since the thermal expansion of the mandrel is constrained by the composite. On the other hand, the composite cylinder is under tensile (Figure 6.27).

Figure 6.28 show the second set of results that represents the transient stage (time = 60.8 sec). Here, cooling is taking place and the global temperature drops back to about 100°C. The shear stress become less severe. The distribution of hoop and radial stresses through the thickness are

uniform. The third set of results representing the cooling stage (time = 526 sec) is shown in Figure 6.29. During cooling stage, the effect of localized heating died out completely. The temperature field, the distribution of hoop and radial stresses are uniform and there are no shear stresses.

For studying the developing of the process-induced thermal stresses during the on-line consolidation process, the temperature and thermal stress distributions along the radial direction are shown in Figure 6.30 through Figure 6.33. Figure 6.30 shows the temperature variations through the thickness at five times. Figure 6.31 through 6.33 show the process-induced thermal stresses developed during the on-line consolidation process. Results are from elements #721 through #733 (figure 6.18). For the final state of thermal stresses, the mandrel is near stress-free and the composite is under small tensile stress in radial direction and compression in the hoop direction.

The analysis of process-induced stresses presented in this work can be used to study the impact of processing parameters such as nippoint temperature and winding speed, to further investigate the residual stresses, and to realize the potential of the on-line consolidation technique for manufacturing composite parts.

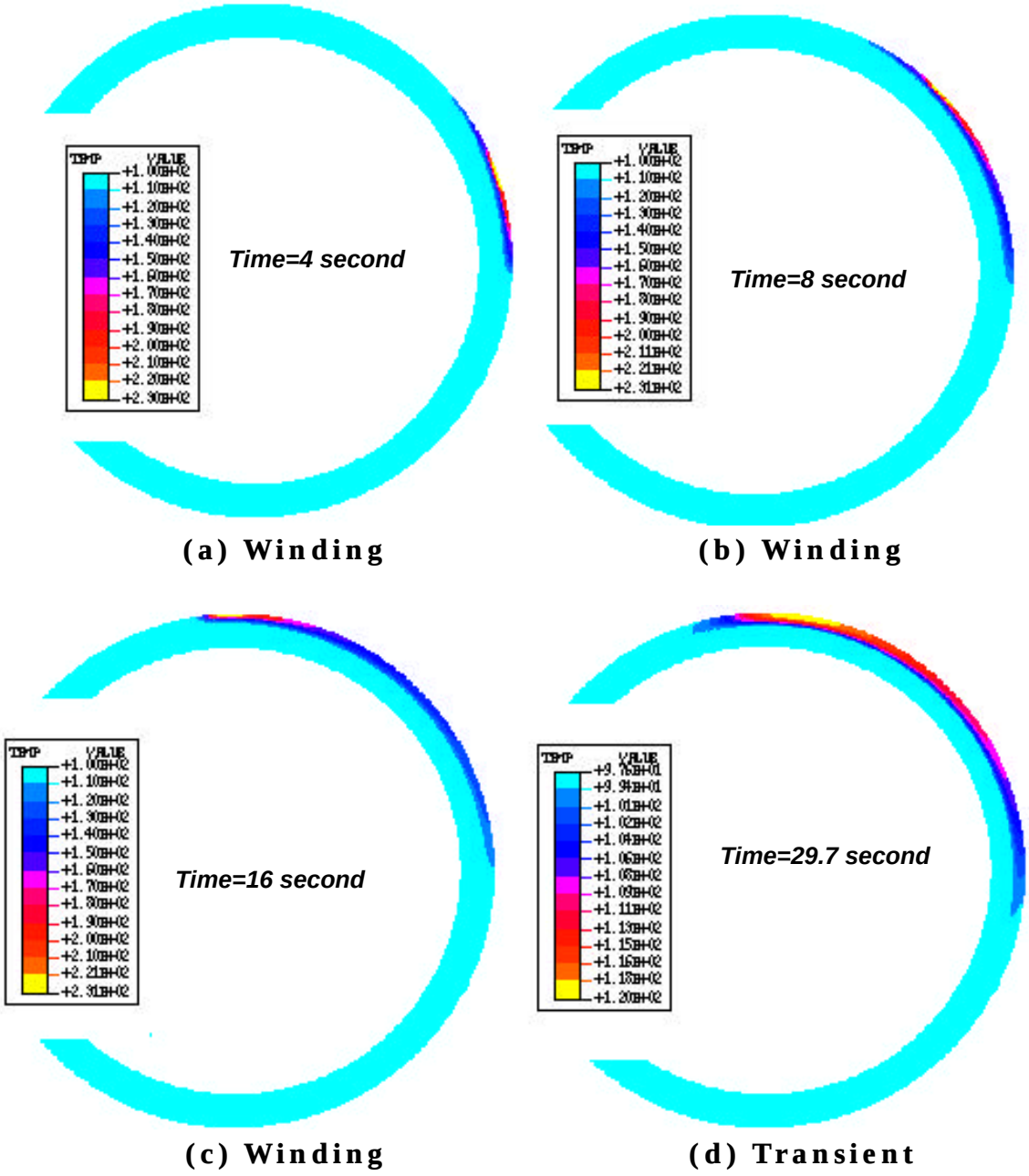

Figure 6.23 Contour plots of the temperature field at four times. Temperatures are in °C.

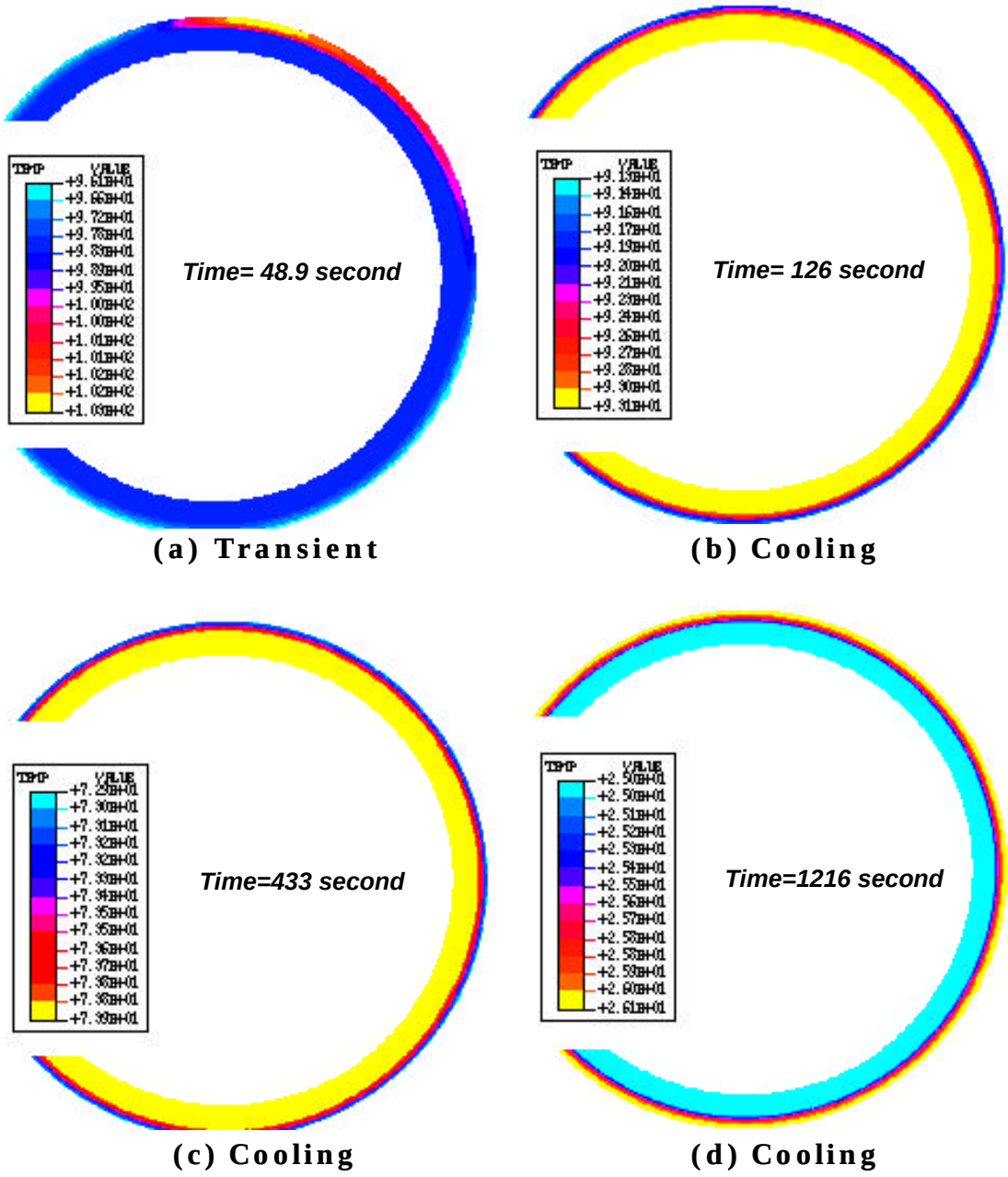

Figure 6.24 Contour plots of the temperature field at four times. Temperatures are in °C.

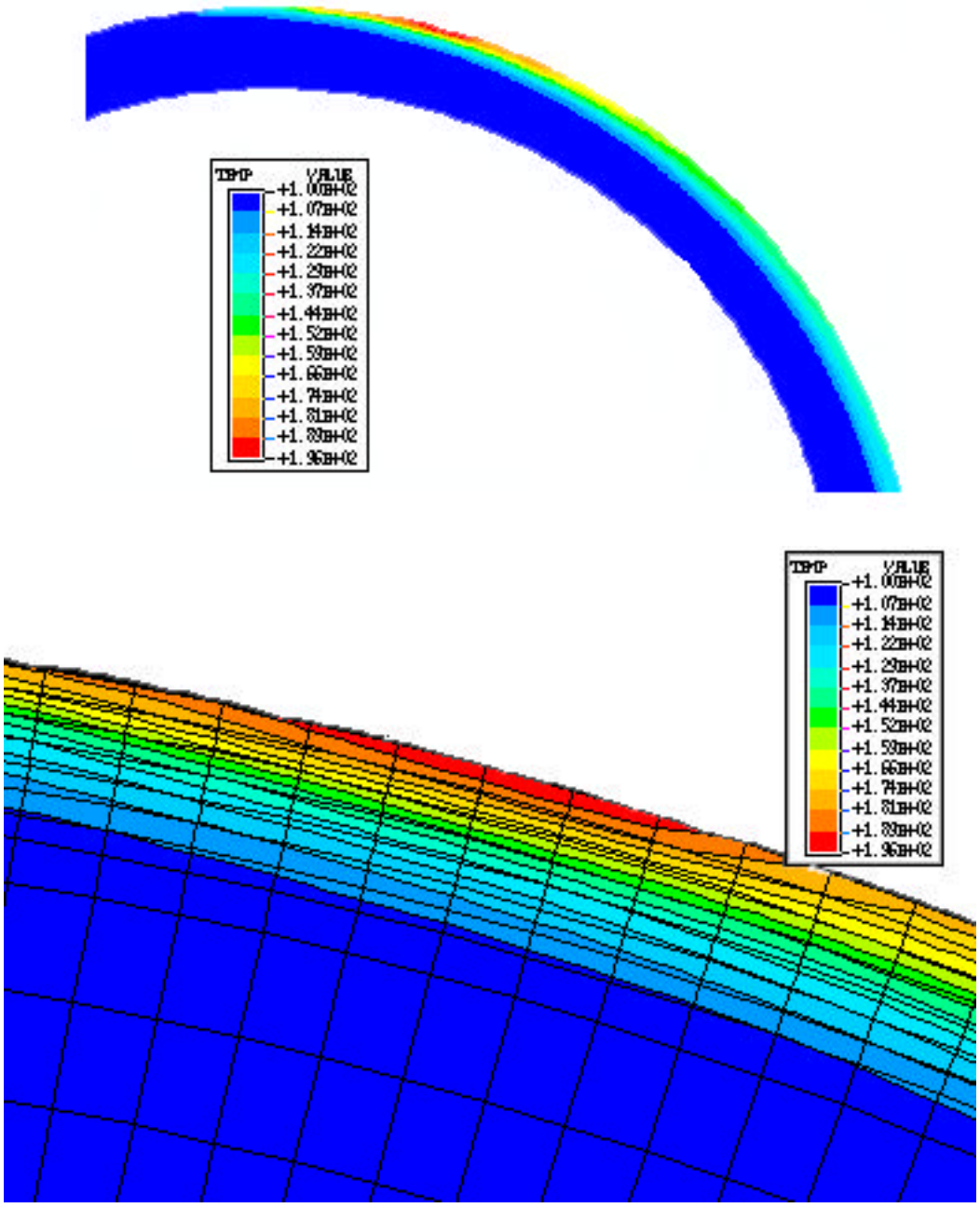

Figure 6.25 Temperature contour plot at time = 13.74 second. Temperatures are in °C.

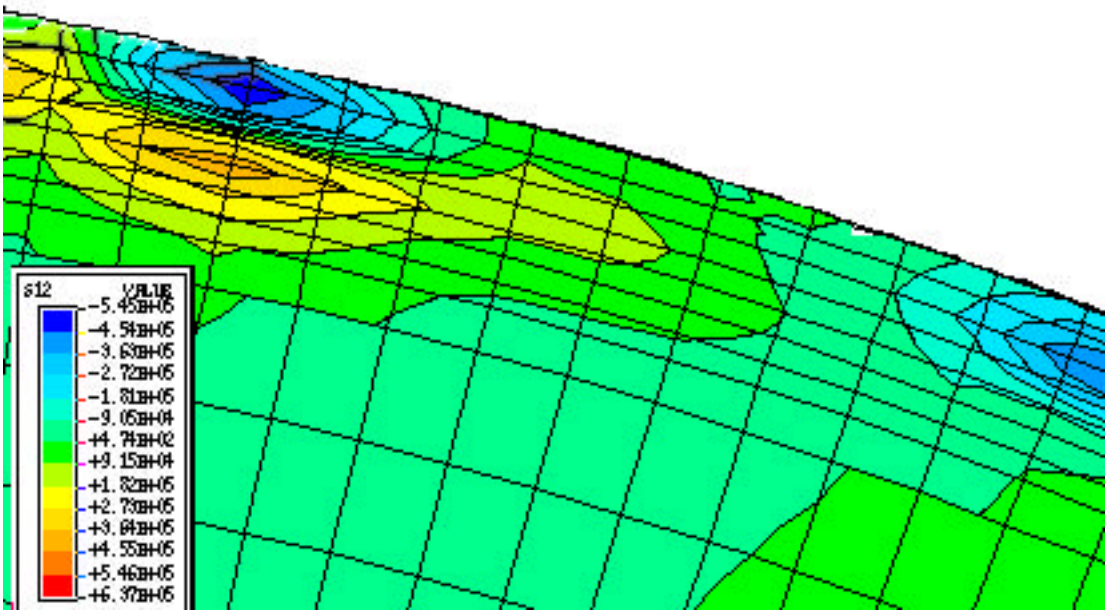

(a)

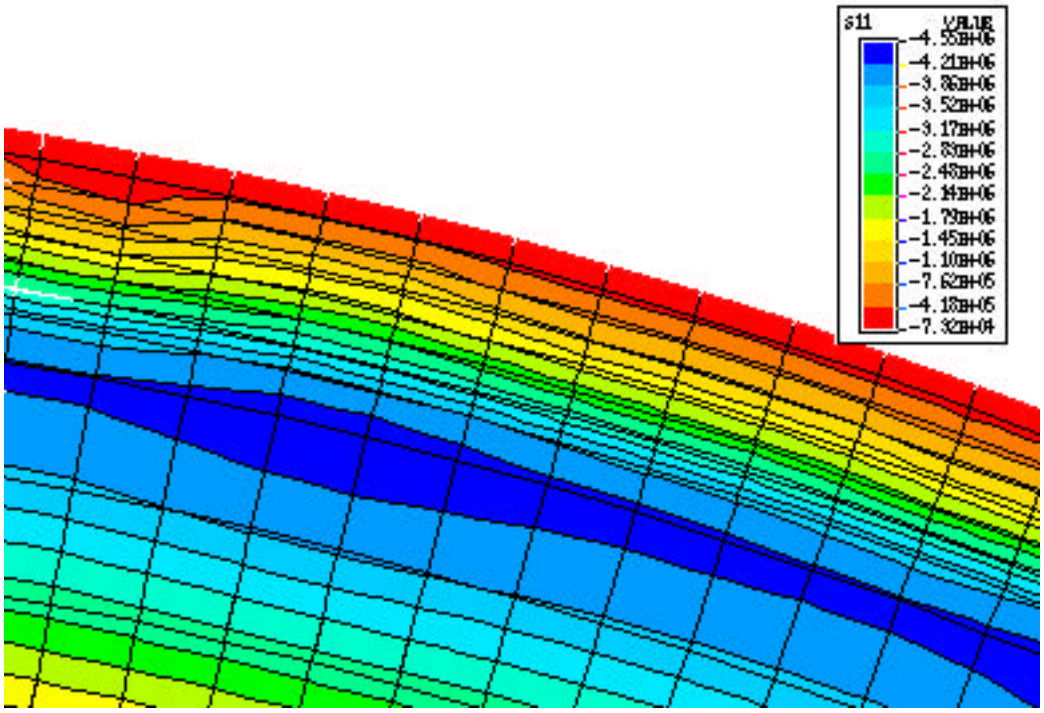

(b)

Figure 6.26 Process-induced shear (a) and radial stress (b) at time = 13.74 second. Stresses are in Pa.

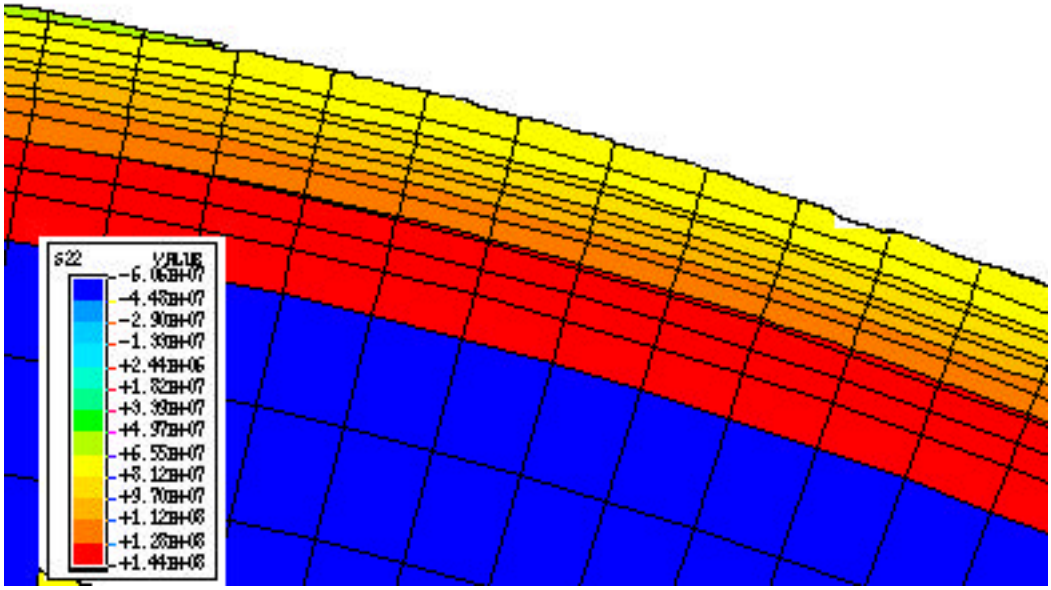

Figure 6.27 Process-induced hoop stress at time = 13.74 second. Stresses are in Pa.

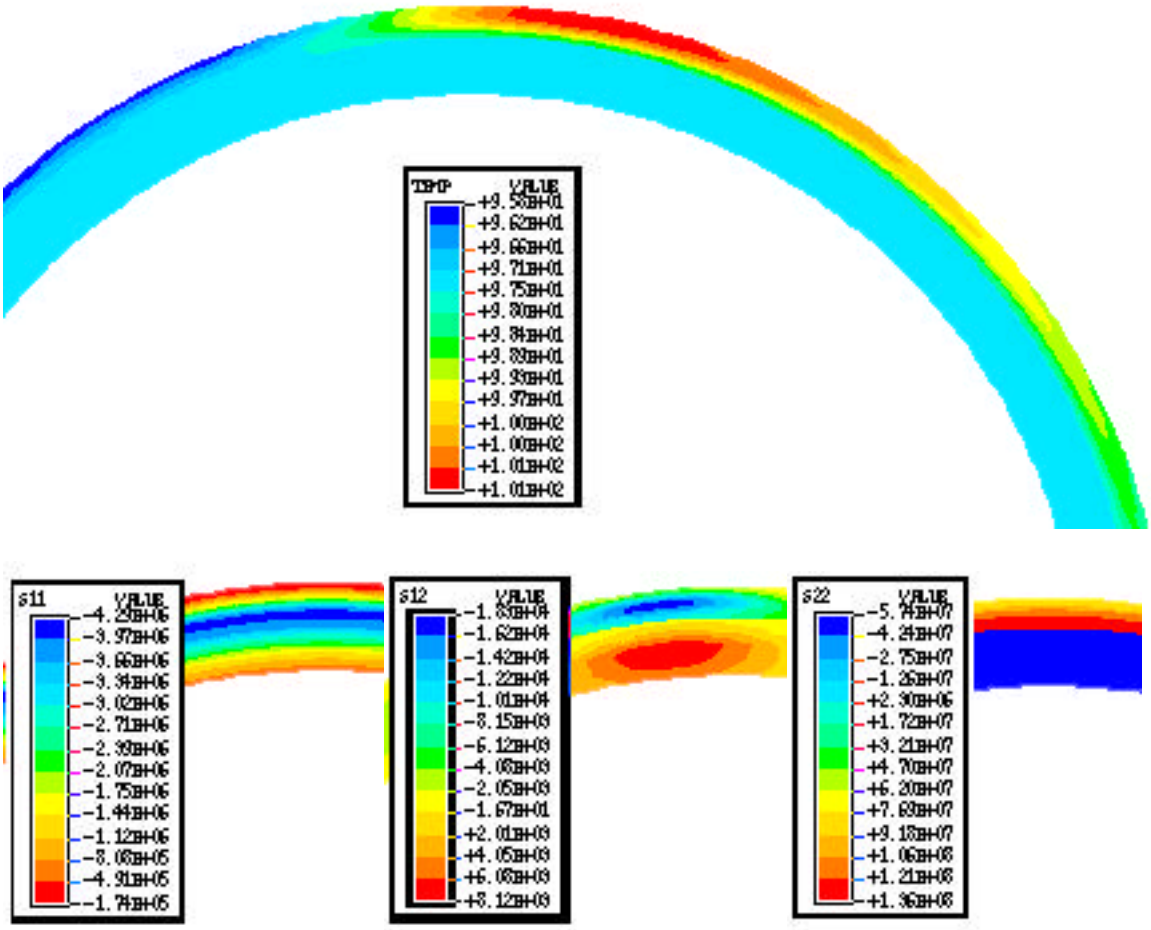

Figure 6.28 Isotherms and process-induced stresses at time = 60.8 second. Temperatures are in °C. Stresses are in Pa.

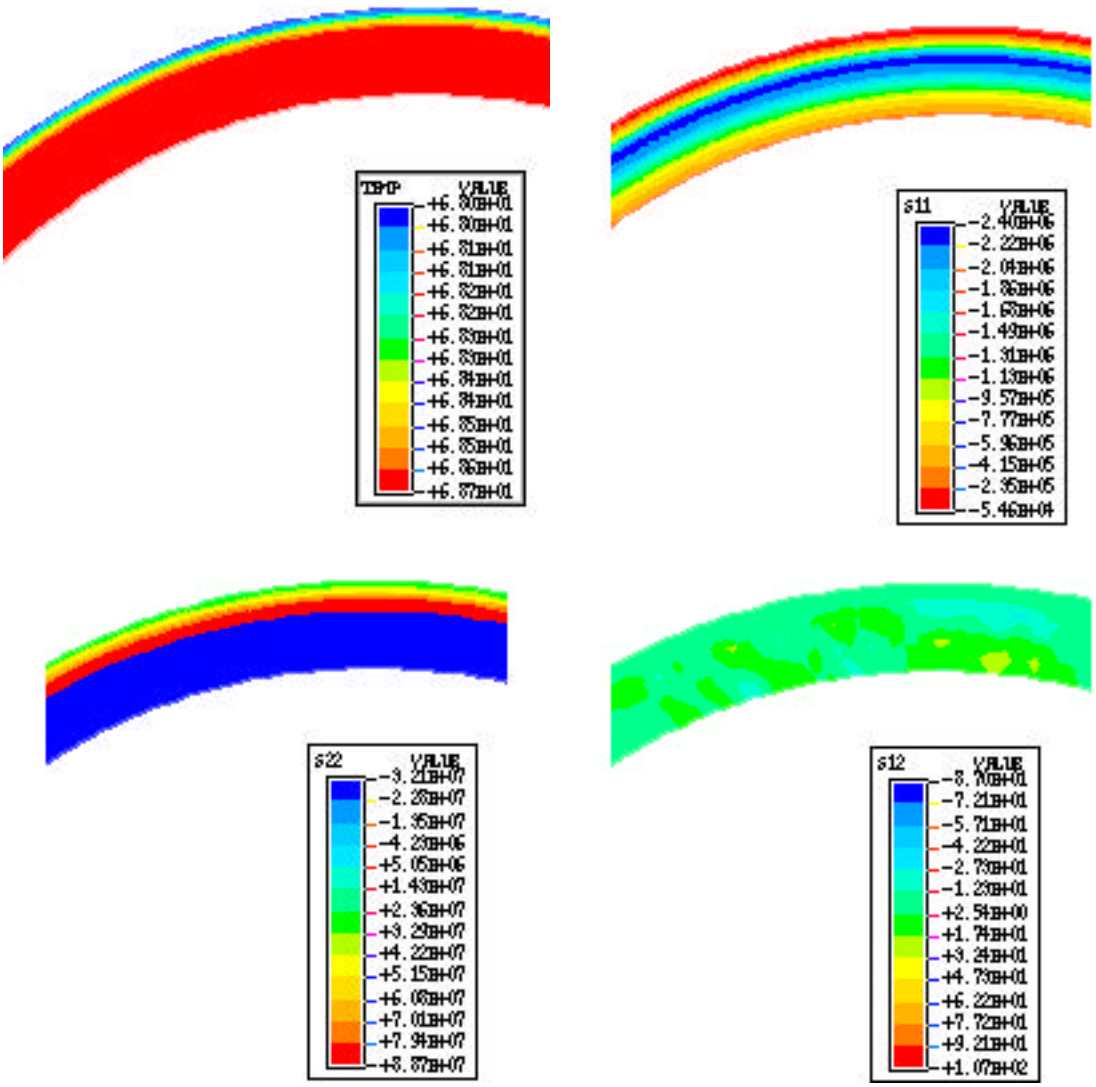

Figure 6.29 Isotherms and process-induced stresses at time = 526 second. Temperatures are in °C. Stresses are in Pa.

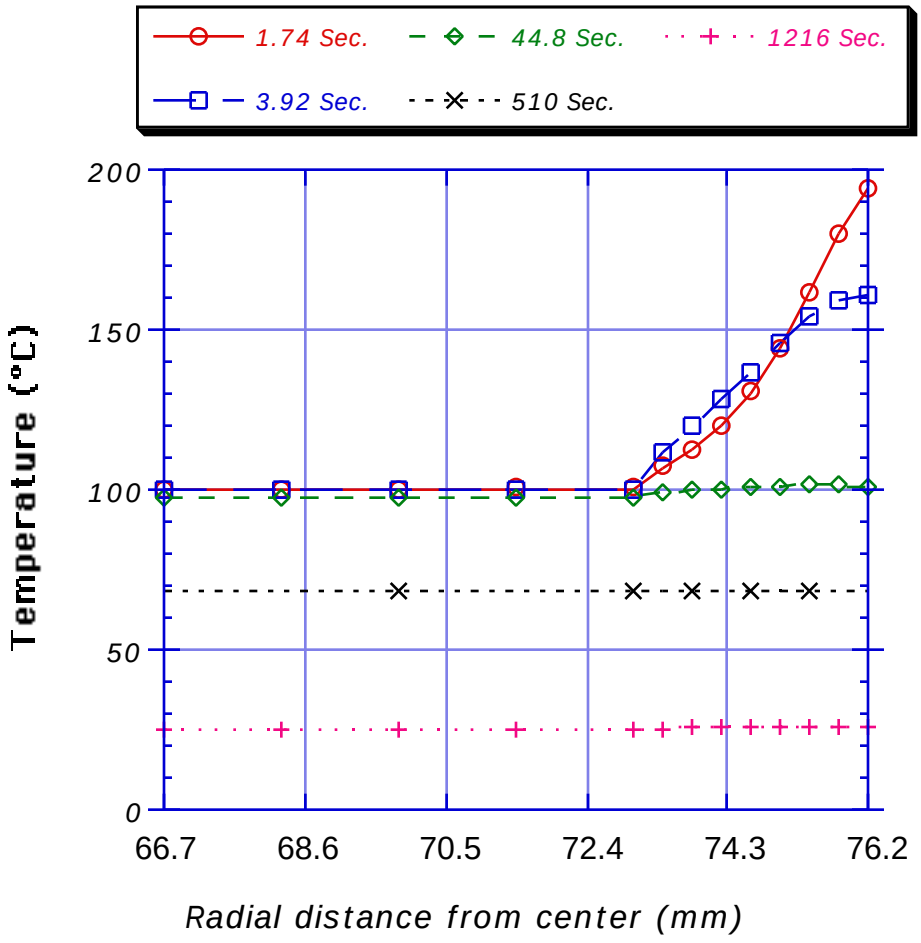

Figure 6.30 Temperature distribution across the thickness at five times during manufacturing process.

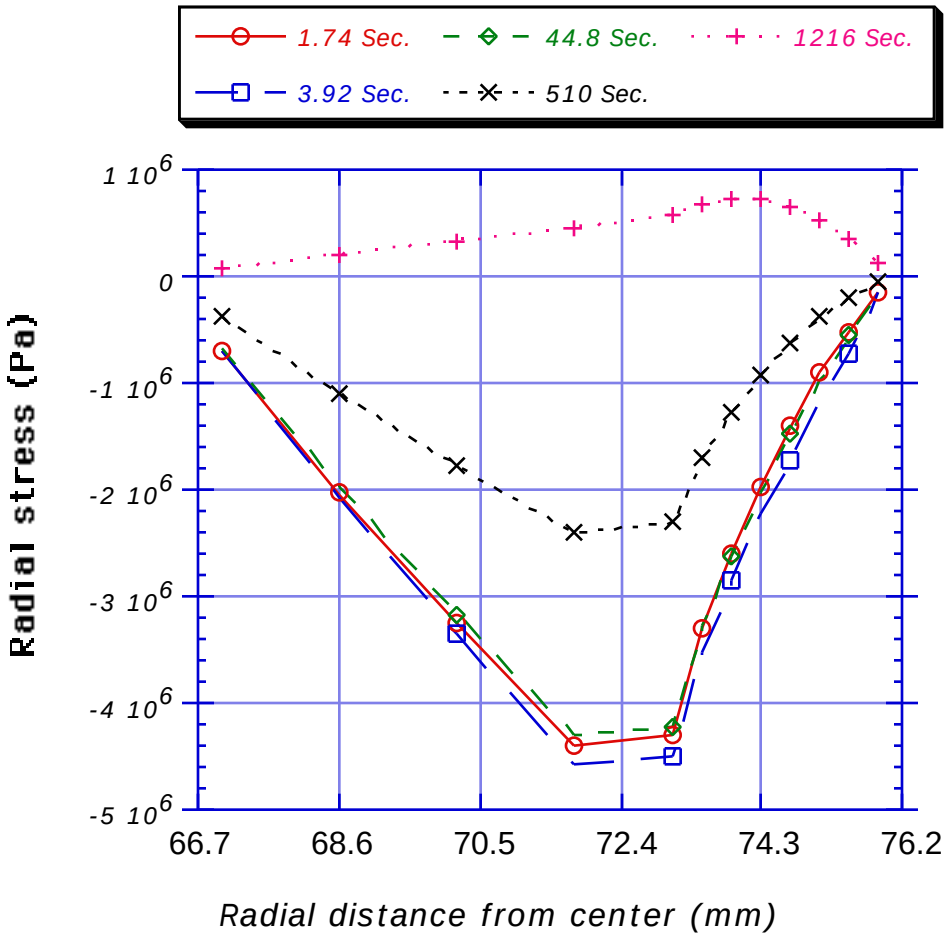

Figure 6.31 Thermal stresses in radial direction at five times during manufacturing process.

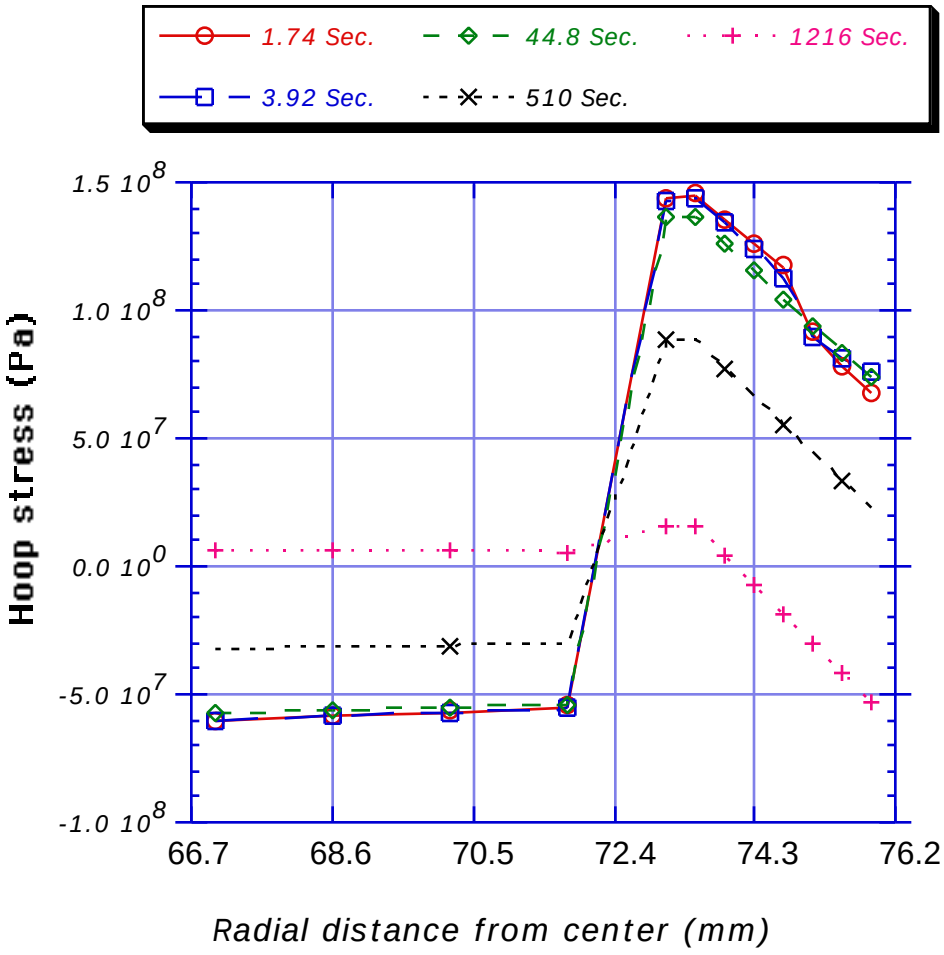

Figure 6.32 Thermal stresses in hoop direction at five times during manufacturing process.

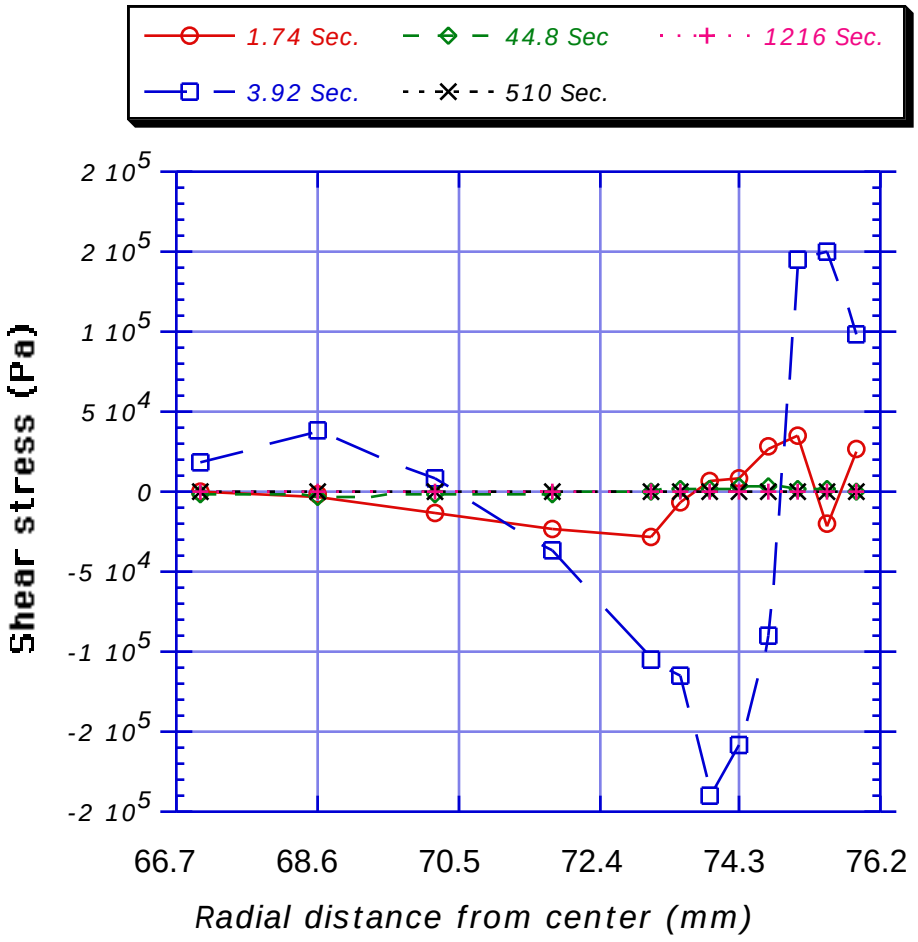

Figure 6.33 Shear thermal stresses at five times during manufacturing process.

7 Concluding Remarks

7.1 Summary

An on-line consolidation system which includes a computer-controlled filament winding machine and consolidation head assembly, has been designed, constructed, and installed in Hancock Hall at Virginia Tech. The successful completion of the facility allows us to intensively investigate the feasibility of this relatively new manufacturing technique for thermoplastic composites.

The on-line consolidation system was used to manufacture composite cylinders from 6.35 mm wide APC-2 towpreg (carbon fiber and PEEK) from Fiberite, Inc. The winding pattern was generated by the computer software, CADWIND®. The winding procedure was performed on a computer controlled two-axis filament winding machine. All cylinders investigated are hoop-wound and have an inner diameter of 146 mm (5.75 in).

The processing window for the on-line consolidation system was determined by adjusting the three system processing parameters, namely

roller pressure, winding speed, and nippoint temperature. To simplify the approach a step further, a fixed roller pressure of 380 kPa (55 psi) was chosen for fabricating all cylinders. The present study was focused on the impact of winding speed and nippoint temperature on composite quality. A two-factor central composite design of experiments was used to define the combination of processing parameters, to systematically study the processing window, and to maximize the quality of composite parts. The levels for winding speed range from about 4-10 mm/s and the nippoint temperature has a high value of 660°C (1220°F) and a low value of 493°C (920°F). Nine composite cylinders, 26-ply thick and 19 mm (3/4 in) wide were fabricated under the prescribed processing conditions given by the experimental design. The winding time ranges from 77 to 172 minutes.

To gage the overall quality, density and void content tests were performed on all composite cylinders. The density measurements was performed in accordance with ASTM standard D792-91. The void content was calculated based on ASTM standard D2734-91. Micrographs of the cross sections of each consolidated part are used to qualitatively describe the consolidation for a set of processing conditions. The degree of crystallinity of the consolidated cylinders under different processing conditions was measured by differential scanning calorimetry (DSC). Finally, the interlaminar shear strength of consolidated parts was measured based on ASTM standard D2344.

Micrographs of the composite cylinder cross-sections show that complete intimate contact and a uniform fiber distribution at the interply

interface are possible with on-line consolidation. Composite cylinders with less than 1% void content were achieved in spite of an average void content of 7% for APC-2 towpreg. Void content tests assure us that consolidating the thermoplastic prepreg layer by layer helps to squeeze out the air entrapped in the raw material. To study how ILSS varies with different processing conditions, a response surface was constructed. A second order linear regression analysis was used to determine the ILSS response surface.

An in-situ measurement system was constructed to acquire temperature data during the winding process. A total of eight thermocouples were placed between different layers during winding. It was found that the winding speed had a significant impact on the maximum temperature inside the composite cylinder. However, the temperature was well below melting point of APC-2 composite.

In order to investigate the transient heat transfer occuring during on-line consolidation, ABAQUS finite element models of the different phases of the consolidation process were constructed. First, the fundamental equations involved in transient heat transfer and the finite element formulations in ABAQUS were discussed. Then, an ABAQUS finite element model that took into account all components involved in the on-line consolidation process was constructed. The transient temperature field for a stationary heat source was solved and the calculated temperature history was compared with data obtained by the in-situ measurement system. A convective heat transfer coefficient equal to 260 $w/m^2°K$ was obtained by matching the calculated

temperature history to in-situ measurement data. The impact of film coefficient was also investigated.

To predict temperature distribution during winding, mandrel rotation was indirectly modeled by moving the heat source along the circumferential direction of the stationary mandrel. The winding speed was modeled by incrementally moving the convective boundary conditions, as described in Section 6.3.2 around the outer surface of the composite cylinder. The predictions were about 15% lower than the measured temperatures. Nevertheless the overall prediction captured the transient rather well. Finally, a towpreg heating model was constructed to predict the temperature distribution on the cross section of the incoming towpreg under various processing conditions.

The finite element mesh for thermal stress analysis included the entire composite-mandrel assembly. The thermal boundary conditions consist of two major parts, the winding stage and the cooling stage. The winding part was similar to the boundary conditions used in the winding analysis. Then the heat source was moved away and the cooling stage starts. During cooling, the free convective boundary conditions are applied on all of the outer surface of the composite cylinder and a prescribed temperature was specified at every node on the inner surface of the mandrel. Based on the experimental observation, it took about 20 minutes for the mandrel to cool down to the room temperature.

To evaluate the accuracy of the thermal stress model, isotropic material properties were input into the ABAQUS simulation and the results were

compared to that of an analytical solution as derived in Section 6.4. Overall, the simulation results agreed with analytical solution. To predict the process-induced thermal stresses, temperature-dependent material properties were applied to the model. The APC-2 composite was modeled as an orthotropic media with temperature-dependent material properties and the aluminum mandrel was modeled as an isotropic solid with constant material properties. The temperature distribution and thermal stresses were investigated during the winding and cooling processes.

7.2 Conclusions

Results from mechanical and physical tests on the composite cylinders have shown that the present on-line consolidation (OLC) system is capable of performing all tasks needed for investigating the fundamentals involved in the OLC process without adding secondary preheating components. The interlaminar shear strength (ILSS) was found very sensitive to both winding speed and nippoint temperature. Thus, the ILSS test was considered an excellent screening method for evaluating various processing conditions. Under optimum processing conditions, an ILSS of 58 MPa and a void content less than 1% was achieved with APC-2 towpreg. An experimental design was used to select the processing conditions and to define the processing window. The processing window is defined as the conditions under the shaded area in contour plot (Figure 4.22) which yield an ILSS of 50 MPa or better. For the processing range investigated in the study, higher nippoint temperature and lower winding speed yield higher ILSS and lower void content. The thermal

degradation was not a concern due to high heating rate and short dwelling time associated with the on-line consolidation process.

The winding simulation model confirms the experimental observation from in-situ measurements that the single air-heater design was not able to create a melt zone on the substrate surface. Therefore, the heater was focused directly at the towpreg which was much easier to melt thoroughly due to its size. The path of towpreg through guide roller was also changed to enlarge melt zone on the incoming towpreg. The towpreg heat transfer simulation provided operational limits that avoid insufficient melting and thermal degradation. The process-induced thermal stress analysis was used to determine the temperature distribution and thermal stresses during the winding and cooling processes. During winding, localized heating results in in-plane shear stresses near the heat affected zone. During the cooling, virtually no in-plane shear existed due to no temperature change throughout the composite-mandrel assembly. After processing, a compressive hoop stress was predicted inside the composite cylinder. The on-line consolidation models developed in the present study can be used as a computer-aided-design tool for developing new OLC systems by simply changing the boundary conditions or the material properties.

Though still at its developing stage, with ever increasing knowledge of the fundamentals involved in the process and the very merit of the thermoplastic materials such as toughness, recyclability, and reparability, the on-line consolidation technology will find its positions in many industrial applications in the very near future.

7.3 Future work

For future work, the following activities are recommended:

- Investigate the impact of compaction pressure on the quality of the consolidated cylinders.
- Expand the range of processing parameters beyond the ones currently studied.
- Study the non-isothermal crystallization mechanism of the PEEK resin.
- Modify the in-situ measurement to incorporate process-induced strains measurements.
- Apply the on-line consolidation technique to powder coated towpreg.
- Investigate the resin flow behavior under compaction roller.
- Improve the winding speed by pre-heating the incoming towpreg and mandrel assembly.
- Use contact elements between composite and mandrel to simulate the separation during cooling.

References

[1] Coffenberry, B. S., D. E. Hauber and M. Cirino. “Low Cost Alternative: In-Situ Consolidated Thermoplastic Composite Structures” *38th International SAMPE Symposium,* pp.1640-1650 (1993).

[2] Ghasemi Nejhad, M. N., R. D. Cope and S. I. Güçeri," Thermal Analysis of In-situ Thermoplastic Composite Tape Laying" *Journal of Thermoplastic Composite Materials,* 4:20-45 (1991).

[3] Wells, G. M. and K. F. McAnulty. “Computer Aided Winding Using Non-Geodesic Trajectories,” Proceedings, Sixth International Conference on Composite Materials, Second European Conference on Composite Materials, ICCM & ECCM, 1:1.161-1.173 (1987).

[4] Ghasemi Nejhad, M. N. "Issues Related to Processability during the Manufacture of Thermoplastic Composites Using On-Line Consolidation Techniques" *Journal of Thermoplastic Composite Materials,* 6:130-146 (1993).

[5] Zoller, P. “Solidification Processes in Thermoplastics and Their Role in the Development of Internal Stresses in Composites” *ASC 3rd Technical Conference*, pp. 439-448 (1988).

[6] Ghasemi Nejhad, M. N., J. W. Gillespie and R. D. Cope. “Processing Stresses for Thermoplastic Filament Winding Using the Divergence Method” *Heat Transfer Effects in Materials Processing ASME HTD-Vol. 233* , 33-43 (1992).

[7] Gillespie, J. W. Jr. and T. J. Chapman. “The Influence of Residual Stresses on Mode I Interlaminar Fracture of Thermoplastic Composites” *Journal of Thermoplastics Composites Materials* , 6:160-174 (1993).

[8] Tzeng, J. T. and R. B. Pipes. “Thermal Residual Stress Analysis for In Situ and Post-Consolidated Composite Ring” *Composites Manufacturing,* 3(4): 273-279 (1992).

[9] Lawrence, W. E., J.-A. E. Manson, J. C. Seferis, J. W. Gillespie, Jr. and R. B. Pipes. “Prediction of Residual Stress in Continuous Fiber Semicrystalline Thermoplastic Composites: A Kinetic-Viscoelastic Approach” *ASC 5th Technical Conference*, pp. 401-414 (1990).

[10] White, S. R. and H. T. Hahn. “Process Modeling of Composite Materials: Residual Stress Development During Cure. Part I. Model Formulation” *Journal of Composite Materials* , 26(16): 2402-2422 (1992).

[11] White, S. R. and H. T. Hahn. “Process Modeling of Composite Materials: Residual Stress Development During Cure. Part I. Experimental Validation” *Journal of Composite Materials* , 26(16): 2423-2453 (1992).

[12] Li, M. C. and A. C. Loos. "Thermoplastic Composite Consolidation", Center for Composite Materials and Structures, Report CCMS-94-01, VPI-E-94-02, Virginia Polytechnic Institute and State University, Blacksburg, Virginia (1994).

[13] Chapman, T. J., J. W. Gillespie, Jr., J.-A. E. Manson, R. B. Pipes and J. C. Seferis. “Thermal Skin/Core Residual stresses Induced During Cooling of Thermoplastic Matrix Composites” *ASC 3rd Technical Conference*, : 449-458 (1988).

[14] Unger, W. J. and J. S. Hansen. “The Effect of Thermal Processing on Residual Strain Development in Unidirectional Graphite Fibre Reinforced PEEK” *Journal of Composite Materials,* 27(1):59-82 (1993).

[15] Denault, J. and T. Vu-Khanh. “Crystallization and Fiber/Matrix Interaction During the Molding of PEEK/Carbon Composites” *Polymer Composites*, 13(5): 361-371 (1992).

[16] Benatar, A. and T. G. Gutowski. "A Review of Methods for Fusion Bonding Thermoplastic Composites" *SAMPE Journal,* 23:33-39 (1987).

[17] Egerton, M. W. and M. B. Gruber. “Thermoplastic Filament Winding Demonstrating Economics and Properties Via In-Situ Consolidation” *33rd International SAMPE Symposium,* : 35-46 (1988).

[18] Güçeri, S. I. “Transport Phenomena in On-line Consolidation of Thermoplastic Composites” *Transport Phenomena in Material Processing and Manufacturing* ASME HTD-Vol. 196, 11-21 (1992).

[19] Tung, C. M., D. S. Gnanamuthu, R. J. Moores and C. L. Leung. “Effect of Laser Radiation on the Rapid Processing of Graphite-Reinforced Composites” *32nd International SAMPE Symposium,* p. 476-483 (1987).

[20] Agarwal V., S. I. Güçeri, R. L. McCullough and J. M. Schultz. "Thermal Characterization of Laser-Assisted Consolidation Process" *Journal of Thermoplastic Composite Materials,* 5:115-135 (1992).

[21] Beyeler, E., W. Phillips and S. I. Güçeri, "Experimental Investigation of Laser-Assisted Thermoplastic Tape Consolidation" *Journal of Thermoplastic Composite Materials,* 1:107-121 (1988).

[22] Irwin, R. G. and S. I. Güçeri, "Recent Advances in Laser Heated On-line Consolidation of Thermoplastic Composites" *Heat Transfer Effects in Materials Processing ASME HTD-Vol. 233* , 53-60 (1992).

[23] Hinkley, J. A. , R. W. Grenoble and J. M. Marchello. "Rapid Welding of Thermoplastic Towpreg Ribbon" *40th International SAMPE Symposium,* p. 1560-1571 (1995).

[24] Muzzy, J., L. Norpoth and B. Varughese. "Characterization of Thermoplastic Composites for Processing" *SAMPE Journal;,* 25:23-29 (1989).

[25] Gutowski, T. G. "A Resin Flow/Fiber Deformation Model for Composites" *SAMPE Quarterly*, 16(4):58-64 (1985).

[26] Gutowski, T. G., Z. Cai, J. Kingery and S. J. Wineman "Resin Flow/Fiber Deformation Experiments" *SAMPE Quarterly*, 17(4):54-58 (1986).

[27] Bastien, L. J. and J. W. Gillespie, Jr. "A Non-Isothermal Healing Model for Strength and Toughness of Fusion Bonded Joints of Amorphous Thermoplastics" *Polymer Engineering and Science*, 31(24): 1720-1730 (1991).

[28] Dara, P. H. and A. C. Loos "Thermoplastic Matrix Composite Processing Model," Center for Composite Materials and Structures, Report CCMS-85-10, VPI-E-85-21, Virginia Polytechnic Institute and State University, Blacksburg, Virginia (1985).

[29] Velisaris, C. N. and J. C. Seferis. "Crystallization Kinetics of Polyetheretherketone (PEEK) Matrices" *Polymer Engineering and Science*, 26(22): 1574-1581 (1986).

[30] Velisaris, C. N. and J. C. Seferis. "Heat Transfer Effects on the Processing-Structure Relation of Polyetheretherketone (PEEK) Based Composites" *Polymer Engineering and Science*, 28(9): 583-591 (1988).

[31] Lee, Y and R. S. Porter. "Crystallization of Poly(etheretherketone) (PEEK) in Carbon Fiber Composites" *Polymer Engineering and Science*, 26(8): 633-639 (1986).

[32] Denault, J. and T. Vu-Khanh. “Crystallization and Fiber/Matrix Interaction During the Molding of PEEK/Carbon Composites” *Polymer Composites*, 13(5): 361-371 (1992).

[33] Talbott, M. F., G. S. Springer and L. A. Berglund. “The Effects of Crystallinity on the Mechanical Properties of PEEK Polymer and Graphite Fiber Reinforced PEEK” *Journal of Composite Materials*, 21(11): 1056-1081 (1987).

[34] Colton, J. and D. Leach. "Processing Parameters for Filament Winding Thick-Section PEEK/Carbon Fiber Composites" *Polymer Composites*, 13(6): 427-434 (1992).

[35] Grove, S. M. “Thermal Modeling of Tape Laying with Continuous Carbon Fiber-Reinforced Thermoplastic” *Composites*, 19(2) 367-375 (1988).

[36] Beyeler, E. P. and S. I. Güçeri, “Thermal Analysis of Laser-Assisted Thermoplastic-Matrix Composite Tape Consolidation” *ASME Journal of Heat Transfer*, 110:424-430 (1988).

[37] Ghasemi Nejhad, M. N., R. D. Cope and S. I. Güçeri, "Thermal Analysis of In-Situ Thermoplastic-Matrix Composite Filament Winding" *ASME Journal of Heat Transfer*, 113:304-313 (1991).

[38] Roderic, C. D., S. T. Holmes, K. V. Steiner and J. W. Gillespie, Jr. “Integrated Process Models for Control of Thermoplastic Tow Placement with On-line Consolidation” *25th International SAMPE Technical Conference* pp.713-724 (1993).

[39] Cirino, M., T. P. Watson and D. E. Hauber. “Composite Structure Fabrication with In-Situ Consolidation of APC-2/AS4” *36th International SAMPE Symposium*, pp. 2184-2196 (1991).

[40] Buijs, J.A.H.M. and P. J. Nederveen. "A Study of Consolidation in Filament Winding with Thermoplastic Prepregs" *Journal of Thermoplastic Composite Materials*, 5:276-286 (1992).

[41] Mazumdar, S. K. and S. V. Hoa. “Experimental Determination of Process Parameters for Laser Assisted Processing of PEEK/Carbon Thermoplastic Composites” *38th International SAMPE Symposium*, pp. 189-203 (1993).

[42] Mazumdar, S. K. and S. V. Hoa. “Determination of Manufacturing Conditions for Hot-Gas-Aided Thermoplastic Tape Winding” *Journal of Thermoplastic Composite Materials*, 9:35:53 (1996).

[43] Carpenter, C. E. and Colton, J. S. “On-line Consolidation Mechanism in Thermoplastic Filament Winding (Tape Laying)” *38th International SAMPE Symposium,* pp. 205-216 (1993).

[44] Wood, D. and S. C. Mantell. “Application of Statistical Design of Experiments to Thermoplastic Tape Laying” *38th International SAMPE Symposium,* pp. 154-161 (1993).

[45] Carpenter, C. E. and J. S. Colton. "On-Line Consolidation Mechanisms in Thermoplastic Filament Winding" *Polymer Composites*, 15(1):55-63 (1994).

[46] Don, R. C., S. T. Holmes, K. V. Steiner and J. W. Gillespie, Jr. “Integrated Process Models for Control of Thermoplastic Tow Placement with On-Line Consolidation” *25th International SAMPE Technical Conference*, p. 713-724 (1993).

[47] Lauke, B. and K. Friedrich. "Evaluation of Processing Parameters of Thermoplastic Composites Fabricated by Filament Winding" *Composites Manufacturing*, 4(2): 93-101 (1993).

[48] Liu, K. S. and S. W. Tsai. "A Mathematical Model for an In-Situ Consolidation of Thermoplastic Composites" to be published.

[49] Mantell, S. C. and G. S. Springer. “Manufacturing Process Models for Thermoplastic Composites” *Journal of Composite Materials*, 26(16): 2348-2377 (1992).

[50] Sharp, R., S. Holmes, and C. Woodall, "Material Selection/Fabrication Issues for Thermoplastic Fiber Placement" *Journal of Thermoplastic Composite Materials*, 8:2-14 (1995).

[51] Gruber, M. B. "Thermoplastic Tape Laydown and Consolidation", SME EM86-905, Dearborn, Michigan, (1986).

[52] Werdermann, C., K. Friedrich, M. Cirino, and R. B. Pipes, "Design and Fabrication of an On-Line Consolidation Facility for Thermoplastic Composites " *Journal of Thermoplastic Composite Materials*, 2:293-306 (1989).

[53] Haupert, F., C. Chen, and K. Friedrich, “Manufacturing of Thermoplastic composite Parts by Combined Filament Winding and Injection Molding” Proc. ICCM 10, Canada 1995.

[54] Hauber, D. E., D. J. Hardtmann, K. B. Bubeck, “Recent Advances in Thermoplastic Composite Fabrication Using ROWS” *35th International SAMPE Symposium* pp.767:772 (1990).

[55] Steiner, K. V. “Development of a Robotic filament Winding workstation for Complex Geometry” *35th International SAMPE Symposium* pp.757:766 (1990).

[56] Hümmler, J., S-K Lee, and K. V. Steiner, “Recent Advances in Robotic filament Winding” *36th International SAMPE Symposium* pp.2142:2156 (1991).

[57] Felderhoff, K. D. and K. V. Steiner, “A New Compact Robotic Head for Thermoplastic Fiber Placement” *38th International SAMPE Symposium* pp.138:151 (1993).

[58] Mazumdar, S. K. and S. V. Hoa. “Processing of PEEK/Carbon Thermoplastic Composites Using Hot Nitrogen Gas by Tape Winding Technique” *Heat and Mass Transfer in Materials Processing and Manufacturing ASME HTD-Vol. 261,* 115-126 (1993).

[59] Wagner, P. and J. S. Colton. "On-Line Consolidation of Thermoplastic Towpreg Composites in Filament Winding" *Polymer Composites*, 15(6):436-441 (1994).

[60] Roderic, C. D., R. Pitchumani and J. W. Gillespie, Jr. “Simulation of the Transient Thermoplastic Fiber Placement” *39th International SAMPE Symposium* pp.1521-1535 (1994).

[61] Steiner, K. V., R. Pitchumani, B. M. Bauer and J. W. Gillespie, Jr. “Experimental Verification of Modeling and Control for Thermoplastic Tow Placement” *40th International SAMPE Symposium* pp.1550-1559 (1995).

[62] Bullock, D. E. and J. Boyce, "On-Line Consolidation of Thermoplastic Matrix Composite Tape Using Ultrasonic Heating", *39th International SAMPE Symposium,* 1500-1506 (1994).

[63] Lee, W. I. and G. S. Springer. “A Model of the Manufacturing Process of Thermoplastic Matrix Composites” *Journal of Composite Materials*, 21:1017-1055 (1987).

[64] Mantell, S. C., Q. Wang and G. S. Springer. “Processing Thermoplastic Composites in a Press and by Tape Laying - Experimental Results” *Journal of Composite Materials*, 26(16): 2378-2401 (1992).

[65] Li, M. C. and A. C. Loos "Thermoplastic Matrix Composite Processing Model," Center for Composite Materials and Structures, Report CCMS-94-02, VPI-E-94-21, Virginia Polytechnic Institute and State University, Blacksburg, Virginia (1994).

[66] Wang, E. L. and T. G. Gutowski. "Laps and Gaps in Thermoplastic Composites Processing", Composites Manufacturing, 2(2):69-78 (1991).

[67] Wool, R. P., B.-L. Yuan and O. J. McGarel. “Welding of Polymer Interfaces” *Polymer Engineering and Science*, 29(19): 1340-1367 (1989).

[68] Voyutskii, S. S. “Autohesion and Adhesion of High Polymers”, *Polymer Reviews* Interscience Publishers, New York, N. Y., Vol. 4 (1963).

[69] Stacer, R. G. and H. L. Schreucder-Stacer. “Time-Dependent Autohesion” *International Journal of Fracture*, 39:201-2216 (1989).

[70] Li, M. C. and A. C. Loos. “The Effects of Processing on Interply Bond Strength of Thermoplastic Composites” *Journal of Reinforced Plastics and Composites*, 11: 1142-1162 (1992).

[71] Barnes, J. A. and G. E. Byerly. “The Formation of Residual Stresses in Laminated Thermoplastic Composites” *Composites Science and Technology*, 51:479-494 (1993).

[72] van den Niewenhuizen, R. S. C. and A. K. Miller. "Full In-Situ Consolidation of Thermoplastic Matrix Carbon Fiber Composites Materials Using Direct Electrical Heating" *Processing, Design, and Performance of Composite Materials, ASME-MD-Vol.52*, PP.29-43 (1994).

[73] Mason, R. L., R. F. Gunst and J. L. Hess. "Statistical Design and Analysis of Experiments with Applications to Engineering and Science" John Wiley and Sons, Inc. New York (1989).

[74] "ABAQUS™/Standard User's Manual Version 5.5", Hibbet Karlsson and Sorenson, Inc., 1995.

[75] "ABAQUS™/Standard Example Problems Manual Version 5.5", Hibbet Karlsson and Sorenson, Inc., 1995.

[76] "ABAQUS™/Theory Manual Version 4.8", Hibbet Karlsson and Sorenson, Inc., 1989.

[77] Timoshenko, S. P. and J. N. Goodier, "Theory of Elasticity" 3rd Edition McGraw-Hill Book Company, pp. 448-449 (1970).

[78] Boley, B. A. and J. H. Weiner, "Theory of Thermal Stresses", John Wiely & Sons, Inc. New York, pp.288-291 (1960).

APPENDIX A

The law of conservation of energy states that heat added to the system plus the work done by the surroundings on the system is equal to increase of the internal energy of the system. Since the surface force and body force are of no interest in a pure heat transfer problem, the Lagrangian formulation of the energy balance equation for an arbitrary control volume as shown in Figure A.1 can be mathematically expressed as the follows:

$$\int_{\Gamma} \boldsymbol{q}\, d\Gamma + \int_{\Omega} \boldsymbol{r}\, d\Omega = \int_{\Omega} \rho \dot{\boldsymbol{U}}\, d\Omega \qquad \text{(A.1)}$$

where:

$\int_{\Gamma} \boldsymbol{q}\, d\Gamma$ = surface flux term, $\boldsymbol{q}$ positive into the body,

$\int_{\Omega} \boldsymbol{r}\, d\Omega$ = Volumetric flux term (source),

$\int_{\Omega} \rho \dot{\boldsymbol{U}}\, d\Omega$ = storage term,

$\boldsymbol{q}$ = the heat flux per unit of current area crossing surface Γ from surrounding to body (scalar quantity),

$\boldsymbol{r}$ = internal heat generation per unit volume, and

$\dot{\boldsymbol{U}}$ = the material time rate of internal energy.

Substituting $-\tilde{\boldsymbol{q}} \cdot \tilde{\boldsymbol{n}}$ for $\boldsymbol{q}$ in Eq. (A.1), we obtain

$$\int_{\Gamma} -\tilde{\boldsymbol{q}} \cdot \tilde{\boldsymbol{n}}\, d\Gamma + \int_{\Omega} \boldsymbol{r}\, d\Omega = \int_{\Omega} \rho\, \dot{\boldsymbol{U}}\, d\Omega \tag{A.2}$$

or using divergence (Gauss') theorem

$$-\int_{\Omega} \frac{\partial}{\partial \tilde{\boldsymbol{x}}} \cdot \tilde{\boldsymbol{q}}\, d\Omega + \int_{\Omega} \boldsymbol{r}\, d\Omega = \int_{\Omega} \rho\, \dot{\boldsymbol{U}}\, d\Omega\,. \tag{A.3}$$

By rearranging Eq. (A.3) we can write

$$\int_{\Omega} \left(-\frac{\partial}{\partial \tilde{\boldsymbol{x}}} \cdot \tilde{\boldsymbol{q}} + \boldsymbol{r} - \rho\, \dot{\boldsymbol{U}}\right) d\Omega = \boldsymbol{0}\,. \tag{A.4}$$

or

$$-\frac{\partial}{\partial \tilde{\boldsymbol{x}}} \cdot \tilde{\boldsymbol{q}} + \boldsymbol{r} - \rho\, \dot{\boldsymbol{U}} = \boldsymbol{0}\,. \tag{A.5}$$

Since the region Ω is arbitrary, the integrand must be identically equal to zero.

Fourier's law of heat conduction states that the heat flux $\tilde{\boldsymbol{q}}$ is proportional to the temperature gradient $\frac{\partial \boldsymbol{T}}{\partial \tilde{\boldsymbol{x}}}$ and can be expressed as

$$\tilde{\boldsymbol{q}} = -\bar{\bar{\boldsymbol{k}}} \cdot \frac{\partial \boldsymbol{T}}{\partial \tilde{\boldsymbol{x}}} \tag{A.6}$$

where $\bar{\bar{\boldsymbol{k}}}$ is the material's thermal conductivity matrix.

The time rate of internal energy can be rewritten as

$$\dot{\boldsymbol{U}} = \frac{\boldsymbol{dU(T)}}{\boldsymbol{dt}} = \frac{\boldsymbol{dU(T)}}{\boldsymbol{dT}} \frac{\boldsymbol{dT}}{\boldsymbol{dt}} = \frac{\boldsymbol{dU(T)}}{\boldsymbol{dT}} \dot{\boldsymbol{T}} = \boldsymbol{C_p} \dot{\boldsymbol{T}} \tag{A.7}$$

where $\boldsymbol{C_p}$ is the specific heat of the material and is defined as $\frac{\boldsymbol{dU(T)}}{\boldsymbol{dT}} = \boldsymbol{C_p}$. Note that $\boldsymbol{C_p}$ can be temperature dependent in the most general case.

Substituting Eq. (A.6) and Eq. (A.7) into Eq. (A.5), we obtain

$$\frac{\partial}{\partial \tilde{\boldsymbol{x}}} \cdot \bar{\bar{\boldsymbol{k}}} \frac{\partial \boldsymbol{T}}{\partial \tilde{\boldsymbol{x}}} + \boldsymbol{r} = \rho \boldsymbol{C}_p \dot{\boldsymbol{T}} \tag{A.8}$$

or in the matrix form and in the tensor form respectively as

$$\cdot (\bar{\bar{\boldsymbol{k}}} \quad \boldsymbol{T}) + \boldsymbol{r} = \rho \boldsymbol{C}_p \dot{\boldsymbol{T}} \text{ and } (\boldsymbol{K}_{ij} \boldsymbol{T}_{,j})_{,i} + \boldsymbol{r} = \boldsymbol{C}_p \rho \dot{\boldsymbol{T}}. \tag{A.9}$$

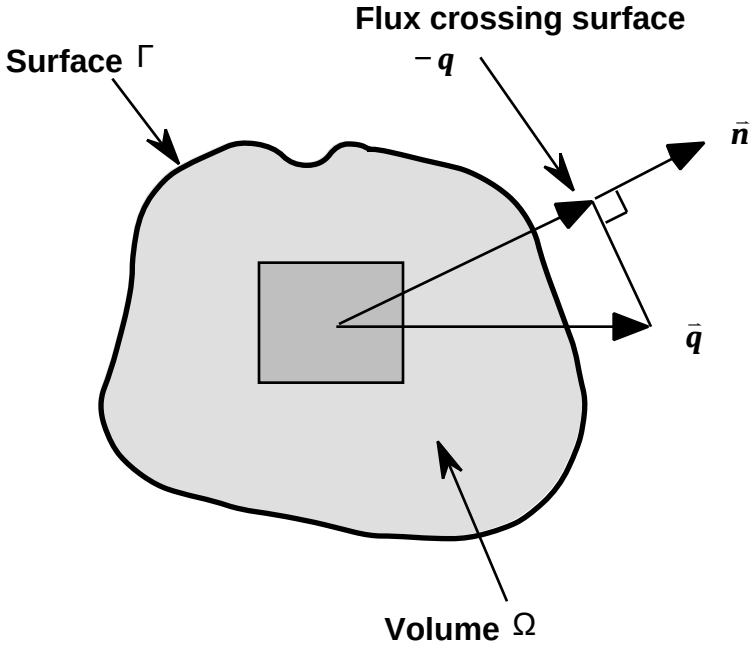

Figure A.1 Arbitrary control volume.

Vita

Po-jen Shih was born on June 27, 1963 in Tainan, Taiwan, Republic of China. In 1986 he graduated from National Cheng Kung University (NCKU) in Taiwan with a bachelor's degree, and in 1991 with a Master's degree in Mechanical Engineering from Oklahoma State University. Since 1991 he entered Virginia Polytechnic Institute and State University and began his pursuit for a Ph.D. degree in Engineering Mechanics.